

# POLITECNICO DI TORINO

Collegio di Ingegneria Chimica e dei Materiali

**Master of Science Course**

**in Ingegneria Chimica e dei Processi Sostenibili**

Master of Science Thesis

## **Benchmark Analysis of Accident Modelling Software Applied to Hydrogen Storage.**



**Politecnico  
di Torino**

### **Tutors**

Micaela Demichela

Elsa Pastor

Eulalia Planas

### **Candidate**

Lorenza Saturnino



*A me stessa.  
Al coraggio di mettermi in gioco.*



## Abstract (English)

Global greenhouse gas emissions have surged to unprecedented levels, prompting a strong focus on decarbonization. Hydrogen, especially when produced renewably, emerges as a promising CO<sub>2</sub>-free energy vector for industry, transport, and power sectors. However, the transition to hydrogen involves significant technical challenges, particularly in continuous production and safe storage. Classified as a hazardous substance under the SEVESO III Directive, hydrogen poses risks of major accidents, necessitating rigorous Quantitative Risk Assessment (QRA).

Accurate consequence estimation is critical for reliable risk assessment. This study conducted a benchmark analysis of Phast, HyRAM, and ALOHA software tools to evaluate their capabilities in modelling the dispersion and ignition of gaseous hydrogen from pressurized tank leaks, focusing on the accuracy of their results.

Real-world experimental data from three studies were used to validate simulation outcomes, covering pressures from 60 to 400 bar and hole diameters from 0.5 mm to 52.5 mm. Assumptions were made for missing parameters, including weather conditions, with ambient temperatures set at 10°C for night-time and 20°C for daytime experiments, and atmospheric stability classified using the Pasquill method.

ALOHA demonstrated significant limitations in this study. It was unable to produce results for most experimental studies involving small and medium-scale hydrogen jets because it does not display distances shorter than 10 meters and is restricted to simulating vertical jet fires only.

The comparison of Phast and HyRAM revealed that both tools generally underestimated hydrogen concentrations, with Phast performing slightly better than HyRAM, especially at higher concentrations. Atmospheric stability influenced dispersion but not jet fire characteristics. Both tools tended to overpredict flame length, except in the smallest release hole simulations. For large-scale jet fires, Phast overpredicted radiation, while HyRAM underpredicted it.

## Abstract (Italian)

Le emissioni globali di gas serra hanno raggiunto livelli senza precedenti, spingendo verso un forte interesse per la decarbonizzazione. L'idrogeno, soprattutto quando prodotto in modo rinnovabile, emerge come un promettente vettore energetico privo di emissioni di CO<sub>2</sub> per l'industria, il trasporto e il settore energetico. Tuttavia, la transizione da combustibili fossili a idrogeno presenta significative sfide tecniche, soprattutto per quanto riguarda la sua produzione continua e la sicurezza dello stoccaggio. Classificato come sostanza pericolosa secondo la direttiva SEVESO III, l'idrogeno, infatti, comporta rischi di incidenti rilevanti, rendendo necessaria una rigorosa Valutazione Quantitativa del Rischio (QRA).

La stima accurata delle conseguenze di un incidente è fondamentale per una valutazione affidabile del rischio. In questa tesi è stata condotta un'analisi comparativa dei software Phast, HyRAM e ALOHA per valutare la loro capacità nella modellazione della dispersione e dell'accensione dell'idrogeno gassoso proveniente da perdite di serbatoi pressurizzati, concentrando l'attenzione sull'accuratezza dei risultati.

Sono stati utilizzati dati sperimentali reali provenienti da tre studi per convalidare le simulazioni, coprendo intervalli di pressione da 60 a 400 bar e diametri dei fori da 0,5 mm a 52,5 mm. Sono state effettuate ipotesi per parametri mancanti, inclusi le condizioni meteorologiche, con temperature ambientali fissate a 10°C per le sperimentazioni notturne e 20°C per quelle diurne, e la stabilità atmosferica è stata classificata utilizzando il metodo di Pasquill.

ALOHA ha mostrato limitazioni significative in questo studio, non producendo risultati per la maggior parte degli esperimenti che coinvolgono jet di idrogeno di dimensioni ridotte e medie, poiché non visualizza distanze inferiori a 10 metri e si limita alla simulazione di jet verticali.

Il confronto tra Phast e HyRAM ha evidenziato che entrambi gli strumenti tendono generalmente a sottostimare le concentrazioni di idrogeno, con Phast che mostra prestazioni leggermente superiori rispetto a HyRAM, soprattutto a concentrazioni più elevate. La stabilità atmosferica influisce sulla dispersione ma non sulle caratteristiche del jet fire. Entrambi gli strumenti tendono a sovrastimare la lunghezza della fiamma, eccetto nelle simulazioni con il foro di rilascio più piccolo. Per i jet fire su larga scala, Phast ha sovrastimato la radiazione, mentre HyRAM l'ha sottostimata.

## Resum (Catalan)

Les emissions mundials de gasos d'efecte hivernacle han augmentat a nivells sense precedents, provocant un fort enfocament en la descarbonització. L'hidrogen, especialment quan es produeix de manera renovable, emergeix com un vector d'energia prometedora i lliure de CO<sub>2</sub> per als sectors de la indústria, el transport i l'energia. Nogensmenys, la transició a l'hidrogen implica desafiaments tècnics significatius, particularment en la producció contínua i l'emmagatzematge segur. Classificat com una substància perillosa segons la Directiva SEVESO III, l'hidrogen planteja riscos d'accidents greus, fet que requereix una rigorosa Avaluació Quantitativa de Riscos (QRA).

L'estimació precisa de les conseqüències és crítica per a una avaluació fiable de riscos. Aquest treball va realitzar una anàlisi de referència de les eines de programari Phast, HyRAM i ALOHA per avaluar les seves capacitats en la modelització de la dispersió i la ignició d'hidrogen gasós de fuites de tancs pressuritzats, centrant-se en la precisió dels seus resultats.

Per validar els resultats de les simulacions s'han utilitzat dades experimentals de tres estudis, cobrint pressions de 60 a 400 bars i diàmetres d'orificis de 0.5 mm a 52.5 mm. Es van fer supòsits per a les variables desconegudes, incloent-hi les condicions meteorològiques, amb temperatures ambientals fixades en 10°C per a experiments nocturns i 20°C per a experiments diürns, i l'estabilitat atmosfèrica classificada utilitzant el mètode Pasquill.

ALOHA presenta limitacions significatives ja que no va poder produir resultats per a la majoria dels estudis experimentals que involucraven dolls d'hidrogen a petita i mitjana escala perquè no proporciona resultats per a distàncies menors a 10 metres i només simula dolls de foc verticals.

La comparació de Phast i HyRAM ha mostrat que ambdues eines generalment subestimen les concentracions d'hidrogen, amb Phast funcionant lleugerament millor que HyRAM, especialment en concentracions més altes. Ambdues eines tendeixen a sobreestimar la longitud de la flama, excepte en les simulacions de l'orifici de fuga més petit. Per a dolls de foc a gran escala, Phast va sobreestimar la radiació, mentre que HyRAM la va subestimar.

## Resumen (Spanish)

Las emisiones mundiales de gases de efecto invernadero han aumentado a niveles sin precedentes, provocando un fuerte enfoque en la descarbonización. El hidrógeno, especialmente cuando se produce de manera renovable, emerge como un vector de energía prometedor y libre de CO<sub>2</sub> para los sectores de la industria, el transporte y la energía. No obstante, la transición al hidrógeno implica desafíos técnicos significativos, particularmente en la producción continua y el almacenamiento seguro. Clasificado como una sustancia peligrosa según la Directiva SEVESO III, el hidrógeno plantea riesgos de accidentes graves, lo que requiere una rigurosa Evaluación Cuantitativa de Riesgos (QRA).

La estimación precisa de las consecuencias es crítica para una evaluación fiable de riesgos. Este trabajo realiza un análisis de referencia de las herramientas de software Phast, HyRAM y ALOHA para evaluar sus capacidades en la modelización de la dispersión y la ignición de hidrógeno gaseoso de fugas de tanques presurizados, centrándose en la precisión de sus resultados.

Para validar los resultados de las simulaciones se han utilizado datos experimentales de tres estudios, cubriendo presiones de 60 a 400 bares y diámetros de orificios de 0.5 mm a 52.5 mm. Se hicieron suposiciones para las variables desconocidas, incluyendo las condiciones meteorológicas, con temperaturas ambientales fijadas en 10°C para experimentos nocturnos y 20°C para experimentos diurnos, y la estabilidad atmosférica clasificada utilizando el método Pasquill.

ALOHA presenta limitaciones significativas ya que no pudo producir resultados para la mayoría de los estudios experimentales que involucraban chorros de hidrógeno a pequeña y mediana escala porque no proporciona resultados para distancias menores a 10 metros y solo simula dardos de fuego verticales.

La comparación de Phast y HyRAM ha mostrado que ambas herramientas generalmente subestiman las concentraciones de hidrógeno, con Phast funcionando ligeramente mejor que HyRAM, especialmente en concentraciones más altas. Ambas herramientas tienden a sobreestimar la longitud de la llama, excepto en las simulaciones del orificio de fuga más pequeño. Para dardos de fuego a gran escala, Phast sobreestimó la radiación, mientras que HyRAM la subestimó.



# Contents

<b>ABSTRACT (ENGLISH)</b>	<b>III</b>
<b>ABSTRACT (ITALIAN)</b>	<b>IV</b>
<b>RESUM (CATALAN)</b>	<b>V</b>
<b>RESUMEN (SPANISH)</b>	<b>VI</b>
<b>CONTENTS</b>	<b>VII</b>
<b>LIST OF FIGURES</b>	<b>IX</b>
<b>LIST OF TABLES</b>	<b>XII</b>
<b>1 INTRODUCTION &amp; OBJECTIVES</b>	<b>15</b>
<b>2 HYDROGEN: PROPERTIES, STORAGE AND SAFETY CONCERNS</b>	<b>17</b>
2.1 Physical and chemical properties	17
2.2 Hydrogen storage	17
2.2.1 Physical-based hydrogen storage	18
2.2.2 Material-based hydrogen storage	21
2.3 Hydrogen safety concerns	23
2.3.1 Material properties-related issues	24
2.3.2 Management-related issues	25
2.4 Hydrogen Incidents and Accidents Database (HIAD 2.1)	27
<b>3 RELEVANT ACCIDENTS INVOLVING HYDROGEN</b>	<b>31</b>
3.1 Hindenburg airship LZ-129 (1937)	31
3.2 Accident at acetylene hydrogenation section of Idemitsu Petrochemicals Co., Ltd. (1973)	33
3.3 The explosion at Laporte Industries Ltd. (1975)	33
3.4 Pressurized tank rupture in Heraeus Quartzglas company (1991)	34
3.5 Detonation in a refuelling station in Kjørbo, Norway (2019)	35
<b>4 CONSEQUENCE ANALYSIS AND SOFTWARE USED</b>	<b>37</b>
4.1 Phast – Process hazard analysis software tool	38
4.2 HyRAM+ – Hydrogen Plus Other Alternative Fuels Risk Assessment Model	39
4.3 ALOHA – Areal Locations of Hazardous Atmospheres	40
<b>5 METHODOLOGY OF A BENCHMARK ANALYSIS</b>	<b>43</b>
5.1 Ground truth data collection and definition of the benchmark exercises	44
5.2 Results collection and comparison	44

5.3	Details on the methodology used in this thesis work.....	45
<b>6</b>	<b>RESULTS</b> _____	<b>49</b>
6.1	Jet Dispersion .....	49
6.1.1	Experimental study.....	49
6.1.2	Modelling.....	51
6.1.3	Results of the simulations .....	52
6.1.4	Discussion .....	57
6.2	Jet Fire .....	60
6.2.1	Experimental study - Compressed hydrogen jet fire flame length .....	60
6.2.1.1	Modelling.....	62
6.2.1.2	Results of the simulations .....	64
6.2.1.3	Discussion .....	69
6.2.2	Experimental study – Large scale hydrogen jet fires .....	71
6.2.2.1	Modelling.....	72
6.2.2.2	Results of the simulations .....	75
6.2.2.3	Discussion .....	80
<b>7</b>	<b>CONCLUSION</b> _____	<b>83</b>
	<b>GLOSSARY</b> _____	<b>85</b>
	<b>REFERENCES</b> _____	<b>86</b>
	<b>ANNEX A: SUSTAINABILITY REPORT</b> _____	<b>91</b>
A.1	Sustainability matrix .....	91
A.1.1	Environmental sustainability .....	91
A.1.2	Economic sustainability .....	92
A.2	Ethical implications.....	92
A.3	Relationship with the Sustainable Development Goals.....	93
	<b>ANNEX B: INPUTS OF DISPERSION SIMULATIONS</b> _____	<b>95</b>
	<b>ANNEX C: INPUTS OF JET FIRE FLAME LENGTH SIMULATIONS</b> ____	<b>98</b>
	<b>ANNEX D: INPUTS OF JET FIRE RADIATION SIMULATIONS</b> _____	<b>102</b>
	<b>RINGRAZIAMENTI</b> _____	<b>105</b>

# List of Figures

Figure 1: Representation of type I, II, III and IV vessels (Barthelemy et al.,2017).	19
Figure 2: (a) 3800 m <sup>3</sup> LH <sub>2</sub> storage tank in NASA. (b) Conceptual diagram of vacuum thermal insulation structure for LH <sub>2</sub> storage tank (Yin et al., 2024).	20
Figure 3: LN <sub>2</sub> precooled Linde-Hampson Cycle (Yin & Ju, 2020).	21
Figure 4: Distribution of Incidents by Sector in HIAD 2.1 Database.	28
Figure 5: Temporal distribution and report quality classes of the accidents collected in HIAD 2.1.	29
Figure 6: Size comparison between Hindenburg LZ-129 and Boeing 747-400 (airship.net).	32
Figure 7: (a) start of the fire, (b) structure collapse (airship.net).	32
Figure 8: Corrosion in the electrolysis cell of Laport Industries Ltd (Great Britain. HM Factory Inspectorate.,1976).	34
Figure 9: The aftermath of the explosion at Heraeus Quartzglas (Markus Sommerfeld, 2021).	35
Figure 10: Plug assembly (Løkke, 2019).	35
Figure 11: Kjørbo incident consequences (Hansen, 2019).	36
Figure 12: Steps of a benchmark analysis.	43
Figure 13: Trend of pressure conditions and hole release diameter used in experimental studies (Carboni et al., 2022).	46
Figure 14: Experimental set up of the jet dispersion experiments (Han et al., 2014).	50
Figure 15: Visualization of hydrogen jets using alumina particles. Nozzle diameter is 0.7mm with varying pressure (Han et al., 2014).	50
Figure 16: Concentration (ppm) in function of downwind distance (m) for the simulated experiment 1.11, with simulation conditions S2.	53
Figure 17: Concentration (ppm) against distance downwind (m) at different times after the release for the simulated experiment 1.1, conditions S2. (a) 1 s, (b) 5 s.	54

Figure 18: Concentration (ppm) against distance downwind (m) at different times after the release for the simulated experiment 1.1, conditions S2. (a) 10 s, (b) after the end of the release (about 300 s).	55
Figure 19: View of the jet at 400 bar from a hole of 0.7 mm, experiment 1.11 (Han et al., 2014).	56
Figure 20: Side view of simulated experiment 1.11 with Phast.	56
Figure 21: Side view of simulated experiment 1.11 with HyRAM.	57
Figure 22: Comparison of Phast results for simulations S1, S2, S3 and S4 of experiment 1.1 (100 bar, 0.5 mm).	58
Figure 23: Comparison of Phast results for simulations S2, S5 and S6 of experiment 1.1 (100 bar, 0.5 mm).	58
Figure 24: Jet dispersion. Comparison between experimental results and simulation results.	59
Figure 25: Schematic representation of the experimental set up used in Carboni et al. experimental study (Carboni et al., 2022).	60
Figure 26: Thermocouple positioning (Carboni et al., 2022).	61
Figure 27: IR image obtained for experiment 2.7, with nozzle diameter of 3 mm and pressure equal to 340 bar (Carboni et al., 2022).	62
Figure 28: Miller model description of a horizontal jet fire (DNV Phast technical documentation).	63
Figure 29: Graph depicting radiation (kW/m <sup>2</sup> ) in function of distance (m) along the centreline of the jet for simulated experiment 2.13 obtained with Phast. Comparison between atmospheric stability class D (a) and B (b).	65
Figure 30: Graph depicting radiation ellipses of the jet for the simulated experiment 2.13 obtained with Phast. Comparison between atmospheric stability class D (top) and B (bottom).	66
Figure 31: Graph generated by Phast to compare the maximum concentration (ppm) in function of downwind distance (m) for the different atmospheric stability classes investigated for the simulated experiment 2.13.	67
Figure 32: HyRAM. Temperature plot of the simulated experiment 2.13.	68
Figure 33: HyRAM. Radiation contours for the simulated experiment 2.13.	68

Figure 34: Jet fire flame length. Comparison between experimental results and simulation results.	69
Figure 35: Schematic of the experimental set up used in “Large-Scale Hydrogen Jet Flame Radiant Fraction Measurements and Modeling” experimental study by Ekoto et al., 2012.	72
Figure 36: Graph generated by Phast representing the radiation ellipse and effect zone results for simulated experiment 3.1.	76
Figure 37: Graph generated by Phast representing the radiation ellipse and effect zone results for simulated experiment 3.2.	76
Figure 38: Graph generated by Phast representing the radiation (kW/m <sup>2</sup> ) in function of the downwind distance (m) for (a) simulated experiment 3.1 and (b) simulated experiment 3.2.	77
Figure 39: Temperature plots for (a) simulated experiment 3.1 and (b) simulated experiment 3.2 obtained with HyRAM.	78
Figure 40: Radiation ellipses for (a) simulated experiment 3.1 and (b) simulated experiment 3.2 obtained with HyRAM.	78
Figure 41: Radiation contours generated by ALOHA for simulated experiments (a) 3.1 and (b) 3.2.	79
Figure 42: Concentration contours generated by ALOHA for simulated experiments (a) 3.1 and (b) 3.2.	79
Figure 43: Jet fire radiation. Comparison between experimental results and simulation results.	81
Figure 44: Side view of the simulated experiment 3.2 one second after the start of the release generated by Phast. LFL and 0.5LFL contours.	82

# List of Tables

Table 1: Hydrogen properties (Cameo chemicals database, International Chemical and Safety Cards).	18
Table 2: Summary of the main H <sub>2</sub> storage methods.	22
Table 3: GHS hydrogen classification.	24
Table 4: Quality classes qualifying HIAD 2.1 events (Campari et al., 2023).	28
Table 5: Overview of pivotal hydrogen accidents.	31
Table 6: Overview of the used software.	38
Table 7: Pasquill classification of atmospheric stability class (Kahl & Chapman, 2018).	47
Table 8: Pressure (bar) and nozzle diameter (mm) conditions used in Han et al. experimental study.	51
Table 9: Wind speed and release elevation conditions tested in jet dispersion simulations.	52
Table 10: Nozzle diameters (mm) and pressure (bar) investigated and wind velocity (m/s) measured during Carboni et al. experimental study.	61
Table 11: Atmospheric stability classes investigated in Phast depending on the wind speed.	63
Table 12: Comparison of the flame lengths for the tests using a 5 mm diameter release nozzle.	70
Table 13: Experimental and ambient conditions reported in Ekoto et al. experimental study.	71
Table 14: Coordinates (x,y,z) used in HyRAM and Phast to identify the position of the radiometers for simulated experiment 3.1.	73
Table 15: Coordinates (x,y,z) used in HyRAM and Phast to identify the position of the radiometers for simulated experiment 3.2.	74
Table 16: Comparison of radiation ellipses dimensions for simulated experiments 3.1 and 3.2.	80
Table 17: Flame length comparison with experimental results.	81







# 1 Introduction & Objectives

Global greenhouse gases emissions are reaching record levels, driving increasing interest in achieving decarbonization, which involves reducing emissions through the adoption of alternative and renewable energy sources, the enhancement of resource efficiencies, the growth of alternative production processes and carbon sequestration.

Starting with the Paris Agreement of 2015, 194 states plus the European Union committed to a collective effort to reduce emissions and mitigate the impacts of climate change. The Paris Agreement marks the beginning of a shift towards achieving a net-zero emissions world. At the European level, the European Green Deal introduced in 2019 presented a roadmap to make the EU economy sustainable by addressing transportation, energy, and industrial sectors such as steel, cement, and chemicals. The principal aim to achieve carbon neutrality by 2050 is codified in the European Climate Law (European Commission, 2021), together with the interim target of a reduction of net greenhouse gas emissions by at least 55% compared to 1990 levels by 2030. The European Climate Law also encourages member states to establish National Energy and Climate Plans, outlining specific objectives to be achieved between 2021 and 2030. In this regard, Spain identifies renewable hydrogen as a way to decarbonize industrial processes and economic sectors where reducing carbon emissions is both pressing and challenging to accomplish (NECP Spain, 2020).

Hydrogen can be used as a chemical, a fuel or an energy carrier and storage, and has many possible applications across industry, transport and power sectors. The main applications of hydrogen include petroleum recovering and refining sector as well as ammonia and methanol production. In addition, when used as energy vector, it does not emit CO<sub>2</sub>, contributing to cleaner energy usage (European Commission, 2020).

Hydrogen widespread adoption is facilitated by existing infrastructure for production, storage, and delivery. Despite being the most abundant element on Earth, it is typically found in water or hydrocarbons, requiring energy for extraction and release. Global production, predominantly from methane steam reforming, currently amounts to around 56 billion kilograms annually (European Commission, 2020). However, there is potential for a renewable production pathway, employing solar-powered water electrolysis, renewable energy sources, biogas reforming or biomass conversion. Renewable hydrogen production and utilization are climate-neutral and emission-free, offering promising prospects for sustainable energy solutions.

One of the primary challenges associated with hydrogen is the safety of its installations, for both production and storage units, as well as its various applications, such as utilization as a vehicle

fuel. Hydrogen is categorized as a hazardous substance according to the SEVESO III Directive, potentially leading to major accidents.

Recently, computational fluid dynamics (CFD) has been increasingly applied in process safety and loss prevention. CFD performs three-dimensional computations involving fluid properties variation, turbulence modelling and chemical reactions, accurately representing the geometry of the flow field. Despite its high accuracy, CFD is computationally expensive, often taking hours for a single scenario and potentially months for multiple scenarios (Shen et al., 2020). In contrast, integral models are widely used for consequence analysis due to their simplicity and lower computational demands. These models rely on empirical formulas derived from experiments, providing conservative estimates.

The primary aim of this thesis is to conduct a benchmark analysis of some of existing software tools that implement integral models. The specific focus will be on accidental releases of hydrogen from storage units. This analysis will evaluate the features, capabilities and limitations of each software tool in modelling hydrogen-related accidents. By comparing simulation results with real data, the thesis will assess the accuracy and conservativeness of the estimates provided by each tool. This evaluation will determine which tool is most suitable for ensuring accurate and reliable risk assessments.

## 2 Hydrogen: properties, storage and safety concerns

### 2.1 Physical and chemical properties

Molecular hydrogen ( $H_2$ ), composed of two hydrogen atoms covalently bonded, is the lightest of all gases. The molecule has linear geometry, with a bond angle of approximately 180 degrees. Hydrogen atoms exist in three different isotopes. The most common isotope, known as protium (H), is the ordinary form of hydrogen. Another stable isotope is deuterium (D), which has a molecular mass of two and is present in natural hydrogen at a proportion of 0.015%. The third isotope of hydrogen is tritium, which is unstable and has an atomic weight of three.

Under standard conditions,  $H_2$  exists as a mixture of two types of molecules: ortho and para hydrogen, distinguished by the spin of their electrons and nuclei. At room temperature, normal hydrogen consists of 25% para-form and 75% ortho-form. However, as the temperature decreases, a new equilibrium is reached, with ortho molecules transitioning into para molecules through an exothermic conversion process (Züttel, 2004). Table 1, in the following page, presents key physical properties of this substance, including its molecular weight, boiling point and melting point.

### 2.2 Hydrogen storage

The challenges to overcome for hydrogen to gradually replace fossil fuels are mainly of a technical nature, involving its continuous production, safe and convenient storage. Hydrogen storage is required in a range of capacities and at various operating conditions to support customer's demand. Unlike fossil fuels, hydrogen has a low energy density, necessitating specific storage conditions to avoid extremely large storage vessels. High pressure, low temperature, or the use of carrying materials, in fact, are necessary to store a sufficient amount of  $H_2$ . Moreover, another critical consideration to choose the storage method is the reversibility of hydrogen uptake and release.

A first classification of storage methods refers to the final use of hydrogen, dividing them in storage for stationary applications and storage methods for mobile applications, designed to integrate hydrogen in vehicles. A second classification divides storage methods into two classes: physical storage technologies and material storage systems.

Table 1: Hydrogen properties (Cameo chemicals database, International Chemical and Safety Cards).

Property	Value	Units
Molecular Weight	2.016	g/mol
Boiling Point (at 1 atm)	-252.8	°C
Melting Point	-259	°C
Critical temperature	-240	°C
Critical pressure	12.8	atm
Vapour Pressure	165320	kPa at 25°C
Solubility in water	1.62	mg/l at 21°C
Relative vapour density (air = 1)	0.067	
Diffusion coefficient (gaseous H <sub>2</sub> )	0.61	cm <sup>2</sup> /s
Joule-Thompson inversion temperature	-71	°C
Auto-ignition Temperature	ICSC: 560 Cameo: 573.89 AIChE: 585	°C
Flammable Limits	4-75	%vol in air
Ignition energy	0.017	mJ
Heat of vaporization at -253°C	447	kJ/kg
Higher Heat of Combustion	141.88	MJ/kg
Lower Heat of Combustion	119.96	MJ/kg

### 2.2.1 Physical-based hydrogen storage

The physical-based H<sub>2</sub> storage methods include storing hydrogen as compressed gas, cryogenic liquid and cryo-compressed gas.

Compressed hydrogen storage is the most conventional method available. Depending on the vessel type, the operating pressure ranges between 20 and 80 MPa. Based on the material combination incorporated in their design, four different types of tanks (Figure 1) are used:

- Type I: These are fully metallic pressure vessels, representing the most conventional and least expensive solution. Made of aluminium or steel alloys, they can contain pressures up to 50 MPa (Moradi & Groth, 2019).
- Type II: Steel pressure vessel with a glass fiber composite overwrap. They offer the highest pressure tolerance due to the load sharing between the two materials.
- Type III: Composite material tanks of fiberglass or carbon fiber wrap with metal liner of aluminium. They can withstand pressures of about 45 MPa. While lighter than other types, they tend to be more expensive.
- Type IV: Fully composite tanks of carbon fiber or carbon glass with thermoplastic polymer liner like HDPE. With a pressure tolerance of up to 100MPa, they are mostly used for mobile applications due to their lightweight nature (Yadav et al., 2021).

Recently, the primary focus has been on developing composite pressure vessels (COPVs) operating at pressures between 35 MPa and 70 MPa (Barthelemy et al., 2017). Despite these advancements, composite pressure vessels still hold a relatively small market share compared to metallic pressure vessels due to their higher costs (Moradi & Groth, 2019). The choice of storage technology is influenced by the final application, necessitating a balance between technical performance and cost-effectiveness. For industrial applications, hydrogen is typically stored at 20-30 MPa in Type I metallic cylinders. In contrast, for onboard vehicle applications, Type III or Type IV COPVs made of carbon fiber composite with a working pressure of 70 MPa are used (Barthelemy et al., 2017).

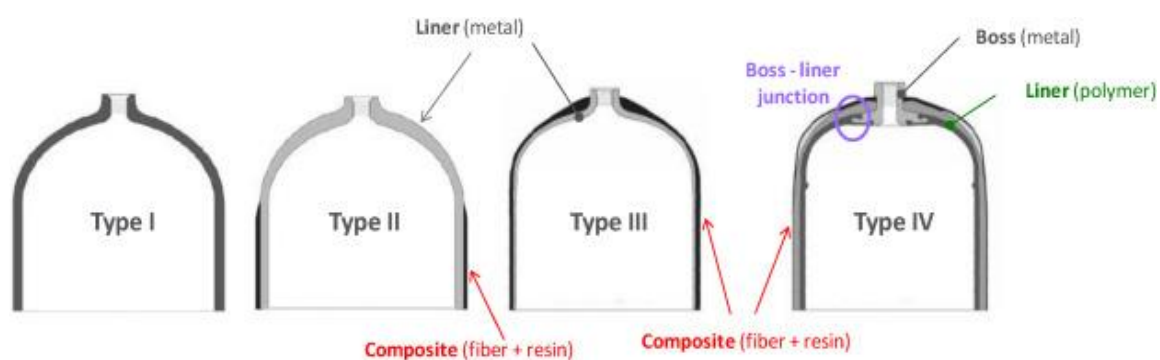


Figure 1: Representation of type I, II, III and IV vessels (Barthelemy et al.,2017).

Gaseous hydrogen storage tanks typically come equipped with pressure relief devices (PRDs) designed to release pressure to prevent rupture or burst failure. For composite vessels and any other materials sensitive to temperature increases, thermally activated pressure relief devices (TPRDs) are required.

When considerable hydrogen quantities need to be stored for extended periods, subterranean reservoirs or well-suited geological formations are used. These structures exhibit integrity even under elevated pressures so they are durable and leak resistant options. The primary method nowadays involves using the artificially built salt caverns, as salt is inert and it would not react with hydrogen. Typically, the volume of these caverns is approximately 700 000 m<sup>3</sup> with a maximum operating pressure of 20 MPa (Muntasir Shovon et al., 2024).

Liquid or cryogenic hydrogen (LH<sub>2</sub>) storage requires to reach H<sub>2</sub> boiling temperature, which is -253°C (20K), and it is carried out at atmospheric pressure. LH<sub>2</sub> storage tanks are equipped with an additional vacuum insulated layer and burst disks (Figure 2b). The challenges associated with liquid hydrogen storage include achieving an energy efficient liquefaction process and securing effective thermal insulation of the storage system in order to reduce the boil-off of hydrogen. This

phenomenon also depends on the vessel size. Theoretically, the optimal shape for the vessel is a sphere (Züttel, 2004), which features the lowest surface-to-volume ratio and because stress and strain are uniformly distributed. An example of this vessel is showed in Figure 2a.

This storage method is often used for medium to large scale storage and delivery like truck delivery and intercontinental hydrogen shipping. A cryogenic tanker can carry 5000 kg of hydrogen (Moradi & Groth, 2019), which corresponds to approximately 71 m<sup>3</sup> of liquid hydrogen at its boiling point. A disadvantage of this storage method is that at these low temperatures, materials tend to become brittle, thereby raising the risk of vessel failure.

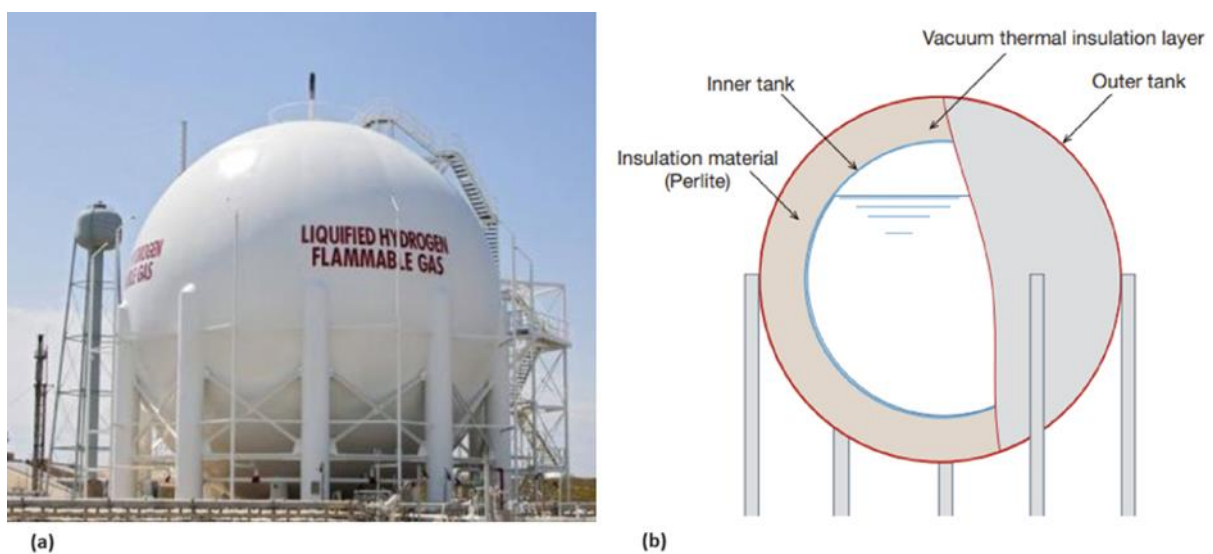


Figure 2: (a) 3800 m<sup>3</sup> LH<sub>2</sub> storage tank in NASA. (b) Conceptual diagram of vacuum thermal insulation structure for LH<sub>2</sub> storage tank (Yin et al., 2024).

The most employed liquefaction cycle is the Linde cycle (Figure 3). In this cycle, the gas undergoes compression initially, followed by cooling in a heat exchanger. Subsequently, it passes through a throttle valve, where it expands, generating some liquid. This liquid is separated from the gas, and the gas is then recirculated back to the heat exchanger and the beginning of the cycle. To achieve cooling when hydrogen expands, it must be below its Joule-Thompson inversion temperature of -72°C. Hence, prior to the Linde cycle, a pre-refrigeration step using nitrogen is employed.

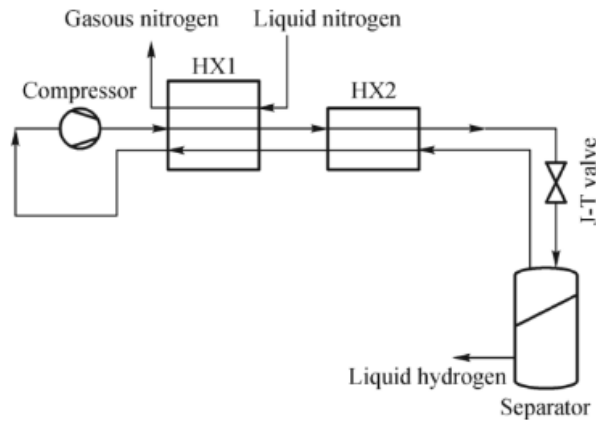


Figure 3: LN<sub>2</sub> precooled Linde-Hampson Cycle (Yin & Ju, 2020).

The latest physical-based method for H<sub>2</sub> storage involves storing it as cryo-compressed gas. In this approach, liquefaction does not occur as hydrogen is cooled to -233°C at a pressure of approximately 25-30 MPa (Muntasir Shovon et al., 2024). The storage vessel consists of a two-layer structure, with an outer vacuum enclosure providing protection against chemical and mechanical inclusions. Presently, this method is not fully developed at an industrial scale compared to the previously mentioned methods.

When modelling the behaviour of hydrogen gas, it is essential to notice that hydrogen is a real gas. However, under certain pressure and temperature conditions, it can approximate the behaviour of an ideal gas. Four assumptions define an ideal gas: negligible volume of gas particles, uniform particle size with no intermolecular attraction or repulsion, random particle movement and perfectly elastic collisions with no energy loss. Given hydrogen's small molecular size, it tends toward ideal behaviour at low pressures or high temperatures. Lower pressure reduces intermolecular forces, while higher temperatures increase molecular movement, thereby decreasing intermolecular interactions. Particularly, a real gas can be accurately described by the ideal gas law at pressures up to 100 bar at normal ambient temperature (“Hydrogen Properties,” 2001). However, since hydrogen is stored as compressed gas at pressures exceeding 100 bar, the ideal gas law is not suitable for accurately describing the gas under these storage conditions.

### 2.2.2 Material-based hydrogen storage

Material-based hydrogen storage can be categorized into two sub-groups: chemical sorption and physical sorption.

In chemical sorption, hydrogen molecules are dissociated into atoms, which are then incorporated into the chemical structure of the solid material. An example of this storage method are metal hydrides, also known as interstitial hydrides, because hydrogen atoms occupy the interstitial sites

within the lattice structure. The formation of metal hydrides is an exothermic process, releasing heat. Therefore, the same amount of heat is required to desorb the hydrogen (endothermic reaction). If desorption occurs above room temperature, the necessary must be provided from an external source. There is a rising interest in transitional metal hydrides due to their high effectiveness in safely and compactly storing significant quantities of hydrogen, as well as their capability to facilitate the reverse process under ambient temperature and pressure.

Among the chemical sorption methods, the utilization of Liquid Organic Hydrogen Carriers (LOHCs) stands out as a promising option. In this system, hydrogen forms chemical bonds with hydrogen-lean molecules, and it can subsequently be released through catalytic dehydrogenation. The liquid carrier remains intact throughout this process and can be reused after dehydrogenation. Additionally, LOHCs are non-corrosive and non-toxic, and they require low storage pressures.

Physical sorption methods rely on materials such as Metal Organic Frameworks (MOFs) or porous carbon materials. In physisorption, gas molecules form weak interactions (Van der Waals forces) with the surface of the solid. The amount of hydrogen adsorbed depends on the characteristics of the solid used as the adsorbent. These materials have the potential to yield high-capacity storage units, with additional benefits including low operating pressures, relatively inexpensive materials, and simple storage system designs. However, physical sorption technologies are not widely adopted as trials have mainly been conducted on a small scale, and the performance criteria are not yet satisfactory compared to other storage methods.

Table 2: Summary of the main H<sub>2</sub> storage methods.

	<b>Storage method</b>	<b>Physical state</b>	<b>Application</b>
<b>Physical based</b>	Compressed gas	Gas	Refuelling stations, vehicle fuel, industrial processes
	Cryo-compressed gas	Gas	Not fully developed at industrial scale
	Cryogenic liquid	Liquid	Truck delivery, intercontinental shipping, aerospace field
<b>Material based</b>	Metal hydrides	Solid	No widespread application
	Chemical sorption in LOHCs	Liquid	No widespread application
	Physisorption in MOFs	Solid	No widespread application



## 2.3 Hydrogen safety concerns


Understanding the safety considerations surrounding hydrogen is crucial for ensuring its reliable, safe, and efficient utilization. It is a colourless, odourless, tasteless molecule, so it is not detectable through human senses. Table 3 presents the Globally Harmonized System (GHS) classification of hydrogen, outlining the corresponding pictograms, hazard statements, and precautionary statements.

According to the International Chemical Safety Card (ICSC) and the Cameo Chemicals datasheet, hydrogen is not considered toxic. However, in high concentrations, it can cause asphyxiation by displacing oxygen in a confined space. The first physical symptoms occur when oxygen concentration reaches the value of 19.5%vol in the atmosphere, while for levels below 6% death occurs (OSHA standard). If stored as a cryogenic liquid, hydrogen poses the risk of frostbite or severe burns if it comes into contact with the skin in the event of a leak.

Hydrogen is classified as an extremely flammable gas and is also categorized as a compressed gas due to its storage under pressure. It exhibits a wide flammability range when mixed with air (4-75% by volume), a low minimum ignition energy (0.017mJ) and a high heat of combustion (141.6 MJ/kg). Due to these characteristics, the ignition can be initiated by several sources including sparks from electrical equipment, electrostatic discharges, pre-existing flames, mechanical friction and impacts (Yang et al., 2021). Fires involving pure hydrogen in air typically produce pale blue flames that are nearly invisible to the naked eye during daylight. These flames emit minimal radiant heat and do not generate smoke.

Safety concerns surrounding hydrogen are not only related to its chemical properties; they also involve how it interacts with various materials and the potential risks during routine handling and operations involving hydrogen. These concerns can be broadly categorized into two main areas: material properties-related issues and management-related issues (Moradi & Groth, 2019).

Table 3: GHS hydrogen classification.

UN/NA number	1049
Pictograms	
Hazard Statements	H220: Extremely flammable gas. H280: Contains gas under pressure; may explode if heated. H281: Contains refrigerated gas; may cause cryogenic burns or injury.
Precautionary Statements	P203: Obtain, read and follow all safety instructions before use. P210: Keep away from heat, hot surface, sparks, open flames and other ignition sources. P222: Do not allow contact with air. P280: Wear protective gloves/ protective clothing/ eye protection/ face protection/ hearing protection/... P282: Wear cold insulating gloves and either face shield or eye protection. P336+P317: Immediately thaw frosted parts with lukewarm water. Do not rub the affected area. Get medical help. P377: Leaking gas fire: Do not extinguish unless the leak can be stopped safely. P381: In case of leakage, eliminate all ignition sources. P403: Store in a well-ventilated place. P410+P403: Protect from sunlight. Store in a well-ventilated place.

### 2.3.1 Material properties-related issues

Material properties-related issues pertain to how hydrogen interacts with different substances it comes into contact with, such as metals or polymers, and how these interactions might lead to safety hazards.

The primary concern arises from the transition of materials from a ductile to a brittle state. This transition can occur in different scenarios, such as compressed hydrogen storage, where it is associated with the phenomenon known as hydrogen embrittlement (HE), or in cryogenic liquid hydrogen storage, where materials are exposed to extremely low temperatures. Hydrogen embrittlement (HE) consists in the degradation of the mechanical properties of metals, leading to potential failures and leaks. Essentially, this embrittlement decreases the material's ability to withstand stress or pressure, making it susceptible to catastrophic failure at levels below its

desirable strength (Dwivedi & Vishwakarma, 2018). Three primary factors contribute to hydrogen embrittlement (HE):

- Material susceptibility: this factor relies on various aspects, including the mechanical properties of the material, its surface conditions, the presence of coatings, and its overall microstructure.
- Environmental conditions: pressure, temperature and exposure time. Additionally, the concentration or quantity of hydrogen to which the material is exposed is a critical determinant: increasing H<sub>2</sub> purity, steel's vulnerability to embrittlement increases (Abohamzeh et al.,2021).
- Stress conditions: they include residual stress within the material, the rate at which strain is applied, and any heat treatments the material has undergone. These stress-related factors can significantly influence the tendency of a material to undergo embrittlement when exposed to hydrogen.

Moreover, the mechanical properties of a material can fluctuate with variations in temperature. Specifically, many materials undergo a transition from a ductile to a brittle state at low temperatures. This transition poses a significant risk, especially in applications involving cryogenic liquid hydrogen, as it can potentially lead to failures in storage tanks or pipelines.

Hydrogen molecules are small, so they can migrate through materials. Migration refers to the rate at which hydrogen molecules pass through the walls or gaps of tanks, interface materials, or piping. This phenomenon becomes more pronounced as material aging, temperature, and operational pressure increase. Safety concerns related to hydrogen losses resulting from permeation are generally minimal for metal-based vessels due to their low permeation rates. However, this becomes a more significant issue for polymer-based vessels, particularly those classified as type IV, which exhibit higher rates of hydrogen permeation (Bengaouer et al., 2009).

When using polymeric or resin vessels, it is also crucial to assess their resistance to high temperatures. Generally, they exhibit lower thermal resistance compared to metallic materials. Consequently, it is essential to analyse how these composites behave in fire scenarios and to establish effective fire protection measures.

### **2.3.2 Management-related issues**

Management-related issues typically arise within routine operations and manifest as instances of hydrogen loss of containment (LOC). A LOC is an unexpected and uncontrolled discharge of material from its primary confinement.

During a LOC event involving compressed hydrogen, a mixture of H<sub>2</sub> and air is formed, often flammable. Immediate ignition of such a leak results in a jet fire - a turbulent diffusion flame

powered by the high momentum of released hydrogen due to pressure differentials between the vessel and the atmosphere. Conversely, delayed ignition allows hydrogen to mix thoroughly with air, creating a flammable atmosphere. In such cases, there is a risk of a flash fire or a vapor cloud explosion (VCE). It is important to note that hydrogen, due to its low molecular weight, exhibits high volatility, making it prone to easy dispersion. Consequently, a confined environment or a high degree of congestion is necessary to trigger an explosion.

When hydrogen leaks into the atmosphere, it expands. If the gas temperature is below its Joule-Thompson inversion temperature, the expansion leads to cooling, whereas above it, the gas temperature rises due to expansion. For example, air's inversion temperature is approximately 385°C, causing it to cool upon expansion at room temperature. In contrast, hydrogen's inversion temperature is around -71°C (202K). Consequently, when compressed hydrogen is released into the atmosphere, it heats up as it expands, potentially reaching the autoignition temperature.

In addition, hydrogen flames are typically invisible to the naked eye, posing risks of equipment, structural, and human damage due to thermal radiation and direct flame exposure, which could trigger cascading effects.

Both cryogenic liquid and pressurized gaseous vessels face the risk of mechanical explosion when exposed to thermal radiation or high temperatures. Following such an explosion, the contents of the vessel typically ignite and burn. These situations are identified as the outcomes of a domino effect, where a primary initiating accident sets off a chain of events that amplify the consequences of the initial one.

During a release of liquid hydrogen, a two-phase flow dispersion occurs, followed by the vaporization of hydrogen and the formation of a flammable cloud. If the vaporization at the leak point is instantaneous and ignition follows, a flash fire may start inside the pipelines or the vessel. Alternatively, in the case of partial vaporization, the escaping hydrogen absorbs heat from the atmosphere, forming a boiling film while causing freezing of the surrounding solid ground.

Another potential hazard associated with LH<sub>2</sub> storage is a boiling liquid expanding vapor explosion (BLEVE). This occurs when external heat exposure causes a rise in temperature and pressure inside the vessel, leading to its rupture. In the moment of rupture, the liquid's temperature exceeds its boiling point at atmospheric pressure, causing instantaneous vaporization of the entire liquid content. The consequences of such an event include the formation of pressure waves, fragment projection, and the creation of a flammable cloud. In the case of hydrogen, ignition of this cloud is probable, resulting in a fireball.

## 2.4 Hydrogen Incidents and Accidents Database (HIAD 2.1)

Reducing the likelihood of undesired events such as loss of containment (LOC) and subsequent accidents can be achieved through preventive measures, such as regular inspection and maintenance activities. A crucial strategy for enhancing industrial safety involves drawing lessons from past accidents. Specifically in the context of hydrogen, safety reporting systems play a vital role by gathering and organizing information on hydrogen-related incidents and failures.

The Joint Research Centre (JRC) of the European Commission developed the Hydrogen Accidents and Incidents Database HIAD in the frame of the European Network of Excellence HySafe in 2006 (Campari et al., 2023) and upgraded to version 2.1 in 2023. This database collects information from the French database ARIA, the European database eMARS, the British database IChemE, the Japanese database RISCAD, various American databases, scientific articles, newspapers and industrial reports.

Within the database spanning from 1937 to 2023, 752 accidents are recorded, with a notable concentration observed between 1990 and 2019. Among the various sectors, the chemical and petrochemical industry stands out with the largest share of incidents at 54% (Figure 4). Following there are hydrogen transport and distribution at 13% and hydrogen power plants at 8%. Hydrogen production represents 2% of the accidents, while the remaining sectors contribute only minor shares.

Each accident in the database is assigned a quality rating ranging from 2 to 5, denoting the level of detail and comprehensiveness of available information, as outlined in Table 4. The quality labels are highlighted alongside the temporal distribution of the events in Figure 5, providing insight into the reliability and depth of data for each recorded accident.

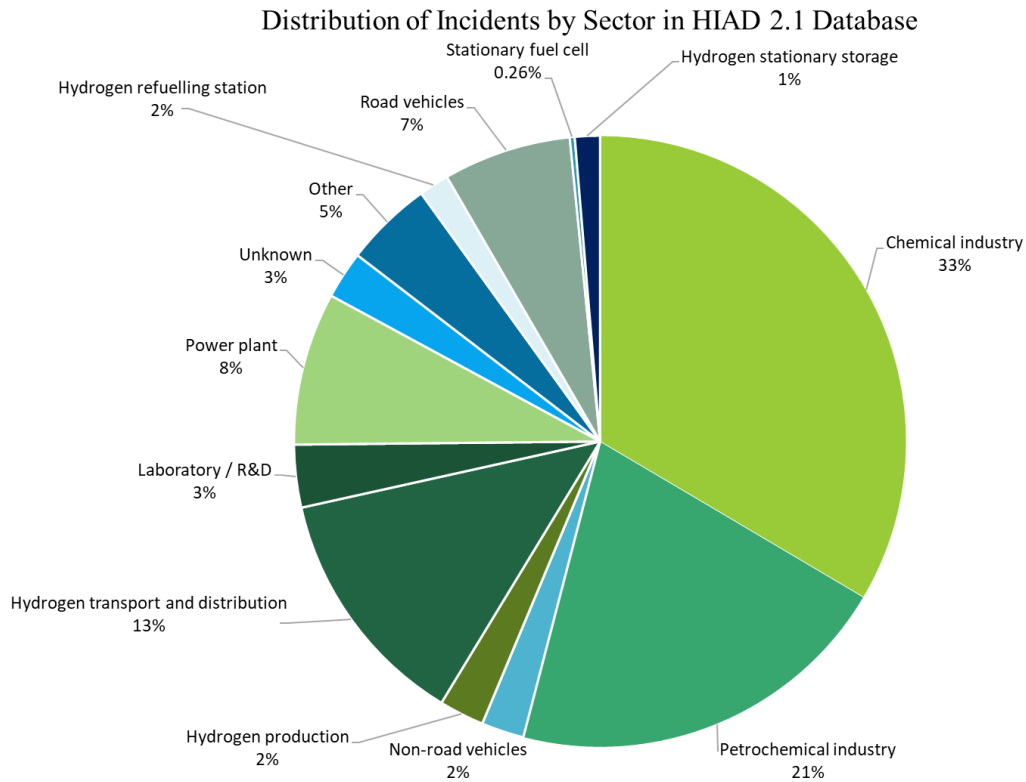


Figure 4: Distribution of Incidents by Sector in HIAD 2.1 Database.

Table 4: Quality classes qualifying HIAD 2.1 events (Campari et al., 2023).

<b>2: Low Quality</b>	Most quantitative descriptors are missing, the event narrative is enough to understand qualitatively the course of the event.
<b>3: Good Quality</b>	Most key descriptors are in place but still some important descriptors missing, impeding general return of experience.
<b>4: High Quality</b>	Root cause analysis and lesson learned are available, traceable and good sources, etc.
<b>5: Very High Quality</b>	Most of the key descriptors are in place, plus a detailed root cause analysis, return of experience useable for general recommendations, traceable and good sources with good technical details and general conclusions.

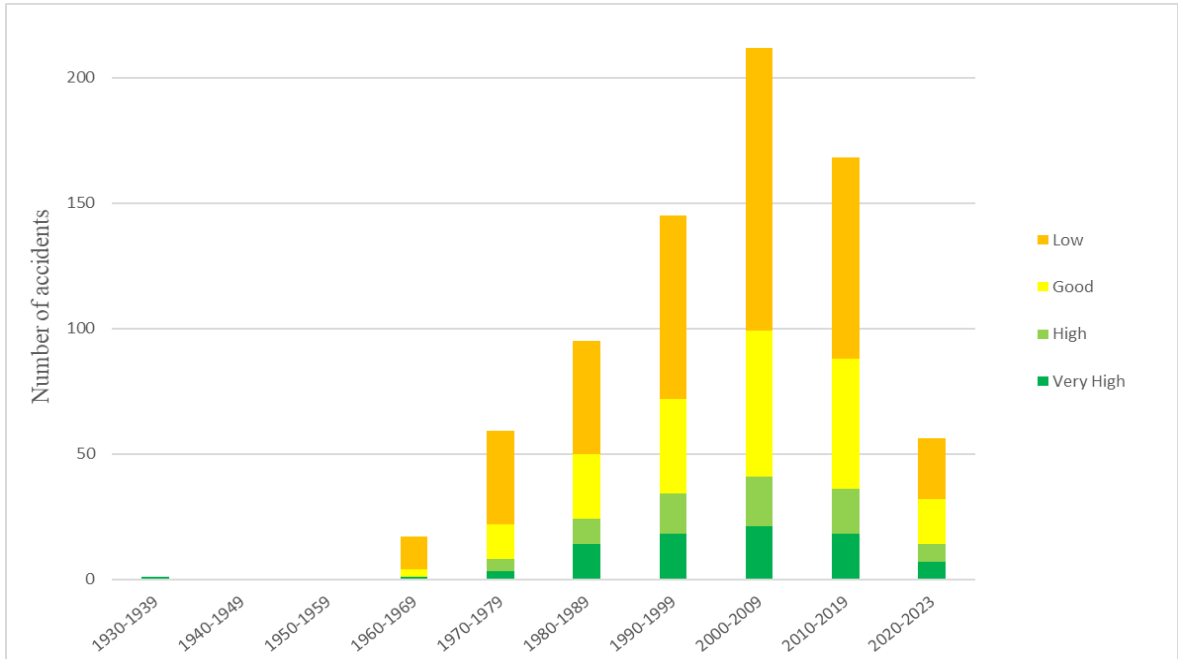


Figure 5: Temporal distribution and report quality classes of the accidents collected in HIAD 2.1.





### 3 Relevant accidents involving hydrogen

The purpose of this chapter is to provide a brief description of various pivotal accidents that historically played a role in increasing awareness concerning the handling, production and use of hydrogen. A summarized overview of these incidents is outlined in Table 5.

Table 5: Overview of pivotal hydrogen accidents.

	Year	Quantity of Hydrogen involved	Causes	Consequences	Deaths
<b>Hindenburg airship LZ-129</b>	1937	200000 m <sup>3</sup>	Leak	Fire	35
<b>Acetylene hydrogenation section of Idemitsu Petrochemicals Co., Ltd.</b>	1973	Not provided	Runaway reaction	Explosion and fire	1
<b>Laporte Industries Ltd electrolyser</b>	1975	Equivalent to 22 kg TNT	Corrosion	Explosion	1
<b>Pressurized tank in Heraeus Quartzglas</b>	1991	370 kg at 44.1 bar	Corrosion/Fatigue	Explosion	0
<b>Kjørbo</b>	2019	Between 1.5 and 3 kg at 900 bar	Management factors	Explosion	0

#### 3.1 Hindenburg airship LZ-129 (1937)

The most well known accident event related to hydrogen the Hindenburg disaster. The Hindenburg, airship LZ-129, was the largest airship ever built, 245m long with a diameter of 41.2 m (Figure 6). It held about 200 000 m<sup>3</sup> of gas inside sixteen compartments made of two layers of cotton fabric and an impermeable layer between the two. It was originally designed for helium usage, but Germany at that time was unable to purchase helium from the US, the Zeppelin

Transport Company of Germany was forced to use hydrogen to fill the dirigible (Cadwallader & Herring, 1999). Hydrogen gas pressure inside each compartment was between 124 and 249 Pa above atmospheric pressure and it made the aircraft lighter than air.



Figure 6: Size comparison between Hindenburg LZ-129 and Boeing 747-400 (airship.net).

On May 6, 1937, the Hindenburg airship was on its journey from Frankfurt, Germany, to Lakehurst, New Jersey. During the trip, the airship encountered adverse weather conditions, with wind and rain slowing its progress. At 6:00 pm, the Hindenburg approached the landing field and began the docking procedure. During this process, hydrogen was vented from the gas cells to maintain the airship's stability, while water ballast was dropped to balance it.

However, as the airship approached the mooring mast, a small flame appeared near the rear (Figure 7, a) and quickly escalated into a massive fire. The fire spread rapidly along the airship, causing it to collapse within seconds (Figure 7, b). Subsequent investigations indicated that the fire had originated near gas cells 4 and 5 and then spread along the rear of the airship. Possible gas combustion ignitors were discussed, including the pressure sensor, outgoing radio transmissions, mechanical friction, chemical reactions, electrical energy, but the most probable cause seemed to be electrostatic energy. Despite the severity of the incident, the mooring mast remained intact, suggesting that the event was primarily a fire rather than an explosion.

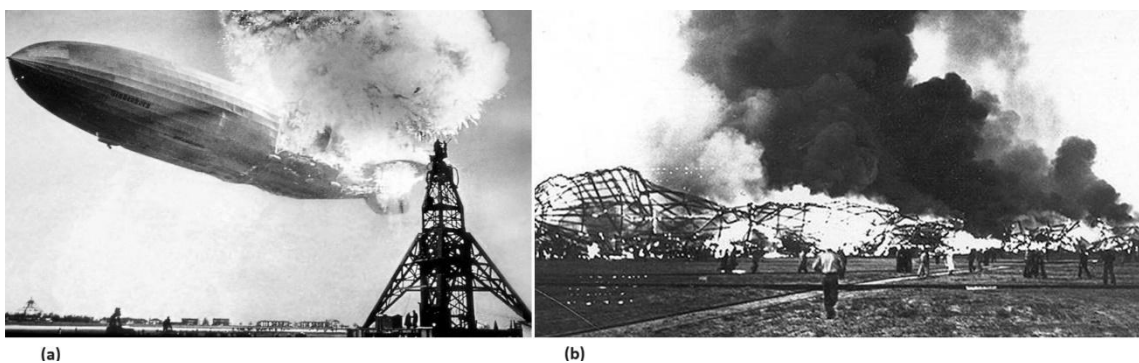


Figure 7: (a) start of the fire, (b) structure collapse (airship.net).

### **3.2 Accident at acetylene hydrogenation section of Idemitsu Petrochemicals Co., Ltd. (1973)**

On July 7<sup>th</sup>, 1973, an explosion and subsequent fire occurred in the acetylene hydrogenation section of the Tokuyama factory, part of the ethylene plant owned by Idemitsu Petrochemicals Co., Ltd. In Japan. The accident was triggered by an emergency shutdown procedure initiated due to the closure of an instrument air valve, which led to the failure of all associated instruments. As a result, the flare stack, designed to burn off excess gas, ignited a sizable flame.

During the restart process, errors in hydrogen feed control led to repeated starts and stops of hydrogen supply. This resulted in the excessive injection of hydrogen, causing nearly complete hydrogenation of the ethylene in the reactor. Furthermore, the presence of catalysts favoured the exothermic decomposition reaction of ethylene, leading to a rapid rise in temperature inside the reactor. Eventually, the intense heat caused the outlet piping to crack, resulting in the leakage and subsequent ignition of ethylene and hydrogen.

The sequence of events culminated in an explosion followed by a fireball spanning approximately 60 meters in diameter, lasting for about 5 seconds (Okuyama et al., 1973). The intense heat from the fire destroyed a considerable amount of equipment, including several distillation columns and heat exchangers. The incident resulted in the loss of one life.

### **3.3 The explosion at Laporte Industries Ltd. (1975)**

The facility conducted various chemical and pharmaceutical processes involving hydrogen. The explosion occurred within the Lurgi Electrolytor process plant, where hydrogen was generated through the electrolysis of potassium hydroxide solution. Oxygen, a byproduct of the process, was also produced and discharged as waste.

The explosion likely originated in the oxygen separation drum, which had been contaminated with leaked hydrogen. The ingress of hydrogen into the oxygen drum was attributed to corrosion/erosion in the electrolysis cells, as indicated in Figure 8. The deterioration of the cells likely began days before the accident. Although there was a system in place for monitoring the purity of the hydrogen and oxygen streams through hourly gas analyses conducted by process operators, evidence suggested that these analyses were not consistently performed. Instead, assumed values were sometimes recorded in the process record.

It was estimated that, on the basis of the damages, the oxygen drum exploded contained a mixture of 13.5% hydrogen and 86.5% oxygen and the explosion produced a shock wave equivalent to 22

kg of TNT (Great Britain. HM Factory Inspectorate., 1976). Despite the potential for significant damage in the neighbouring area due to the described explosion, no such damage occurred. This can be attributed to the construction of the building housing the electrolysis plant, which was designed to minimize the impact of any explosion by directing the blast upward.

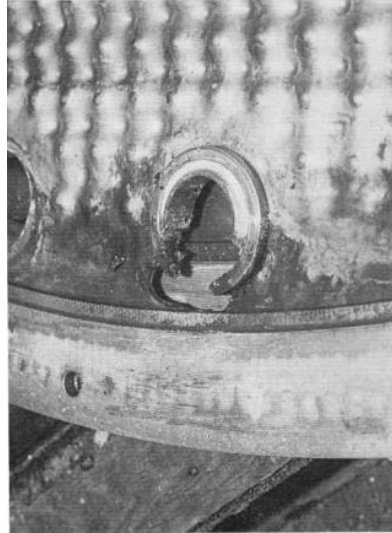


Figure 8: Corrosion in the electrolysis cell of Laport Industries Ltd (Great Britain. HM Factory Inspectorate.,1976).

### **3.4 Pressurized tank rupture in Heraeus Quartzglas company (1991)**

In 1991, at Hanau, Germany, an incident occurred at a facility manufacturing optical fibers, involving the explosion of a 100 m<sup>3</sup> tank containing 370 kg of hydrogen pressurized at approximately 44.1bar. Typically, the vessel maintained this operational pressure, undergoing refill cycles multiple times per week whenever pressure levels fell below 15 bar. The last refill occurred less than two hours before the explosion and this frequent filling of the repository accelerated the weakening process of the tank (ARIA database, event number 2903).

The rupture resulted from a semi-lenticular fatigue crack, measuring 760 mm in length and 20 mm in depth, within a wall thickness of 22 mm. The presence of hydrogen gas accelerated the growth of the crack, estimated to be six to seven times faster compared to other gases (E. Behrend & Dr. U. Schmidtchen, 1995). Subsequent investigations revealed that the tank had been modified to be positioned vertically, also leading to increased tension on the tank welds (Cadwallader & Herring, 1999).

The resulting pressure wave caused damage to buildings within a radius up to 1000 m, with debris from the tank found several hundred meters away (Figure 9). Authorities decided to set a safety perimeter of 500 m, stopping road and rail traffic and evacuating the population.



Figure 9: The aftermath of the explosion at Heraeus Quartzglas (Markus Sommerfeld, 2021).

### 3.5 Detonation in a refuelling station in Kjørbo, Norway (2019)

On June 10, 2019, a detonation occurred in the refuelling station of Kjørbo, Norway, following a major leak estimated to be between 1.5 and 3 kg of hydrogen within three seconds from a high-pressure storage (900 bar). The event occurred shortly after a refuelling, as the compressor started refilling the high-pressure tank. The initial condition was that the green bolts were properly torqued while the blue bolts were not. This condition led to the failure of the red seal, causing a small leak in the red sealing area which began to deteriorate. The leak exceeded the capacity of the leak bore, resulting in a pressure increase inside the blue sealing area. The insufficient pre-tension of the bolts then lifted the plug, causing an immediate failure of the blue seals (Løkke, 2019), as shown in Figure 10. The accident did not result in any fatalities, but the estimated material damage amounted to one million euros. Some parts of the fence that absorbed the explosion were projected approximately 15-20 meters away (Figure 11). Damage to surrounding buildings up to 65 meters away suggests the occurrence of a detonation.

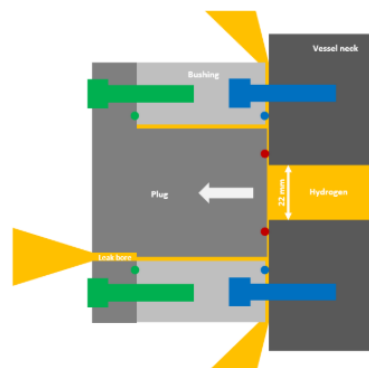


Figure 10: Plug assembly (Løkke, 2019).



Figure 11: Kjørbo incident consequences (Hansen, 2019).

## 4 Consequence analysis and software used

The incidents previously described emphasize the immediate need to address hydrogen system safety in order to prevent further occurrences that could permanently damage public perception of hydrogen. A Quantitative Risk Assessment (QRA) is crucial for identifying hazards and developing strategies to reduce risk in hydrogen infrastructure. It is a formal and systematic tool used to quantify the overall risk of a process or system and identify specific factors contributing to that risk (West et al., 2022). QRA is dependent on the determination of a probability of failure combined with the consequence of failure.




Consequence analysis focuses on evaluating the potential impacts of accidents on both human health and the environment. In consequence analysis, each failure scenario is examined individually. This involves assessing the dispersion resulting from accidental releases, which can cause hazardous events such as jet fires or explosions, generating heat radiation and overpressures. Many of the assumptions in QRA are contained within the consequence analysis (Marx et al., 2001). The intent of the simplification is to represent a group of conditions that result in the most severe consequences. The analysis is biased toward over-predicting the risk. It is always preferable to overpredict risks rather than underpredict them or introduce so many assumptions that the accuracy of risk assessment becomes uncertain (Marx et al., 2001).

Recently, computational fluid dynamics (CFD) has been increasingly applied in process safety and loss prevention (Shen et al., 2020). CFD codes perform three-dimensional computations of fluid properties variation, turbulence modelling, and chemical reactions, while also accurately representing the geometry of the flow field. The geometry is divided into volumetric cells, and a set of partial differential equations is solved iteratively for each cell to calculate changes at every time step. This makes accurate simulations using CFD computationally very costly, particularly when high levels of accuracy are required (Rum et al., 2018). Consequently, using CFD for consequence modelling can take hours for a single run, and running multiple scenarios can extend this timeframe to months (Shen et al., 2020).

In contrast, integral models are widely used for consequence analysis due to their simplicity and lower computational demands. These models rely on empirical formulas derived from various experiments, making them quick and easy to use (Fiorucci et al., n.d.). They provide conservative estimates because they do not account for the specific geometry of a given scenario. This conservative nature means they tend to overestimate the consequences, ensuring a margin of safety (Shen et al., 2020).

Various software tools are available for conducting consequence analysis. Each of these tools is based on different models to simulate the release, dispersion, radiation, and overpressure resulting from a loss of containment event involving a particular substance at specific pressure and temperature conditions. These calculations also take into account environmental factors such as wind speed, atmospheric stability class and ambient temperature. An error in consequence estimation is directly associated to an error on the estimated risk (Vianello et al., 2014). This emphasizes the necessity of comparing existing software tools to determine their respective strengths and limitations. In this thesis work, a comparison of the software listed in Table 6, analysing hydrogen storage systems, is carried out.

Table 6: Overview of the used software.

	Name	Version	Availability
	Phast	9.0	No open source
	HyRAM+	5.1.1	Open source
	ALOHA	5.4.7	Open source

#### 4.1 Phast – Process hazard analysis software tool

Phast (Process Hazard Analysis Software Tool) is a proprietary consequence analysis tool developed by the Norwegian company DNV. It offers capabilities for modelling various loss of containment scenarios, including discharge, dispersion, fires, explosions, and toxic effects. Phast delivers key results through intuitive 2D graphs, immersive 3D views and comprehensive reports available in both Word and Excel formats (DNV, 2024).

The software relies on a comprehensive database of substances and enables users to create custom mixtures. Utilizing the Multi-Component modelling method, the software conducts rigorous thermodynamic calculations to determine mixture properties accurately. Users can specify various types of equipment, including pressure vessels, atmospheric storage tanks, long pipelines, and warehouses. For each equipment type users can define initiating events such as catastrophic ruptures, leaks, and line ruptures. Upon creating loss of containment scenarios, Phast automatically



assesses the type and magnitude of consequence effects. It performs calculations for discharge, pool vaporization, and dispersion, considering potential outcomes like jet fires, pool fires, flash fires, fireballs, and explosions. The software also supports a range of standalone models, which are used when the user has knowledge of the source term. In such cases, discharge and dispersion calculations are not performed. One of the main limitations is that, when simulating a catastrophic tank rupture, all energy from the rupture is converted into overpressure, without accounting for the kinetic energy of the fragments, leading to an overestimation of the overpressure.

Furthermore, Phast includes a model for simulating fires in warehouses, focusing on the effects of the fire as a toxic plume containing a mixture of toxic combustion products like HCl, HBr, HF, NO<sub>2</sub>, and SO<sub>2</sub>. It ignores non-toxic products such as water, carbon dioxide, and carbon monoxide. Additionally, the model does not consider the potential release of excess air and nitrogen into the atmosphere along with the toxic combustion products, which affects the calculation of the toxic dose.

The software workspace provides predefined parameters and weather conditions, but users have the flexibility to customize model parameters according to their requirements. Additionally, users can define new weather conditions by specifying atmospheric stability class and wind velocity. However, Phast has constraints on simulating wind velocity. The software issues a warning for wind velocities below 1 m/s and does not allow simulations for wind speeds below 0.1 m/s.

Phast 9.0 includes a CFD extension for conducting computational fluid dynamics simulations for dispersion, jet fires, and pool fires. This extension allows users to assess the influence of three-dimensional surroundings, such as firewalls and other obstacles, while evaluating the effects of various wind speeds and directions. The resulting outputs include flame shapes, temperature distributions, and radiation levels, which are depicted as isosurfaces and isocontours in a three-dimensional viewer. However, the CFD extension has limitations. Being a simplified version, many parameters are automatically set. Moreover, detailed technical documentation is lacking and the few examples provided within the software indicate that the calculations can be time-consuming.

## **4.2 HyRAM+ – Hydrogen Plus Other Alternative Fuels Risk Assessment Model**

Hydrogen Plus Other Alternative Fuels Risk Assessment Models (HyRAM+) is an open-source software toolkit developed by Sandia National Laboratories. It is used for evaluating the safety of infrastructure related to the use, delivery, and storage of hydrogen, as well as other alternative fuels

such as methane and propane. The software allows to quantify risk of accident scenarios, predict physical effects and characterize the impact of hydrogen hazards.

The software toolkit offers two user modes: "QRA mode," which integrates a documented Quantitative Risk Assessment (QRA) approach with consequence models comprising physics models and probit functions and "Physics mode," allowing for the independent implementation of hydrogen behaviour models for releases, flames, and overpressures (Groth & Hecht, 2017).

In the Physics mode HyRAM can evaluate concentration profiles for unignited jet/plumes, jet flames characteristics, overpressure from the delayed ignition of a plume and time histories of concentration, flammable mass and overpressure due to accumulation and delayed ignition in an enclosure (Ehrhart et al., 2023). This mode also includes four other tabs where a certain parameter is calculated in function of specific provided inputs:

- In the temperature, pressure and density tab, the user enters two known quantities to determine the third one.
- In the tank mass parameter tab three inputs among the temperature, pressure, volume and mass must be provided in order to calculate the fourth.
- The mass flowrate tab is used to determine mass flow rates for either a steady release or a blowdown type release. The required inputs are the temperature, pressure inside the tank and ambient pressure, volume of the tank, orifice diameter and discharge coefficient.
- The TNT mass equivalence tab instead evaluates the TNT mass corresponding to the energy released during the explosion of a certain mass of hydrogen (or alternative fuel).

HyRAM allows users to perform calculations for either a single component or a user-defined mixture of available components within the program. In addition to hydrogen, only a limited database of substances is implemented. This database contains hydrocarbons with up to six carbon atoms, carbon dioxide and nitrogen.

HyRAM has some notable limitations. It does not account for the effects of wind and weather conditions, meaning users cannot specify wind velocity or atmospheric stability class. Additionally, it is not possible to specify the elevation of a release, which prevents the software from considering potential interactions with the ground.

### **4.3 ALOHA – Areal Locations of Hazardous Atmospheres**

ALOHA (Areal Locations of Hazardous Atmospheres) is an open-source tool part of the CAMEO software suit (Computer-Aided Management of Emergency Operations), developed by EPA (Environmental Protection Agency) from the United States and the NOAA (National Oceanic and

Atmospheric Administration). It is a tool widely used for risk analysis worldwide to model many release scenarios like toxic gas clouds, BLEVEs, jet fires, vapour cloud explosions and pool fires. ALOHA evaluates toxicity, flammability, thermal radiation and overpressure hazards depending on the release scenario and generates a variety of output, including threat zone pictures, threats at specific locations and source strength graphs (NOAA, 2020).

ALOHA relies on a comprehensive set of inputs to provide thorough assessments of accident scenarios. This includes data like the accident location, date, and time, as well as atmospheric and terrain conditions. Additionally, the software requires information about the substance involved and uses an internal database to retrieve the properties. ALOHA generates various outputs tailored to the specific hazards associated with substance. When modelling a continuous release, it generates a dispersion plot over an XY surface, illustrating the plume's spread. Conversely, for an instantaneous release scenario, the plot depicts the sweep of the toxic cloud. It also provides a graph detailing the source term's evolution over time. For scenarios involving flammable substances, ALOHA presents graphs outlining the flammable area's extent based on the substance's Upper Flammability Limit (UFL) and Lower Flammability Limit (LFL). It furnishes data on the distances at which specific radiation and overpressure thresholds are reached upon ignition. These results are complemented by a text summary containing the calculated data.

The accuracy of results obtained using ALOHA depends primarily on the quality of input information provided and, secondarily, on inherent assumptions and limitations within the software itself. The first assumption is considering the wind speed and direction constant throughout the area downwind of a chemical release. Secondly, ALOHA considers that when released, a substance immediately disperses and mixes in the atmosphere, resulting in a bell-shaped concentration curve (Gaussian distribution) within the cloud, with the highest concentration downwind along the centreline. However, this estimation's accuracy diminishes under conditions of reduced atmospheric mixing, such as low wind speeds (less than 1.3m/s) or highly stable atmospheric conditions (stability class E and F) (NOAA and Office of Response and Restoration, 2012). In these cases, the software leads to an underestimation of the concentration levels. Furthermore, ALOHA does not display the threat zone if the maximum distance to a specific toxic level is less than 10 meters, due to concentration patchiness observed near the release source. This phenomenon of irregular concentration distribution occurs in proximity of the release source because the cloud has not yet travelled sufficiently for adequate mixing to occur. ALOHA does not account for the effects of combustion byproducts, particulates, or chemical reactions that may occur between the released gas and atmospheric components such as oxygen or water vapor. Additionally, the released substance must be a pure component, as ALOHA does not support defining mixtures except for a few selected solutions (NOAA & Office of Response and Restoration, 2012).



# 5 Methodology of a benchmark analysis

A benchmark analysis is a method created to compare companies, processes and products operating within the same sector, utilizing specific indicators (Bhutta & Huq, 1999). When employed to compare different software tools, like consequence analysis tools, usually the indicators used are accuracy of results, effectiveness of result visualization, computational efficiency and user interface. Performing a benchmark analysis enables the identification of weaknesses and strengths of the analysed tools, helping to select the most proper one based on investigation objectives, accident characteristics and available resources.

The structured approach guiding the benchmark analysis of consequence analysis software tools is outlined in multiple steps (Figure 12), formulated by the author to ensure a comprehensive evaluation of each software's capabilities. These steps constitute a theoretical framework facilitating a detailed benchmark analysis of consequence modelling software tools. However, this thesis will specifically focus on comparing the results obtained from these tools, with computational efficiency excluded as a factor in the comparison.

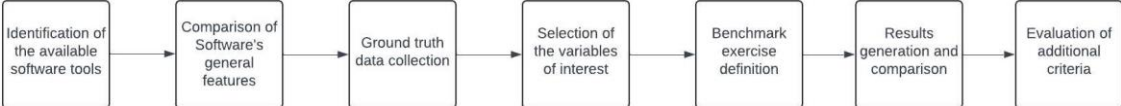


Figure 12: Steps of a benchmark analysis.

After identifying the software to be compared and assessing their availability, taking into account any license requirements, an initial comparison of the overall features of the software tools can be performed. This includes assessing the range of equipment and scenarios they can simulate, as well as the comprehensiveness of the material database containing the properties of simulated substances. During this preliminary analysis phase, it is also possible to evaluate the level of detail in describing specific scenarios. This includes the possibility to specify weather conditions, simulate interactions with external objects, and incorporate a variety of models, offering users the flexibility to select among them. Furthermore, it is crucial to assess the availability of technical documentation and help features.

## **5.1 Ground truth data collection and definition of the benchmark exercises**

Using real-world results as the foundation for the benchmark analysis offers the advantage of providing a ground truth for comparison with simulation outcomes. This stage is perhaps the most difficult during the benchmarking process (Bhutta & Huq, 1999), because collected data must be compatible with the type of results that software tools will produce.

Data extracted from real accident reports could serve as a solid grounding. However, these reports often lack detailed information about the events prior to and during the accidents. Instead, they mainly focus on the immediate effects of the accidents, such as lethality and surrounding damages. An alternative approach may be using results from experimental studies. They provide a comprehensive view of the experimental setup and furnish detailed information about the initiating event, such as the initial conditions of the stored substance or the magnitude of the release that generate the final scenario. Additionally, experimental studies enable access to more detailed scenario data through sensor measurements.

The process of gathering data from experimental results allows the definition of benchmark cases for subsequent analysis. These cases comprise scenarios characterized by well-defined input parameters, including details concerning the substance involved, operating conditions (such as temperature and pressure), the specific equipment involved, the nature of the loss of containment (e.g., leak or catastrophic rupture) and expected outcomes, such as toxic dispersion, jet fire or explosion.

For each scenario under analysis, it is possible to identify the key variables of interest. These variables are selected based on the objectives of the consequence analysis, which aims to provide an accurate and detailed understanding of the major consequences affecting both people and the environment. In toxic dispersion scenarios, the primary variable of interest is the concentration reached at specified distances from the release source. In fire scenarios, critical variables such as radiation reaching specific distances and flame extension play a significant role in establishing the minimum distance required to prevent flame impingement and domino effect. Conversely, in explosion scenarios, the variable that typically causes the most damage is the overpressure.

## **5.2 Results collection and comparison**

Given the variety of the models implemented by different software, it is important to carefully select the most appropriate one for the specific scenario to be simulated. If a selection is not possible, a thorough review of each model's underlying assumptions, as outlined in the technical

documentation, becomes necessary. This review helps identify which models are suitable for use in simulations. Input data should adhere to the specifications outlined in the benchmark exercise and the resulting values must be compared against the measured parameters of the experimental study, considered as the ground truth. In cases where some input data are unavailable, assumptions must be made, but it has to be taken into account that these assumptions will influence the obtained results.

Evaluating the simulation results entails assessing their accuracy, or how closely they align with the real value. In the context of a consequence analysis tool, it is worth noting that it is preferable to overestimate damages, such as concentration, radiation, and overpressure, rather than to underestimate them.

### **5.3 Details on the methodology used in this thesis work**

This thesis work focuses into the characterization of hydrogen jets stemming from leaks through small holes in pipes or tanks. Hydrogen jets are characterized by a primary segment dominated by momentum, followed by a second segment where additional factors such as buoyancy and wind play pivotal roles (Carboni et al., 2022).

Since hydrogen is a flammable substance with a broad flammability range, accurately predicting its dispersion is useful for identifying the distance from the release point at which ignition could occur in the presence of an ignition source. Statistics proves that in the most situations unscheduled hydrogen release will be ignited (Molkov & Saffers, 2013). Once ignited, understanding parameters like flame size or length is essential. Modelling these parameters helps establish safety distances to prevent flame impingement on nearby equipment or objects (Ekoto et al., 2012). Studies in the literature have established the concept of flame length through visible flame observations (Schefer et al., 2007). Flame length, as commonly defined, represents the centreline distance from the tip of the release nozzle to the flame's termination point. In the case of hydrogen, this measurement is often conducted using infrared (IR) and ultraviolet (UV) digital imaging techniques (HyResponders, 2021). Another critical factor is the radiant heat flux, measured in  $\text{kW/m}^2$ , which determines the heat exposure of an object at a specific distance from the jet fire.

To conduct the benchmark analysis and define benchmark exercises, a review of experimental studies was undertaken. Particularly, when addressing pressurized hydrogen, an overview of trends was observed regarding the experimental exploration of pressure and release hole diameters for hydrogen jet characterization over time, as depicted in Figure 13 (Carboni et al., 2022). The evolving technical challenges in hydrogen storage have significantly impacted the investigated

parameters, resulting in experimental conditions shifting towards higher pressure values and smaller release hole diameters.

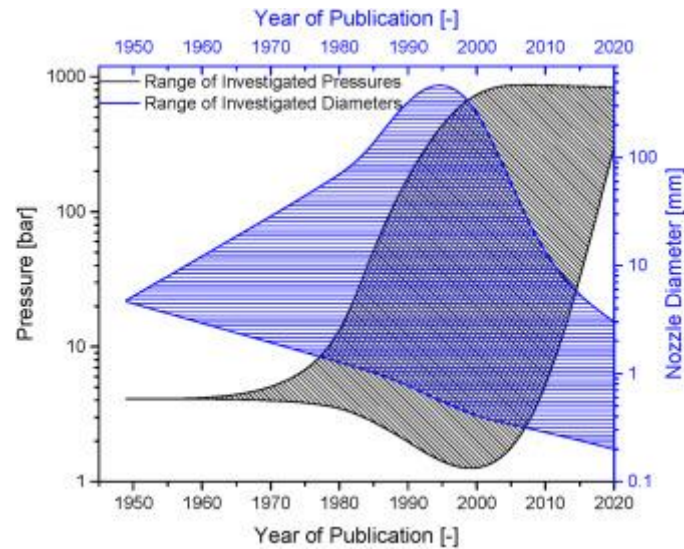


Figure 13: Trend of pressure conditions and hole release diameter used in experimental studies (Carboni et al., 2022).

The selection process for experimental studies, which served as the benchmark for comparing results with software outputs, was guided by two primary factors:

- Completeness of data regarding the experimental setup and conditions. Studies were selected based on their descriptions, ensuring that all relevant parameters were adequately outlined. This approach aimed to provide a thorough comprehension of the experimental context.
- Clarity and extractability of results. Preference was given to studies that presented their results clearly and in a format that facilitated easy extraction. This criterion ensured that the obtained data could be readily compared with results generated by software tools.

When a selected study did not provide all the necessary input parameters, assumptions were made. In this thesis work, many assumptions centred on weather conditions. Particularly, the Pasquill classification was employed to determine the atmospheric stability class (Table 7). Stability class indicates the tendency of the atmosphere to resist or enhance vertical motion. This parameter is influenced by several factors, including temperature changes with altitude (lapse rate), wind speed, time of day, cloud cover and surface roughness. The neutral category D should also be assumed, irrespective of wind speed, for overcast conditions during day or night, and for any sky conditions during the hour preceding or following night.



Table 7: Pasquill classification of atmospheric stability class (Kahl & Chapman, 2018).

Wind speed at 10m from the surface (m/s)	Daytime Insolation			Night-time cloud cover	
	Strong	Moderate	Slight	Thinly overcast or >4/8 low cloud	<3/8 cloud
< 2	A	A – B	B	-	-
2 – 3	A – B	B	C	E	F
3 - 5	B	B – C	C	D	E
5 – 6	C	C – D	D	D	D
> 6	C	D	D	D	D

The simulation results were initially compared based on the type of output generated by the software tools. Subsequently, they were qualitatively compared with the results of experimental studies using scatter plots. This comparison aimed to visualize the deviation between the calculated results and the experimental data.



## 6 Results

### 6.1 Jet Dispersion

In this section, the aim was to evaluate the modelling capabilities of the software tools in simulating the dispersion of gaseous hydrogen from a hole in a pressurized tank. The benchmark exercise was based on the study titled “Experimental investigation of highly pressurized hydrogen release through a small hole” by Han et al. (2014).

#### 6.1.1 Experimental study

The schematic representation of the experimental setup is shown in Figure 14. Gaseous hydrogen, stored in a pressurized tank, was introduced into a cylindrical chamber with a volume of 0.7 L. The release to ambient air occurred through a round hole positioned at the centre of the chamber's base. The chamber's pressure remained constant, ensuring a steady release flow rate. Hydrogen concentration was measured along the jet centreline using five gas samplers placed at distances of 1 m, 3 m, 5 m, 7 m, and 9 m from the jet release point. The typical sampling time was 12 s after the beginning of the release.

Since near the jet exit, the buoyancy is negligible in comparison to the jet inertia, the hydrogen jets were assumed to be straight and axisymmetric (Han et al., 2014). Therefore, the jet centreline was considered to be straight and horizontal at the same height as the release elevation. In verifying this assumption, a laser was employed to visualize the hydrogen jet, as hydrogen itself is colourless. The laser illuminated  $\text{Al}_2\text{O}_3$  particles, which were ejected from the pressure chamber together with the hydrogen (Han et al., 2014). Figure 15 demonstrates that the jet maintained its near-straight trajectory along the horizontal axis across all images.

The experimental site selected was an outdoor paved area enclosed by three-story buildings on three sides. This geometric configuration was chosen to minimize the crosswind effect, which could potentially underestimate the concentration along the centreline (Han et al., 2014). All the experiments were performed after 10 pm, when the land-sea breeze tended to be calm, in almost cloudless nights (Han et al., 2014).

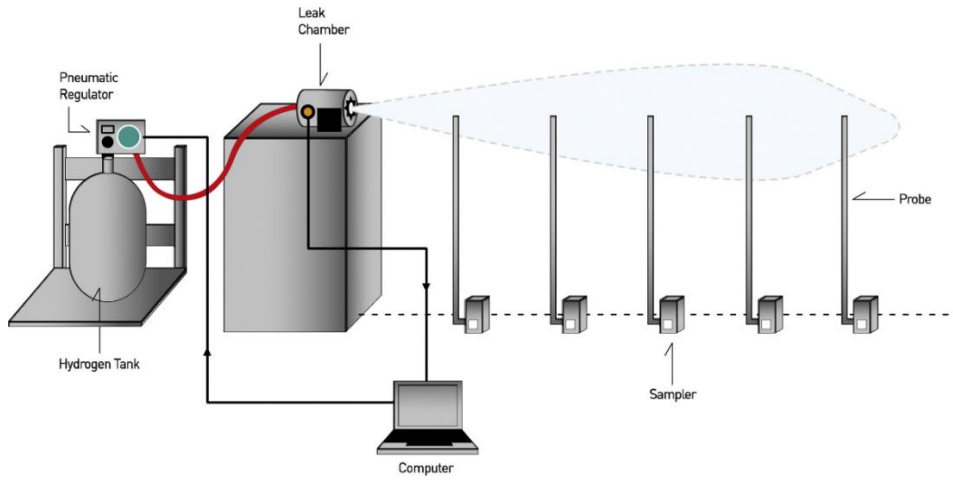
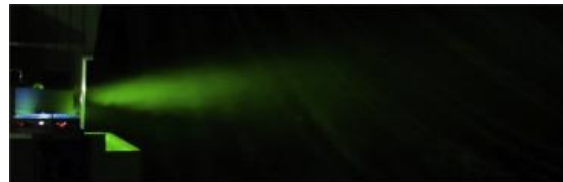
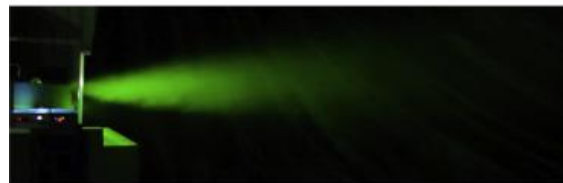


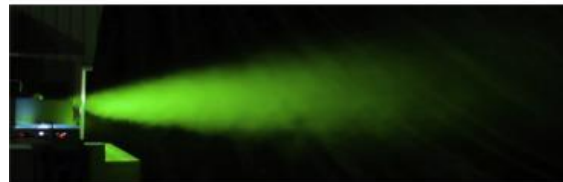
Figure 14: Experimental set up of the jet dispersion experiments (Han et al., 2014).



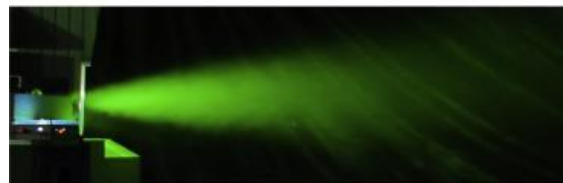
(a)  $P_0=100$  bar



(b)  $P_0=200$  bar



(c)  $P_0=300$  bar



(c)  $P_0=400$  bar

Figure 15: Visualization of hydrogen jets using alumina particles. Nozzle diameter is 0.7mm with varying pressure (Han et al., 2014).

A total of eleven experiments were conducted, with hydrogen pressure ranging from 100 bar to 400 bar and hole diameters varying between 0.5 mm and 1 mm. Table 8 provides a schematic representation of the experimental conditions.

Table 8: Pressure (bar) and nozzle diameter (mm) conditions used in Han et al. experimental study.

Experiment ID	Pressure (bar)	Nozzle diameter (mm)
1.1	100	0.5
1.2	100	0.7
1.3	100	1
1.4	200	0.5
1.5	200	0.7
1.6	200	1
1.7	300	0.5
1.8	300	0.7
1.9	300	1
1.10	400	0.5
1.11	400	0.7

Data on wind velocity and atmospheric stability class were not provided in the paper. Additionally, information regarding the height of the release chamber and the volume of the tank was not specified. However, Han et al. suggested that the tank's volume could be considered infinite, implying it was large enough to continuously supply hydrogen to the release chamber until the jet reached a steady state, moment in which the concentrations were measured.

### 6.1.2 Modelling

Due to missing input data in Han et al.'s paper, assumptions were necessary. Firstly, to characterize the storage conditions, a pressurized tank with a volume equivalent to 50 L was assumed. This selection was based on the standard dimensions commonly found in hydrogen pressure vessels. Additionally, the temperature of the hydrogen within the vessel was presumed to be equal to the ambient temperature, assumed to be 10°C, as the experiments were conducted during the nighttime. The atmospheric stability class was set to F, indicating a moderately stable atmosphere. With only the information that "the land-sea breeze tended to be calm" (Han et al., 2014), the wind velocity tested conditions were 0.1 m/s, 1 m/s, and 2 m/s. Also considering the unknown release elevation, simulations were conducted at different heights from the ground: 0.5 m, 1 m, 1.5 m, and 2 m. Table 9 outlines all the conditions examined. The initiating event resulting in the jet was a horizontal leak, with a constant mass flowrate.

Table 9: Wind speed and release elevation conditions tested in jet dispersion simulations.

Simulation ID	Wind velocity (m/s)	Elevation of the release (m)
S1	1	0.5
S2	1	1
S3	1	1.5
S4	1	2
S5	0.1	1
S6	2	1

Exclusively in Phast, the variation of wind velocity and release elevation was possible, as HyRAM lacks the implementation of wind and atmospheric stability effects and does not account for release elevation. Therefore, simulations detailed in Table 9 were exclusively performed using Phast. Conversely, in HyRAM, only one set of simulations was conducted, as the only parameters to be specified were the diameter of the release orifice and the hydrogen tank pressure. While HyRAM necessitates the specification of the discharge coefficient, Phast calculates it automatically. Therefore, the discharge coefficient determined by Phast served as an input parameter in HyRAM. In the Physics calculation mode of HyRAM, plume dispersion calculations only required the leak diameter, equivalent to the nozzle diameter, and the angle formed by the jet direction from the horizontal axis. As the release was horizontal, this angle was set to zero.

The use of ALOHA software for these simulated experiments was not feasible due to the relatively small dimensions of the jets. Specifically, the jet dimensions were below 10 m, which is the threshold for representing results with ALOHA.

### 6.1.3 Results of the simulations

To assess dispersion, Phast generated a graph plotting concentration against downwind distance at a specified height of interest. This height was matched to the release elevation, corresponding also to the jet centreline, to replicate the positioning of experimental probes illustrated in Figure 14. As an example, Figure 16 displays the graph produced for the simulated experiment conducted at 400 bar, with a release hole diameter of 0.7 mm. The simulation considered a wind velocity of 1 m/s and the release occurring at a height of 1 m. Across all analysed scenarios, the concentration exhibits hyperbolic decay when plotted against downwind distance. In Phast, it is also possible to observe the concentration's evolution over time. Specifically, the graph in Figure 16 depicts the concentration calculated at 12 seconds, corresponding to the sampling time referenced by Han et al. This feature facilitated determining the time after the start of the release at which the jet reached a stationary state (Figure 17 and Figure 18). This was found to be nearly 10 seconds, aligning with the estimation made by Han et al. in their experimental study. Additionally, the software simulates concentration decay when the hydrogen release ceases, as shown in Figure 18 (b).

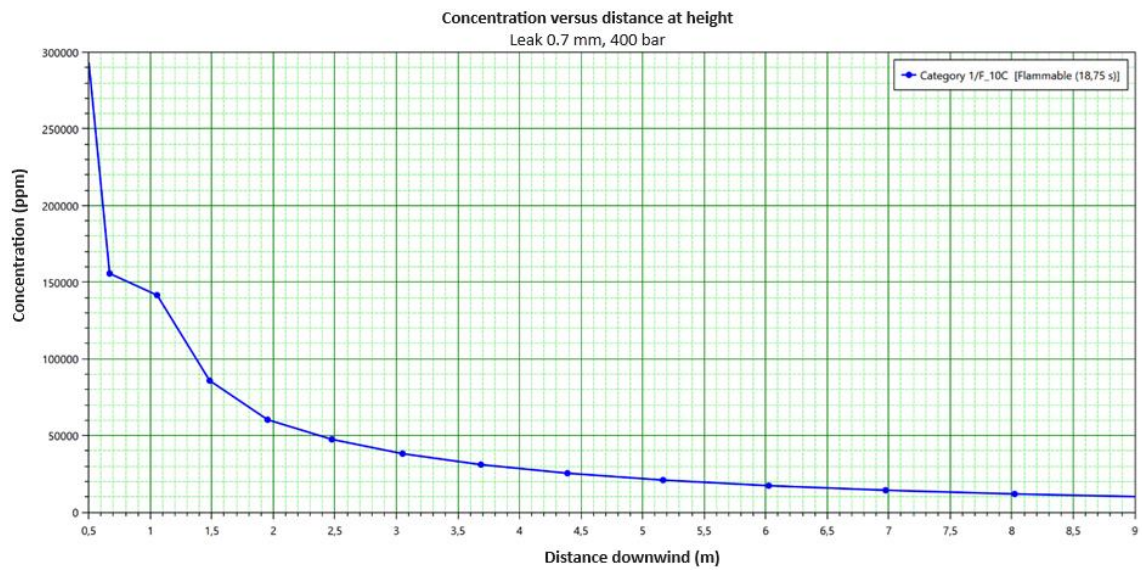
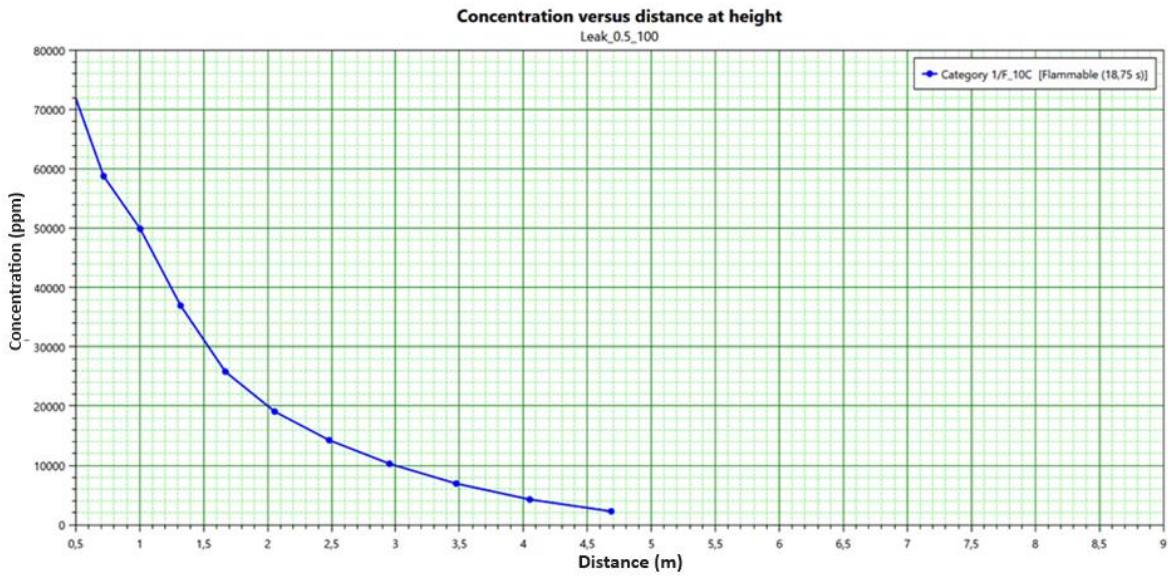
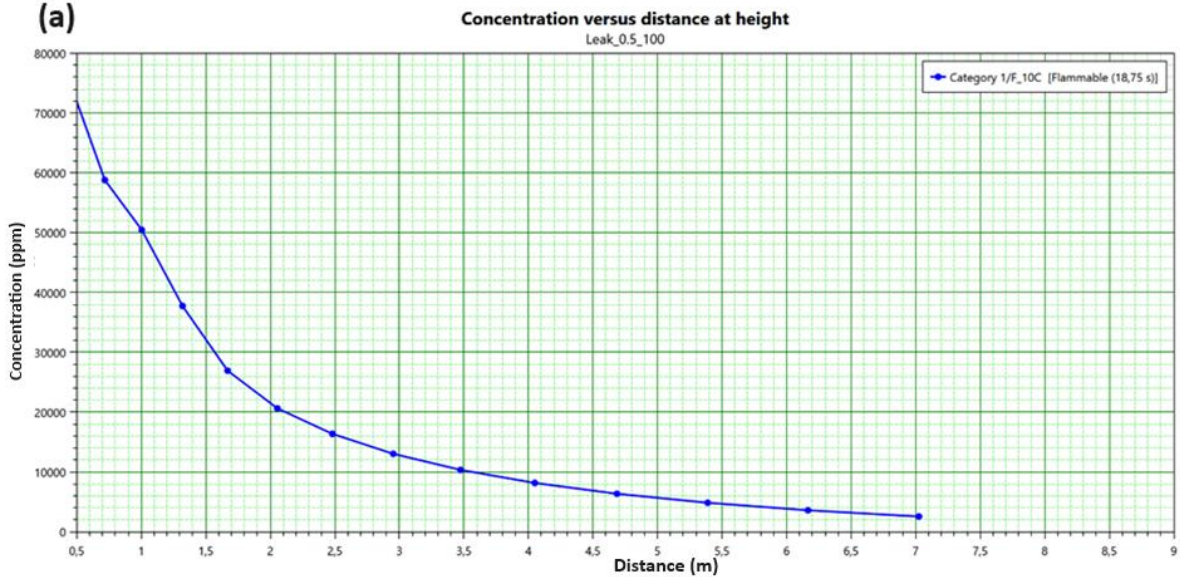


Figure 16: Concentration (ppm) in function of downwind distance (m) for the simulated experiment 1.11, with simulation conditions S2.



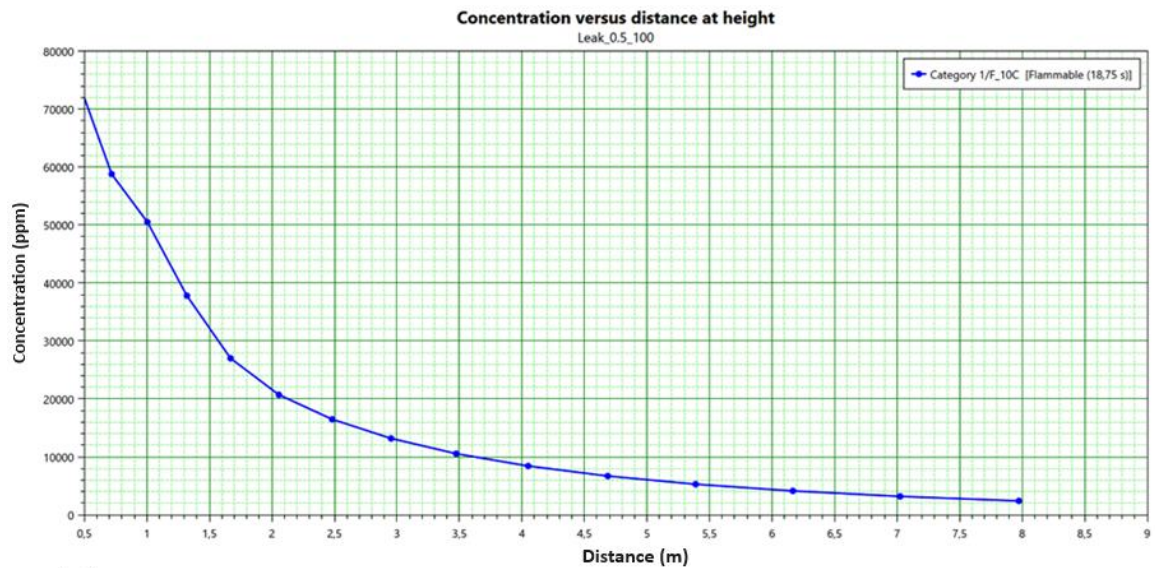
**(a)**



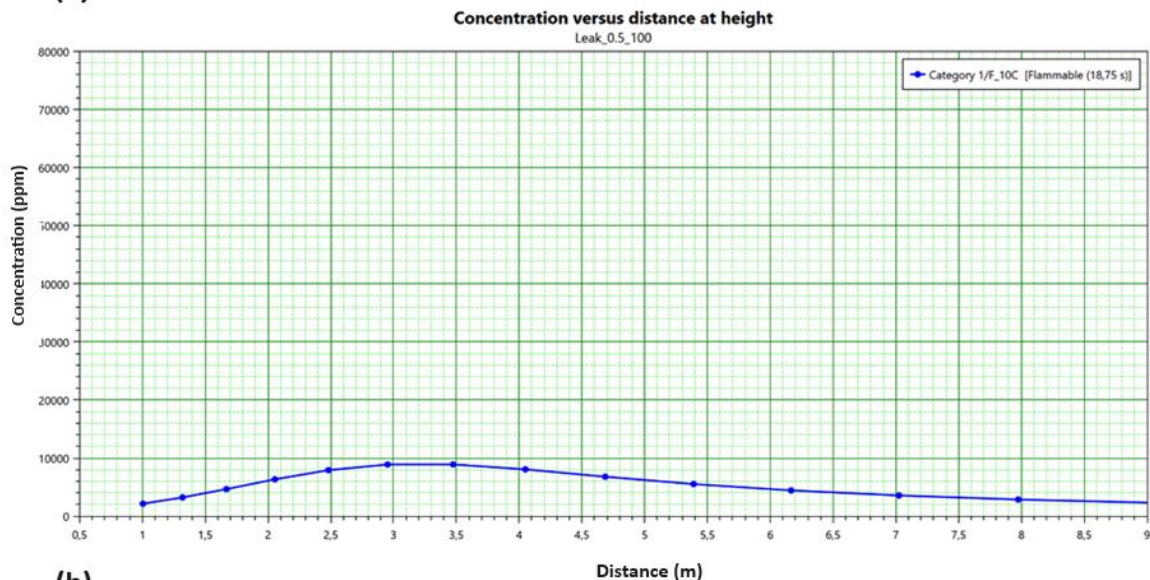
**(b)**

Figure 17: Concentration (ppm) against distance downwind (m) at different times after the release for the simulated experiment 1.1, conditions S2. (a) 1 s, (b) 5 s.





(a)



(b)

Figure 18: Concentration (ppm) against distance downwind (m) at different times after the release for the simulated experiment 1.1, conditions S2. (a) 10 s, (b) after the end of the release (about 300 s).

HyRAM, on the other hand, provided the distance at which a specified concentration level was reached. Extracting the results involved employing a trial-and-error method to establish the concentration at specific distances of 1 m, 3 m, 5 m, 7 m, and 9 m. It is important to note that the concentration value considered was the one along the centreline.

Both software tools also generated a side view of the jet, allowing a comparison with the images presented in Figure 15. In Figure 19, Figure 20 and Figure 21 the three side views for the hydrogen leak at 400 bar through a hole measuring 0.7 mm are shown. It is important to note that there is a difference in the axis reference system between the two software tools.

Specifically, in both Phast and HyRAM, the x-axis indicates the direction of the release. Meanwhile, in Phast, the z-axis is perpendicular to the ground, with its origin at ground level. On

the other hand, in HyRAM, the y-axis denotes the direction perpendicular to the ground and its origin represents the release point.

From Phast's side view (Figure 20), it is evident that the jet is not axisymmetric. The height of the centreline increases as the distance from the source increases. This observation suggests that the software accounts for the buoyancy effect.

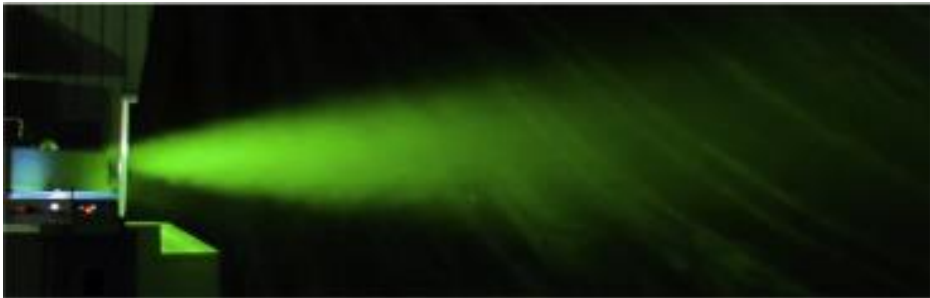


Figure 19: View of the jet at 400 bar from a hole of 0.7 mm, experiment 1.11 (Han et al., 2014).

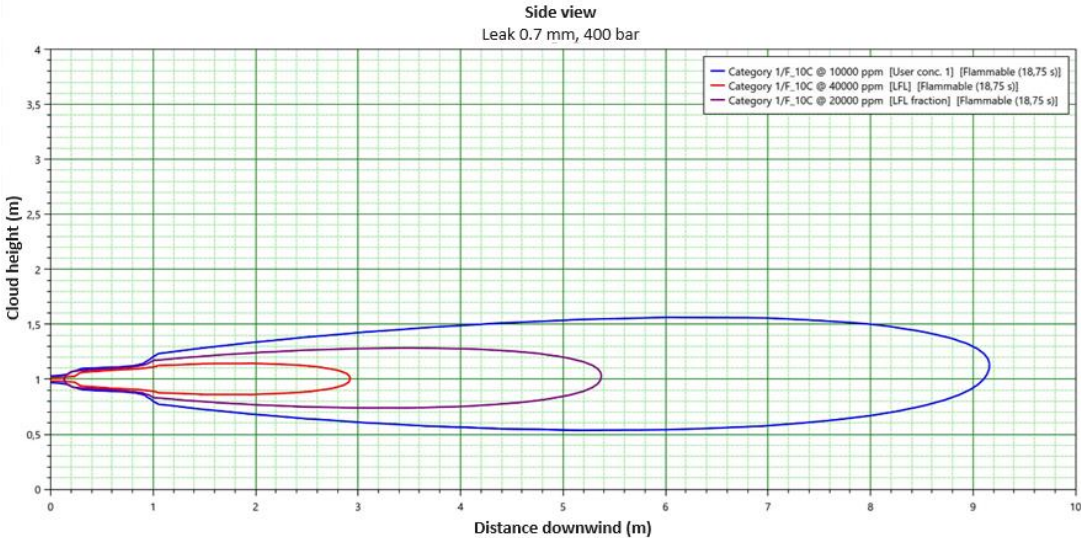


Figure 20: Side view of simulated experiment 1.11 with Phast.

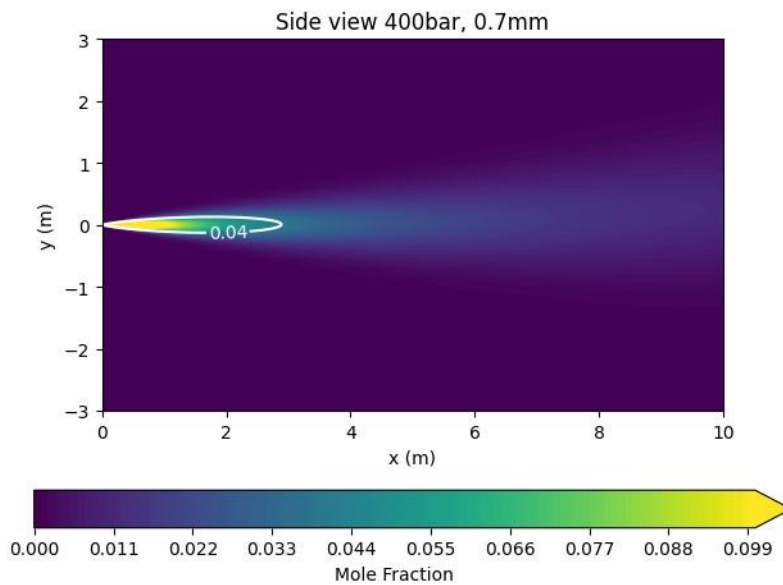


Figure 21: Side view of simulated experiment 1.11 with HyRAM.

#### 6.1.4 Discussion

The objective of comparing the experimental results with the simulation results from the two software tools is to evaluate the accuracy of the software's predictions. Multiple simulations were conducted using Phast, varying wind speed and release elevation as described in Table 9. Before comparing these simulation results with the experimental data, some considerations must be addressed.

For simulations S1, S2, S3, and S4, where the wind speed was set at 1 m/s and the release elevation varied between 0.5 m and 2 m, the results indicated that as the release elevation increased, the calculated concentration at specified downwind distances and at a height equal to the release elevation also increased. In particular, Figure 22 shows that the differences in concentrations were more pronounced at 1 meter downwind, while at greater downwind distances, the concentrations were almost equal for all investigated elevations. Comparing simulations S2, S5, and S6 revealed that variations in wind speed had a more significant impact on the results, with the release elevation maintained at 1 m. For simulations with a release hole diameter of 0.5 mm, the concentration at 1 m from the release point was higher when the wind speed was 2 m/s (Figure 23). In other cases, the concentration calculated by Phast increased as the wind speed decreased for all downwind distances. The results for a wind speed of 1 m/s were in each simulated experiment between the values calculated at 0.1 m/s and 2 m/s. Therefore, it was decided to compare the experimental values with the simulation results obtained using 1 m/s wind speed. In particular, the mean value of the results obtained at different elevations represented the Phast result shown in the comparison.

The results obtained with HyRAM can be directly compared with the experimental results, as the wind speed and release elevation are parameters that cannot be defined in HyRAM.

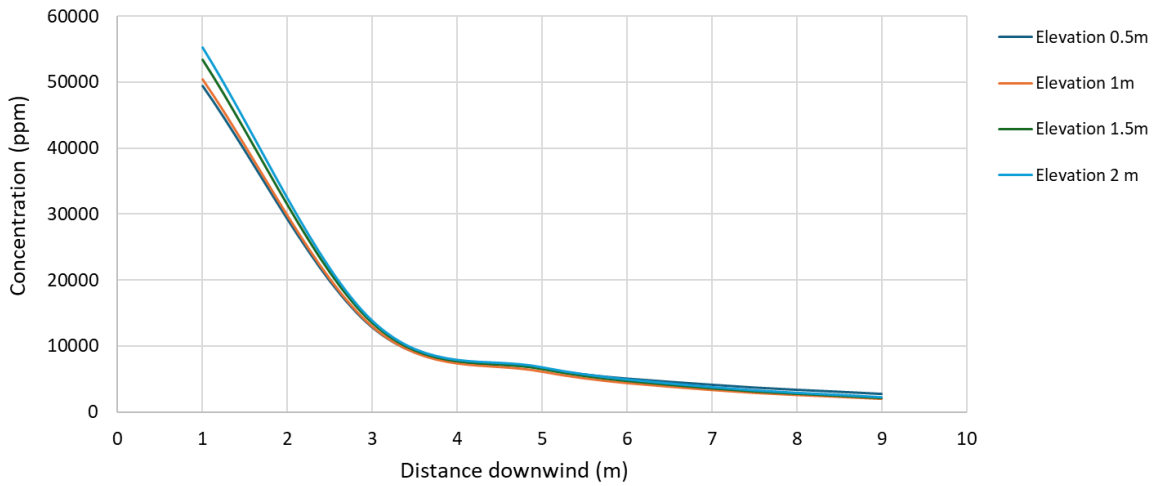


Figure 22: Comparison of Phast results for simulations S1, S2, S3 and S4 of experiment 1.1 (100 bar, 0.5 mm).

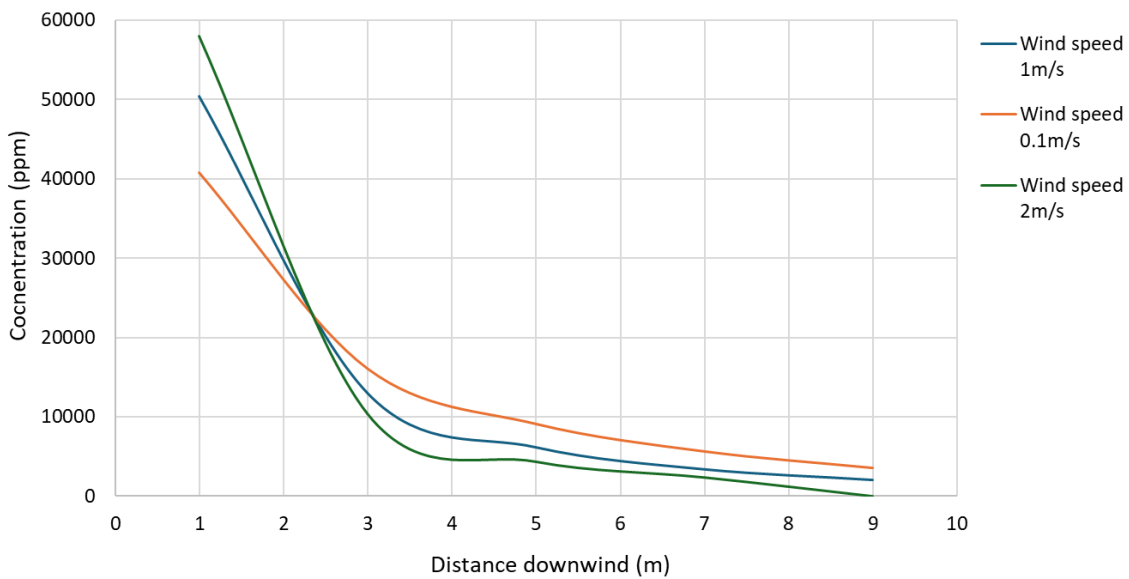


Figure 23: Comparison of Phast results for simulations S2, S5 and S6 of experiment 1.1 (100 bar, 0.5 mm).

The experimental values of concentration used for comparison with the simulation results were extracted from the graphs in the study by Han et al. The concentrations measured in the experimental study were generally quite low, typically below the lower flammability limit of hydrogen (4% vol.). The maximum concentration observed experimentally was 18.5%, measured at a release pressure of 300 bar through a 1 mm diameter hole, 1 meter downwind from the release point.

Both software tools predicted higher concentrations as the release pressure and hole diameter increased, aligning with the experimental observations. Figure 24 illustrates the comparison between the experimental and simulation results. The solid black line, bisector of the first quadrant, represents points where simulation results coincide with experimentally measured values from Han et al.'s study. Each point on this line has equal x and y coordinates corresponding to the experimental values. The simulation results are points with y-coordinate the concentration values calculated by the two software tools and x-coordinate the experimental value. The concentrations in this graph are expressed in terms of the mole fraction of hydrogen.

It can be stated that both software tools generally underestimate the concentrations. However, the underestimation is less pronounced in Phast compared to HyRAM. The discrepancy between the simulation results and the experimental results increases with higher concentration values.

It is important to consider the potential errors that might have occurred while extracting the results from the experimental study. The hydrogen concentrations were presented in graphs where the mole fraction of hydrogen as a function of downwind distance was plotted on a logarithmic scale. This could have introduced inaccuracies in the extracted data.

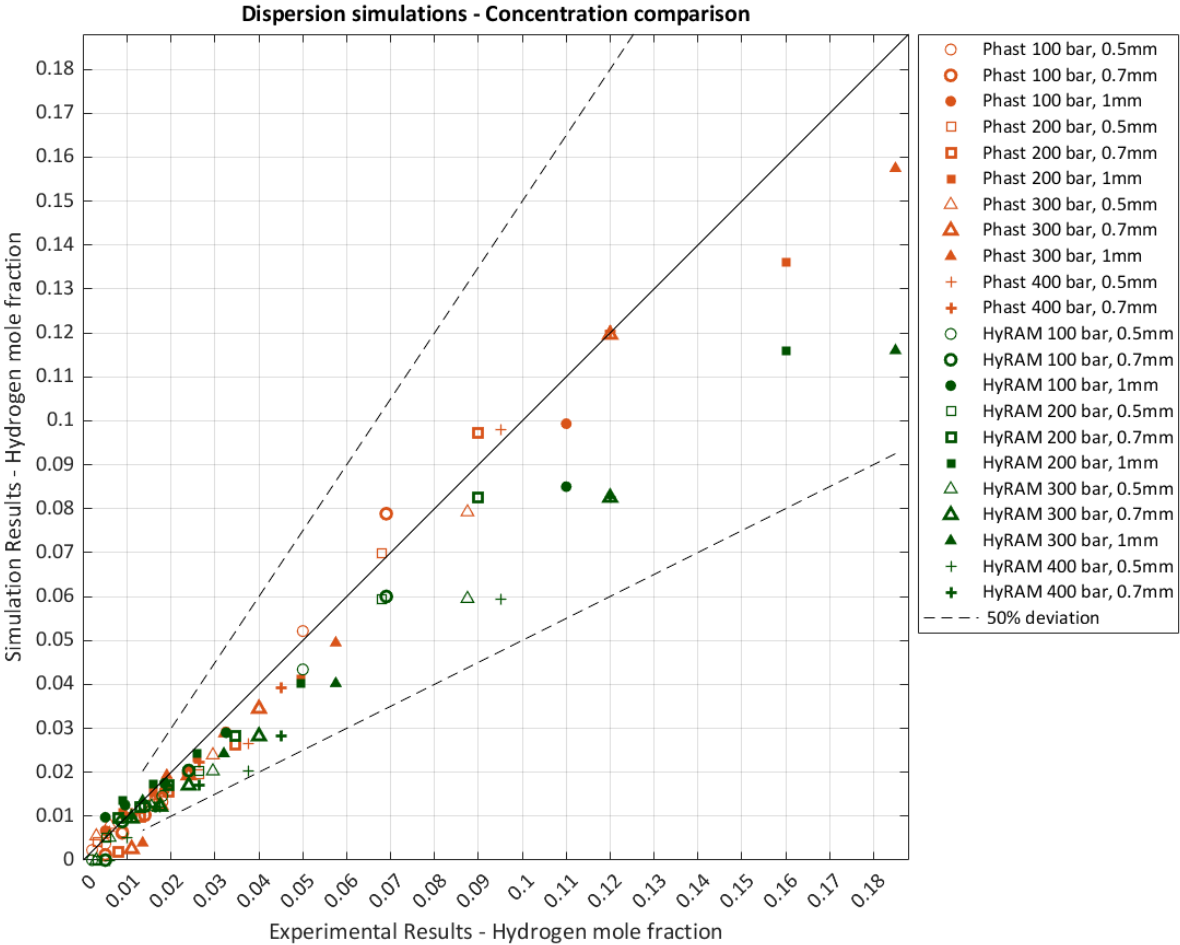


Figure 24: Jet dispersion. Comparison between experimental results and simulation results.

## 6.2 Jet Fire

To assess the predictive capability of the software tools in determining jet fire characteristics, two distinct experimental studies were employed as ground truth. The first study investigated jet fires arising from pressurized hydrogen at ambient pressure and provided the ground truth for the comparison of the flame length, while the second one was used to evaluate the radiation emitted from large-scale hydrogen jet fires and detected at specified distances. This second experimental study allowed to make evaluations also with ALOHA software, as the scales exceeded 10 meters, thereby overcoming the software's limitations.

### 6.2.1 Experimental study - Compressed hydrogen jet fire flame length

The experimental study used as ground truth for the jet fire flame length predictions is titled “Experimental and Numerical Characterization of Hydrogen Jet Fires” by Carboni et al. (2022). In these experiments, pressurized hydrogen was released horizontally at a height of 1 m from the ground. Figure 25 shows a schematic representation of the experimental setup, which included a 0.8 m<sup>3</sup> reservoir with an initial internal pressure of 450 bar. The reservoir was connected to the release nozzles via a pipe with a constant internal diameter of 7 mm. The release nozzles tested had diameters of 1 mm, 3 mm, and 5 mm. A total of 17 tests were performed, varying the nozzle diameters and the storage pressure (Table 10). Wind speed and direction were measured at a height of 3 m by an onsite weather station, with the wind direction mostly coinciding with the direction of the jet throughout the entire campaign (Carboni et al., 2022). The paper did not provide information about atmospheric stability or ambient temperature.

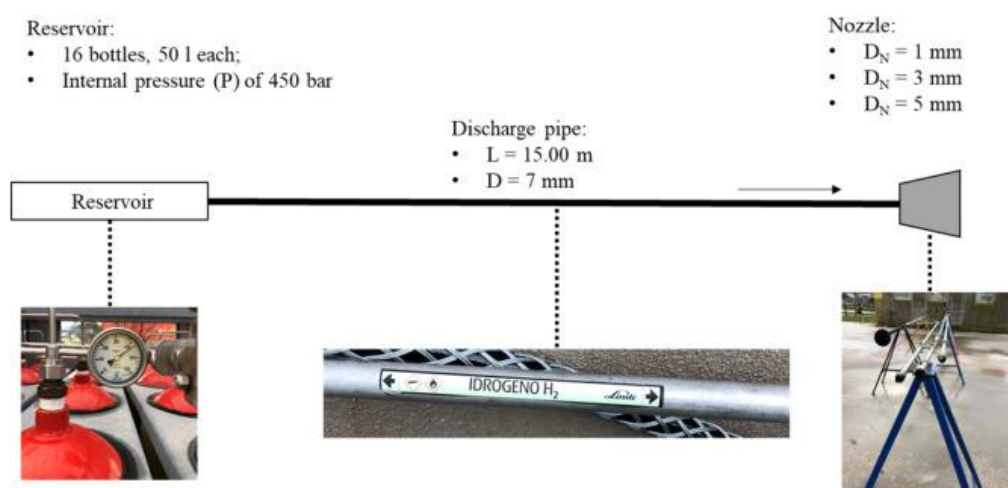


Figure 25: Schematic representation of the experimental set up used in Carboni et al. experimental study (Carboni et al., 2022).

Table 10: Nozzle diameters (mm) and pressure (bar) investigated and wind velocity (m/s) measured during Carboni et al. experimental study.

Experiment ID	Nozzle diameter (mm)	Pressure (bar)	Wind velocity (m/s)
2.1	1	365	1.0
2.2	1	360	0.5
2.3	1	350	0.5
2.4	3	450	2.0
2.5	3	420	2.0
2.6	3	380	2.0
2.7	3	340	1.0
2.8	3	300	2.0
2.9	3	270	0.0
2.10	3	240	1.0
2.11	3	220	0.5
2.12	5	340	0.0
2.13	5	270	2.0
2.14	5	240	0.5
2.15	5	125	2.0
2.16	5	120	2.0
2.17	5	90	1.5

Sixteen type-K thermocouples (Carboni et al., 2022) arranged as shown in Figure 26 were used to record the temperature distribution. The flame structure was characterized using visible and infrared (IR) images taken during the experiments. Carboni et al. stated that the accuracy of the thermocouples and the thermal imaging camera does not significantly impact the estimation of the jet flame length.

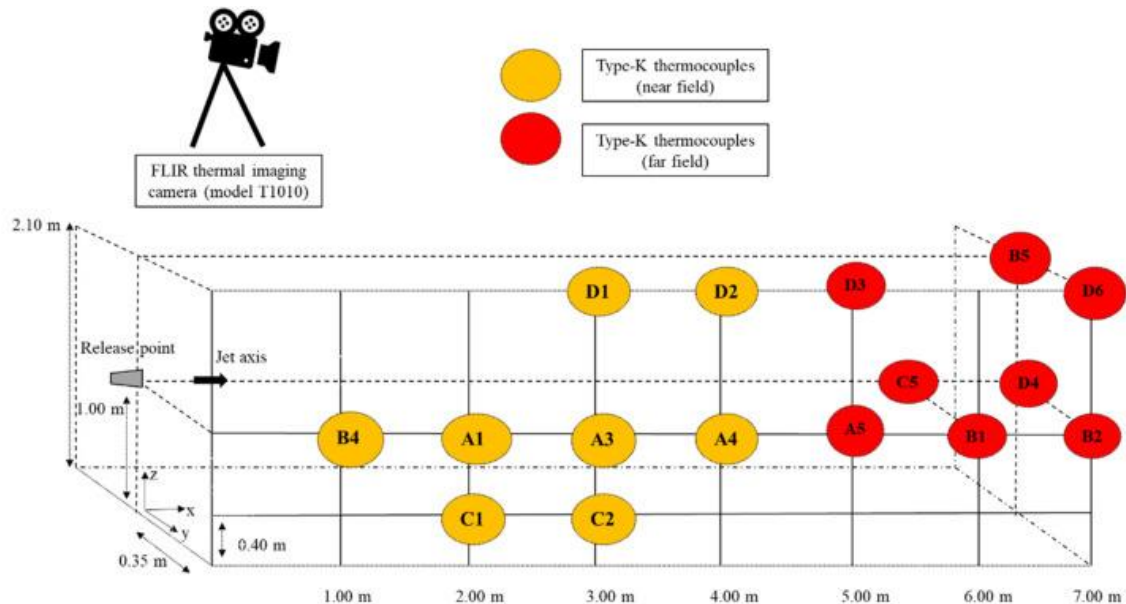


Figure 26: Thermocouple positioning (Carboni et al., 2022).

In the IR images, four different temperature zones were distinguished, corresponding to the temperature ranges  $T > 1400^{\circ}\text{C}$ ,  $800^{\circ}\text{C} < T < 1400^{\circ}\text{C}$ ,  $600^{\circ}\text{C} < T < 800^{\circ}\text{C}$ , and  $T < 400^{\circ}\text{C}$  (Carboni et al., 2022). These zones were indicated by different colours, ranging from dark red to yellow (Figure 27). Cool combustion products appeared outside the jet shape in white. The collected IR images showed that the buoyancy-dominated segment of the flame was inclined at an angle close to  $30^{\circ}$  with respect to the horizontal axis (Carboni et al., 2022).

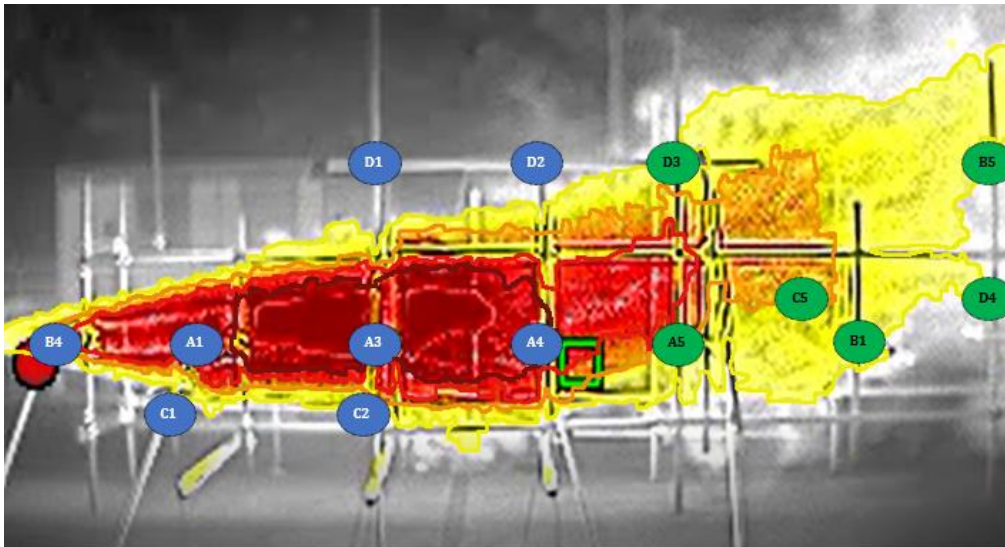


Figure 27: IR image obtained for experiment 2.7, with nozzle diameter of 3 mm and pressure equal to 340 bar (Carboni et al., 2022).

### 6.2.1.1 Modelling

Modelling this experimental study in Phast requires setting detailed weather conditions. Since the experiments were conducted during daytime, an ambient temperature of  $20^{\circ}\text{C}$  was assumed. This temperature was also assumed to be the temperature of the hydrogen inside the reservoir. As no information about atmospheric stability was provided, simulations were conducted for different atmospheric stability classes using the Pasquill classification. The D atmospheric stability class was also used to account for overcast conditions. Table 11 provides the atmospheric stability classes used for the simulations for each wind speed reported in the experimental study.

Phast imposes constraints on the range of wind velocities that can be simulated. Specifically, the minimum wind velocity for which calculations are performed is 0.1 m/s. Additionally, the software issues warnings when wind speeds fall between 0.1 and 1 m/s due to potential inaccuracies observed during the software's validation process (DNV, 2023). This aspect needs to be considered



for simulations corresponding to experiments 2.2, 2.3, 2.9, 2.11, 2.12, and 2.14. Furthermore, when the wind speed reported in the paper was zero, a value of 0.1 m/s was set in Phast.

Table 11: Atmospheric stability classes investigated in Phast depending on the wind speed.

Wind speed (m/s)	Atmospheric stability classes			
0	A	A/B	B	D
1	A	A/B	B	D
1.5	A	A/B	B	D
2	A/B	B	C	D

In Phast, a pressure vessel was defined with a volume equal to that of the reservoir specified by Carboni et al. The pressure varied for each experiment, while the temperature was set to the assumed ambient temperature. The initiating event was set as a horizontal leak from a hole with a diameter corresponding to the nozzle diameter used in each experiment. This hole was positioned at an elevation of 1 m, as depicted in Figure 26.

The software offers the option to select the model for calculating jet fires. Specifically, when dealing with releases of non-hydrocarbon/low-luminosity gases, Phast recommends using the Miller model. In this model, the flame is depicted as a line source consisting of two distinct straight-line segments (Figure 28). The first segment is dominated by momentum, where the flame initially travels straight in the release direction. The second segment is influenced by buoyancy or wind, causing it to travel in a direction determined by buoyancy and wind, forming an angle with respect to the release direction known as the flame lift angle (Miller, 2017). This calculation method applies to both horizontal and vertical jet fires.

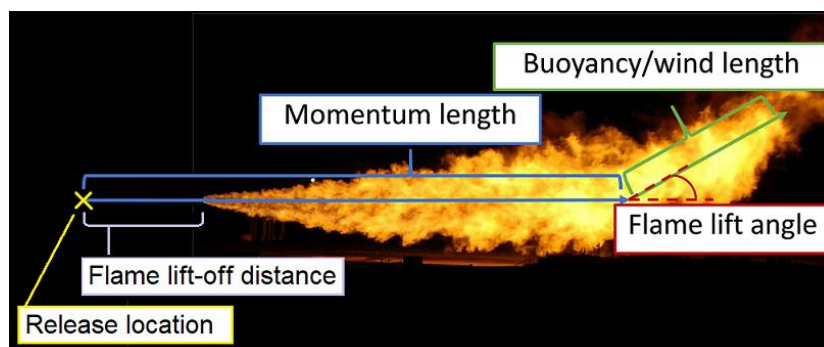


Figure 28: Miller model description of a horizontal jet fire (DNV Phast technical documentation).

The only assumption used in HyRAM was the ambient temperature, which is consistent with the assumption made in Phast. Since HyRAM does not compute the discharge coefficient, the value calculated by Phast was adopted as an input parameter. The only other parameters needed to calculate the characteristics of jet fires are the diameter of the leak, set equal to the nozzle diameter for each experiment, and the release angle, set to zero to define a horizontal release. When the radiative heat flux window is used, another required input is the relative humidity of the ambient, which was set to 0.7, the default value in Phast.

Due to the small scale of the jet fires produced in the experiments conducted by Carboni et al., ALOHA could not be utilized to simulate these conditions.

### **6.2.1.2 Results of the simulations**

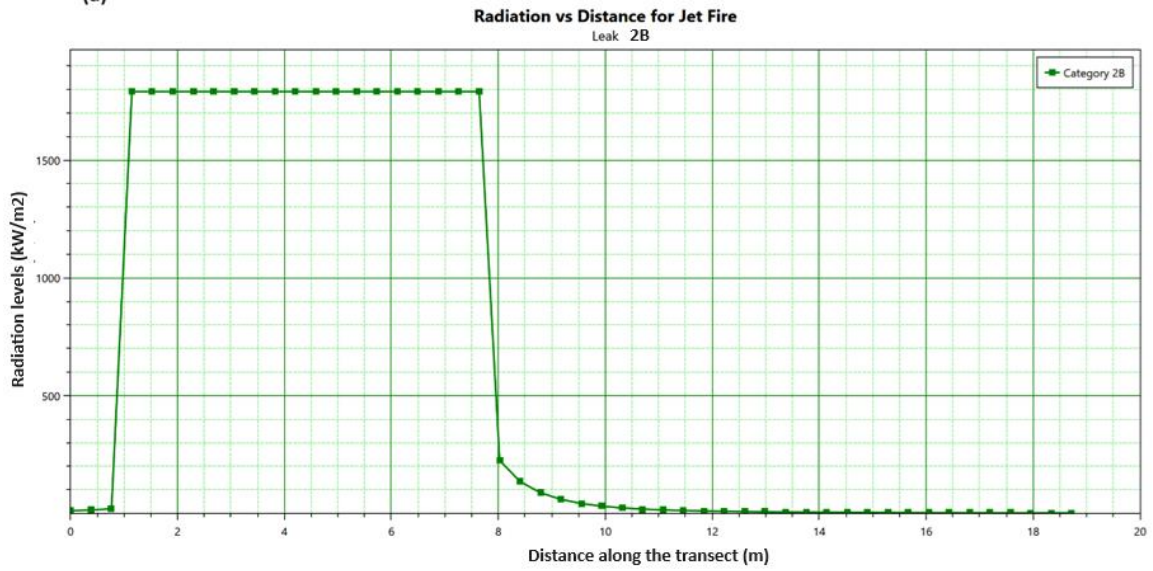
When defining a leak from a pressure vessel, Phast automatically calculates the consequences of each possible scenario resulting from that leak, including jet fire. The software represents through a graph the radiation on the jet fire centreline as a function of the downwind distance at a specified height of interest. Additionally, it generates a radiation ellipse, displaying contours of a defined radiation level in kW/m<sup>2</sup> in the xy-plane, where x indicates the release direction. In this second graph, the z coordinate, corresponding to the height of interest, is constant and set by the user. An example of these two graphs is shown in Figure 29 and Figure 30. The comparison of two atmospheric stability classes (B and D) allows to state that this parameter does not influence the calculation of jet fire characteristics.

The atmospheric stability class primarily influences the dispersion of released hydrogen, as illustrated in Figure 31. Specifically, from class A/B to D, the maximum concentration at a given downwind distance increases. This is because more stable atmospheres (like class D) diminish the vertical motion of air layers, thereby reducing dispersion.

The use of the Miller model to describe the jet fire originated by a hydrogen leak allows to collect as output the values of flame lift-off distance, momentum dominated length, buoyancy/wind dominated length and the total flame length.



(a)



(b)

Figure 29: Graph depicting radiation (kW/m<sup>2</sup>) in function of distance (m) along the centreline of the jet for simulated experiment 2.13 obtained with Phast. Comparison between atmospheric stability class D (a) and B (b).

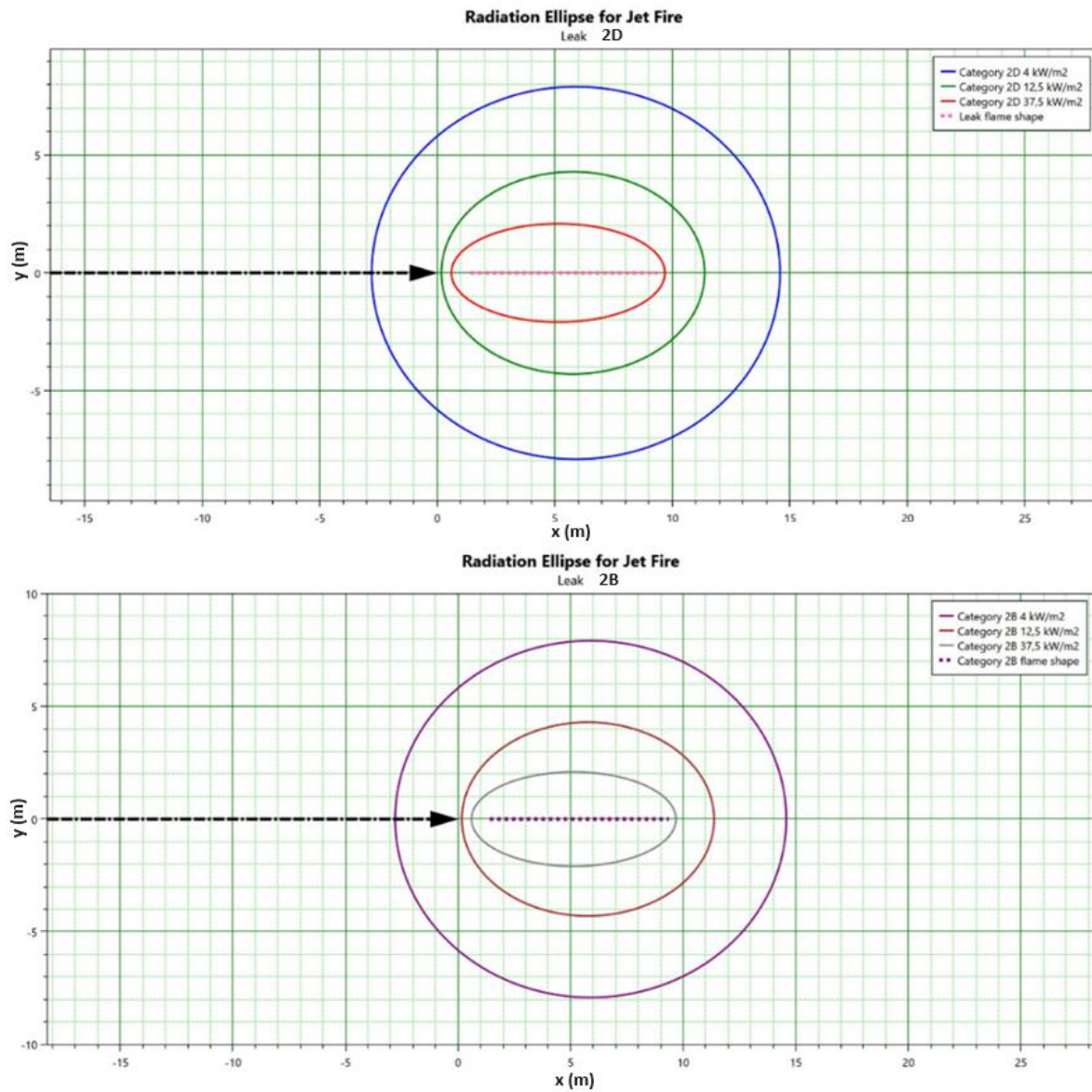


Figure 30: Graph depicting radiation ellipses of the jet for the simulated experiment 2.13 obtained with Phast. Comparison between atmospheric stability class D (top) and B (bottom).

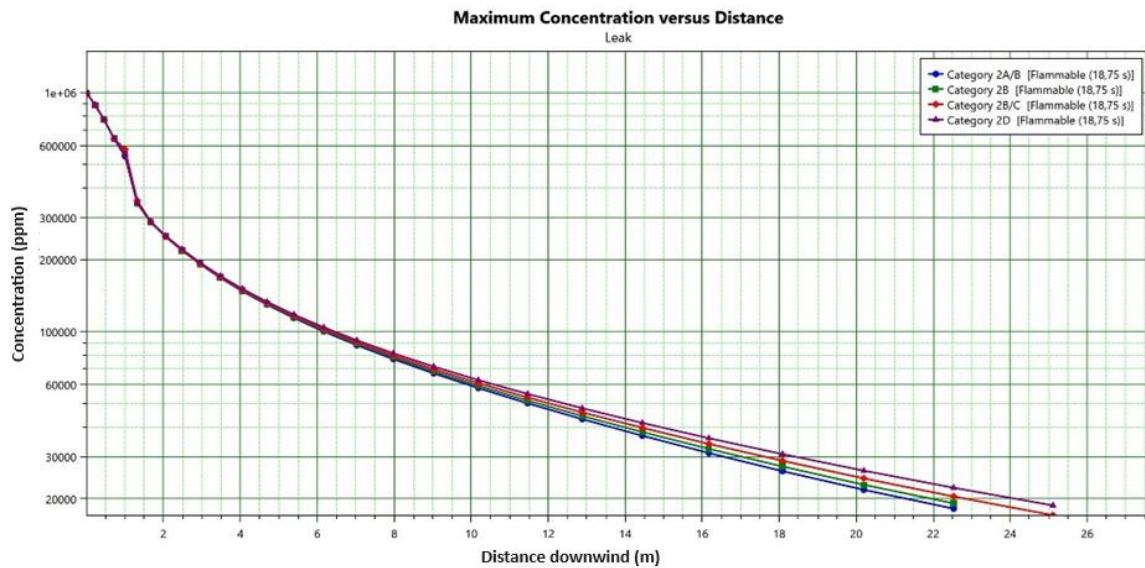


Figure 31: Graph generated by Phast to compare the maximum concentration (ppm) in function of downwind distance (m) for the different atmospheric stability classes investigated for the simulated experiment 2.13.

In HYRAM, a jet flame can be evaluated using two different software features: Flame Temperature/Trajectory and Radiative Heat Flux. With Flame Temperature and Trajectory, the results include a representation of the jet flame with temperature contours highlighted, the mass flow rate exiting the specified release hole, the visible flame length, the total emitted radiative power and the radiant fraction. An example of a temperature plot is shown in Figure 32. The release point is automatically set at the origin of the axis, so the initial part of the jet, where the temperature plot indicates ambient temperature, represents the flame lift-off. Additionally, the flame is not completely straight, indicating that the software accounts for the buoyancy effect.

When using the Radiative Heat Flux window, in addition to the results provided in the Temperature/Trajectory window, contours of specified radiation levels ( $\text{kW}/\text{m}^2$ ) are also provided. An example of this graph is shown in Figure 33, where contour levels of  $3 \text{ kW}/\text{m}^2$ ,  $5 \text{ kW}/\text{m}^2$ , and  $8 \text{ kW}/\text{m}^2$  are displayed. In several EU territories (e.g. Catalonia) (INSTRUCCIÓ 11/2010 SIE, 2010), the first two levels represent the limits used to define the intervention zone and alert zone for an exposure time of 30 seconds, respectively, while the third level indicates the radiation value that can lead to a domino effect.

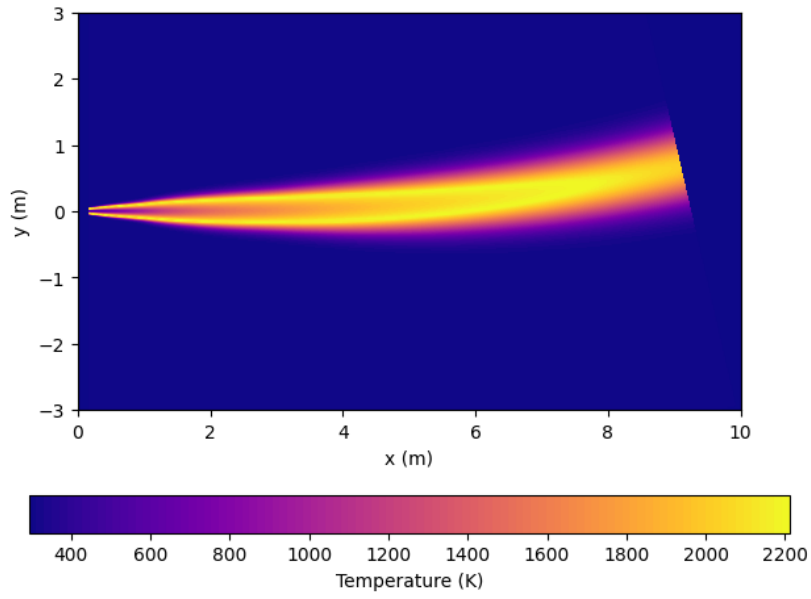


Figure 32: HyRAM. Temperature plot of the simulated experiment 2.13.

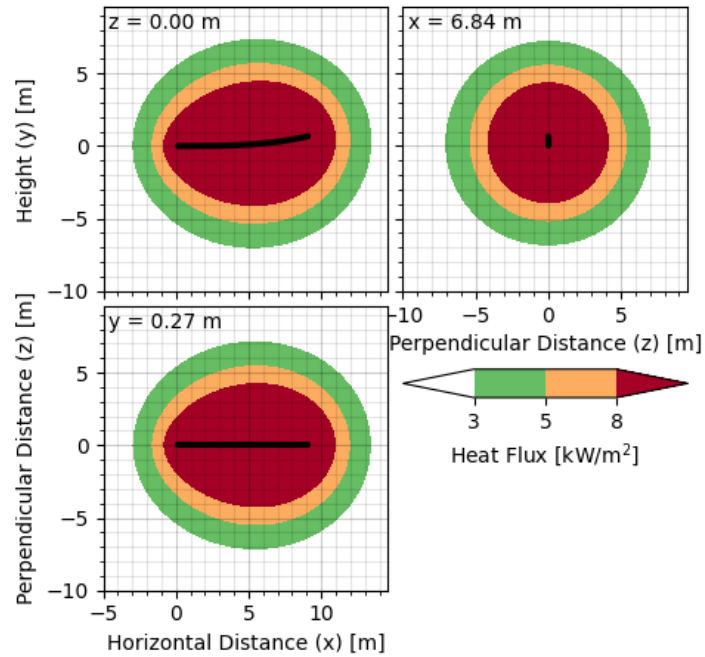


Figure 33: HyRAM. Radiation contours for the simulated experiment 2.13.

6.2.1.3 Discussion

The flame length was experimentally measured by Carboni et al. using visible and infrared digital images recorded during the experiments. The thermal imaging camera had an accuracy of  $\pm 2^{\circ}\text{C}$ , so it did not significantly affect the accuracy in estimating the jet fire flame length (Carboni et al.) which was provided as result in form of a table. The flame lengths of the tested jet fires ranged between 2 m and 7 m.

In Figure 34, a comparison is made between the simulation results and the experimental results. Generally, both software tools tend to overpredict the flame length. The only exceptions, where the flame length was slightly underpredicted, occurred in the simulated experiments involving a release hole with a diameter of 1 mm.

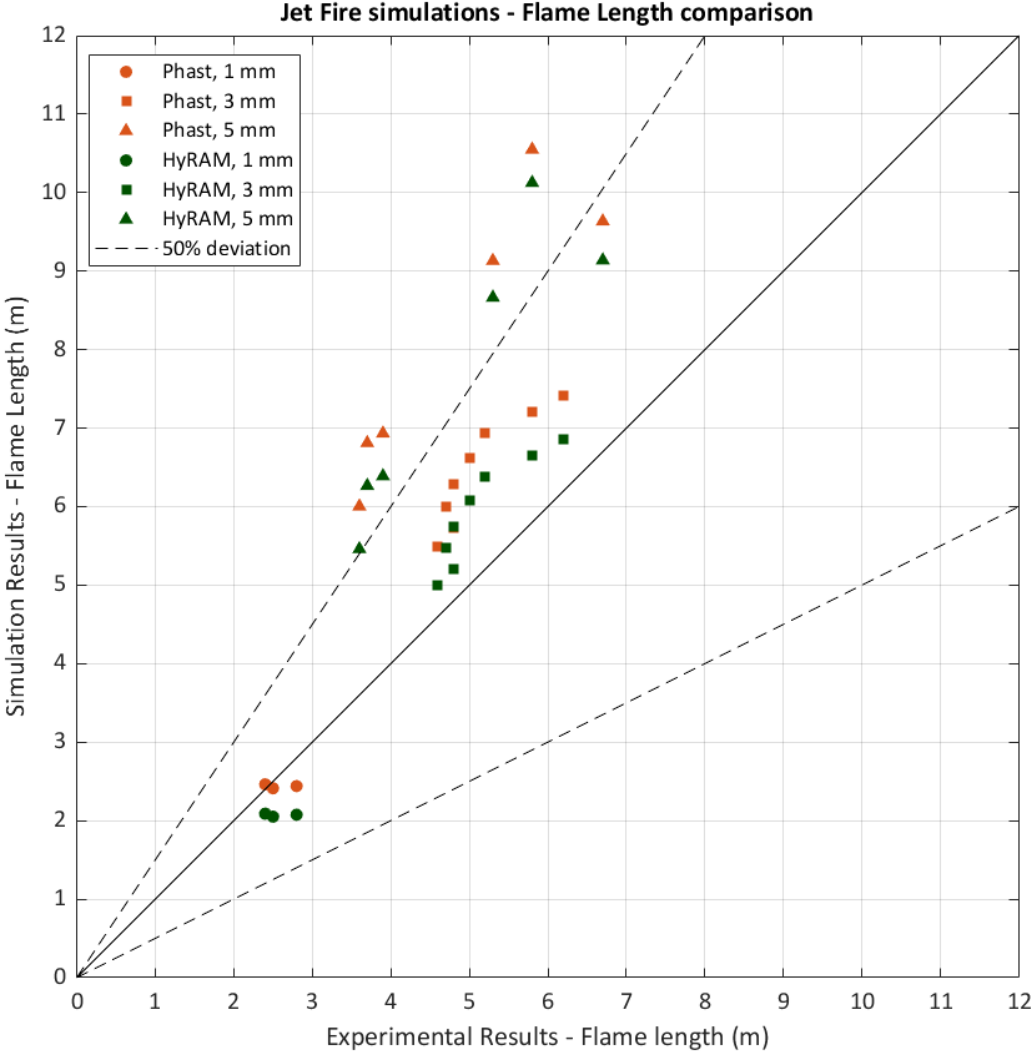


Figure 34: Jet fire flame length. Comparison between experimental results and simulation results.

A pronounced overprediction was observed in the tests conducted with a 5 mm release hole diameter, as shown in Table 12. The discrepancy between the simulated and experimental results was higher than 50%. When hydrogen is released from a pressurized vessel, producing a jet fire, it is expected that, at constant pressure, an increase in the diameter of the release nozzle will result in a longer flame length (HyResponders, 2021). This is because a larger diameter allows more hydrogen to be released and participate in the combustion reaction. Additionally, for a fixed release hole diameter, an increase in pressure should also result in a longer flame length.

Both Phast and HyRAM accurately predicted the theoretical behaviour using an extensively validated correlation for calculating flame length, which is directly proportional to the release nozzle diameter to the first power. During the validation process, HyRAM consistently predicted the flame length of hydrogen jet fires accurately (Ehrhart et al., 2021). Similarly, the Miller model used in Phast has been extensively validated with experimental results from both pilot and full-scale experiments (Miller, 2017).

One reason for the significant difference between measured and simulated flame lengths could be an experimental error in the flame length measurements. In the study by Carboni et al., flame length was determined using a temperature plot contour displayed in an IR image. There is a possibility that the image captured did not represent the stationary phase of the flame, where the maximum flame length occurs, but rather a moment shortly after, when the flame starts to extinguish.

In contrast, Carboni et al. suggest that the unexpectedly low flame lengths measured with a 5 mm release hole, compared to other experiments, are due to the lower pressures at which these specific experiments were conducted. According to their study, this lower pressure could result in mass transfer limitations and reduced turbulence, which in turn limit the availability of reactants and the efficiency of mixing. These factors can slow down the combustion rates, leading to shorter flame lengths despite the larger release hole diameter. Based on this explanation, it may be concluded that the two software tools do not effectively predict the length of jet fire flames when the pressure falls below a certain threshold.

Table 12: Comparison of the flame lengths for the tests using a 5 mm diameter release nozzle.

<b>Test ID</b>	<b>Experimental value (m)</b>	<b>Phast result (m)</b>	<b>HyRAM result (m)</b>
<b>2.12</b>	5.8	10.55	10.13
<b>2.13</b>	6.7	9.63	9.14
<b>2.14</b>	5.3	9.13	8.66
<b>2.15</b>	3.9	6.93	6.39
<b>2.16</b>	3.7	6.81	6.27
<b>2.17</b>	3.6	6.00	5.46



## 6.2.2 Experimental study – Large scale hydrogen jet fires

The benchmark exercise in this case is based on the study “Large-Scale Hydrogen Jet Flame Radiant Fraction Measurements and Modeling” by Ekoto et al. (2012). In the two tests conducted, compressed hydrogen gas at approximately 60 barg was released through a horizontally oriented pipe. For Test 1, the pipe had an internal diameter ( $D_N$ ) of 20.9 mm, and for Test 2, the diameter was 52.5 mm. The release point was situated 3.25 meters above the ground. A 25 m by 15 m concrete pad was positioned in front of the release location to prevent the entrainment of surface dirt particles. Additionally, steel sheeting was placed directly beneath the release path to protect the pad from spallation.

The experimental setup is depicted in Figure 35. Incident thermal radiation was measured at 13 locations using radiometers with an accuracy of  $\pm 5\%$ . Four radiometers (RAD01, RAD02, RAD03, and RAD04) were placed perpendicular to the predicted flame centre, while an additional radiometer (RAD12) was positioned on the opposite side to check for flame symmetry (Ekoto et al., 2012). Four more radiometers (RAD05, RAD06, RAD10, and RAD11) were located 5 meters downstream from the predicted flame centre. Two radiometers (RAD07 and RAD09) were oriented at a  $45^\circ$  angle relative to the release axis. Finally, two sensors were placed along the release axis, one downstream (RAD08) and one upstream (RAD13). Video recordings were acquired at three locations around the test area, while the flame envelope was measured using two IR cameras positioned as shown in Figure 35.

Wind speed and direction, ambient temperature, and relative humidity (RH) were measured approximately 100 meters upstream from the release point. Measurements were taken over discrete averaging periods to ensure that representative mean values were obtained (Ekoto et al., 2012). The boundary and ambient conditions for the two tests are detailed in Table 13, with wind direction indicated by the angle relative to the release direction.

Table 13: Experimental and ambient conditions reported in Ekoto et al. experimental study.

<b>Experiment ID</b>	<b><math>D_N</math> (mm)</b>	<b>P storage (barg)</b>	<b>T storage (K)</b>	<b>RH (%)</b>	<b>T ambient (K)</b>	<b>P ambient (bar)</b>	<b>Wind speed (m/s)</b>	<b>Wind direction (<math>^\circ</math>)</b>
<b>3.1</b>	20.9	59.8	308.7	94.3	280	1.022	2.84	1.5
<b>3.2</b>	52.5	62.1	287.8	94.5	280	1.011	0.83	-43

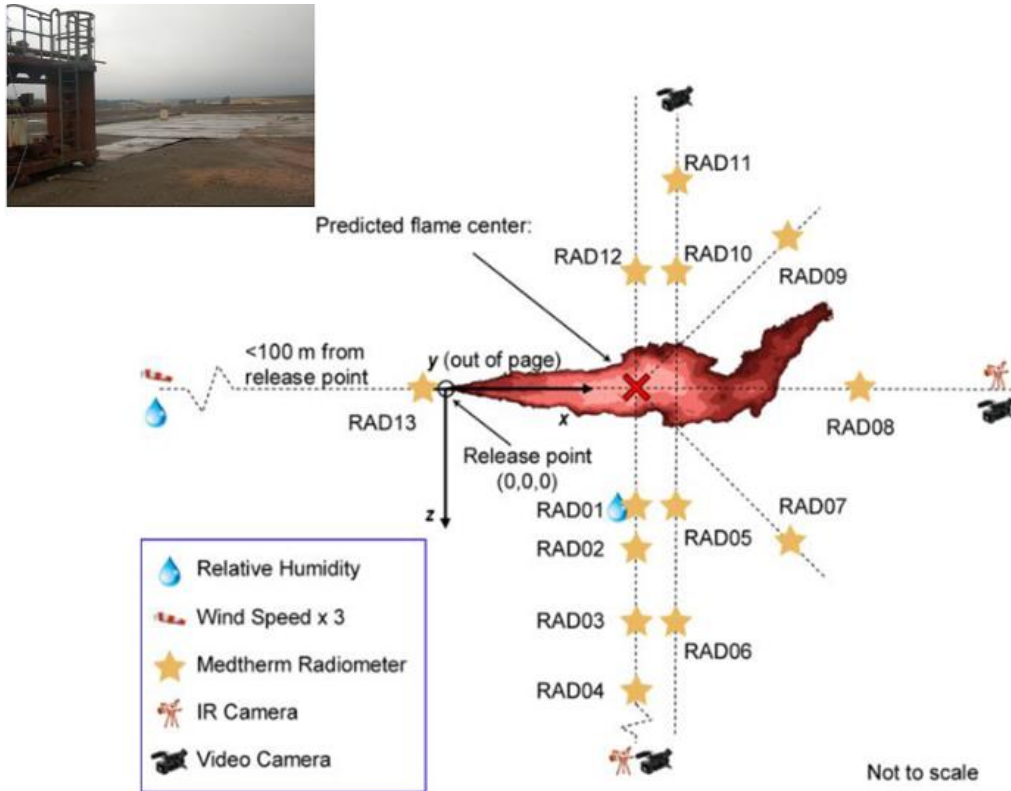


Figure 35: Schematic of the experimental set up used in “Large-Scale Hydrogen Jet Flame Radiant Fraction Measurements and Modeling” experimental study by Ekoto et al., 2012.

### 6.2.2.1 Modelling

This experimental study provided a detailed description of the weather conditions, except for the atmospheric stability class. This parameter was determined based on the Pasquill classification and by examining the photo of the experimental site shown in Figure 35. Given that the site appeared to be completely overcast, the atmospheric stability class was classified as D, regardless of wind speed.

To obtain radiation results at specific points located in the x, y, and z directions, corresponding to the positions of the radiometers, a two-step simulation process was conducted using Phast. Initially, a pressure vessel was defined with operating pressure and temperature conditions as indicated in Table 13. This calculation provided the source term for the jet fire, including the mass flow rate, leak duration and dispersion results. The only results regarding the radiation from the jet fire were the radiation on the jet fire centreline as a function of the downwind distance and the radiation ellipse.

To achieve a more comprehensive set of radiation results, the discharge and dispersion data from the leak were used to create a standalone equipment simulating the jet fire. This model calculates the shape and intensity of the flame and provides a wider range of radiation results. It does not

perform the discharge and dispersion calculations, which are required as inputs. For this reason, the standalone model can be used when the source term of the jet fire is already known. Alternatively, it can be directly created from standard equipment defined in the workspace, where the source term and dispersion calculations are performed by the software.

To retrieve radiation results in HyRAM, the Radiative Heat Flux window was used. The discharge coefficient calculated by Phast was employed as an input parameter. Additionally, the ambient humidity was set to the value specified in the experimental study. HyRAM enables the definition of up to seven different points for radiation calculations simultaneously, while Phast only allows radiation to be calculated at one point at a time.

The coordinates of the radiometers were adapted to the coordinate system used by the two software programs. In the experimental study, the release point was set at the origin of the coordinate system, with the y-axis corresponding to the elevation, where the ground level was identified by the coordinate  $y = -3.25$  m.

In Phast, the release point is located at  $x = 0$  m,  $y = 0$  m, and at the defined elevation, meaning that in Phast the coordinate  $z = 0$  m always represents the ground level. On the other hand, HyRAM uses the coordinate system depicted in Figure 35, where the orientation of the three axes corresponds to the one used in the experimental study. Since HyRAM does not allow the elevation to be specified, the release point is located at the coordinates  $x = 0$  m,  $y = 0$  m, and  $z = 0$  m. Therefore, the coordinates of the radiometers in HyRAM are the same as those reported in the experimental study. Table 14 and Table 15 provide a summary of the coordinates used.

Table 14: Coordinates (x,y,z) used in HyRAM and Phast to identify the position of the radiometers for simulated experiment 3.1.

TEST 1	Experimental and HyRAM			Phast		
	X (m)	Y (m)	Z (m)	X (m)	Y (m)	Z (m)
<b>RAD01</b>	11.0	-2.4	7.5	11.0	7.5	0.85
<b>RAD02</b>	11.0	-1.7	12.5	11.0	12.5	1.55
<b>RAD03</b>	11.0	-1.9	15.0	11.0	15.0	1.35
<b>RAD04</b>	11.0	-0.3	17.5	11.0	17.5	2.95
<b>RAD05</b>	16.0	-2.4	7.5	16.0	7.5	0.85
<b>RAD06</b>	16.0	-1.8	12.5	16.0	12.5	1.45
<b>RAD07</b>	21.6	-1.8	10.6	21.6	10.6	1.45
<b>RAD08</b>	26.0	-1.5	0.0	26.0	0.0	1.75
<b>RAD09</b>	21.6	-1.2	-10.6	21.6	-10.6	2.05
<b>RAD10</b>	16.0	-1.3	-7.5	16.0	-7.5	1.95
<b>RAD11</b>	16.0	-0.5	-12.5	16.0	-12.5	2.75
<b>RAD12</b>	11.0	-1.8	-7.5	11.0	-7.5	1.45
<b>RAD13</b>	-1.0	-1.0	0.0	-1.0	0.0	2.25

Table 15: Coordinates (x,y,z) used in HyRAM and Phast to identify the position of the radiometers for simulated experiment 3.2.

TEST 2	Experimental and HyRAM			Phast		
	X (m)	Y (m)	Z (m)	X (m)	Y (m)	Z (m)
<b>RAD01</b>	23.0	-2.4	15.0	23.0	15.0	0.85
<b>RAD02</b>	23.0	-1.7	20.0	23.0	20.0	1.55
<b>RAD03</b>	23.0	-1.9	30.0	23.0	30.0	1.35
<b>RAD04</b>	23.0	-0.3	40.0	23.0	40.0	2.95
<b>RAD05</b>	28.0	-2.4	15.0	28.0	15.0	0.85
<b>RAD06</b>	28.0	-1.8	30.0	28.0	30.0	1.45
<b>RAD07</b>	40.7	-1.8	17.7	40.7	17.7	1.45
<b>RAD08</b>	48.0	-1.5	0.0	48.0	0.0	1.75
<b>RAD09</b>	40.7	-1.2	-17.7	40.7	-17.7	2.05
<b>RAD10</b>	28.0	-1.3	-15.0	28.0	-15.0	1.95
<b>RAD11</b>	28.0	-0.5	-30	28.0	-30	2.75
<b>RAD12</b>	23.0	-1.8	-15.0	23.0	-15.0	1.45
<b>RAD13</b>	-1.0	-1.0	0.0	-1.0	0.0	2.25

For ALOHA simulations, the site location and specific times of the experiments were required as inputs. The study of Ekoto et al. specify that the experiments took place on the Spadeadam Test Site in North Cumbria, UK. The latitude of 55°1'30''N and longitude of 2°36'8''W (GeoHack) of the site were specified in ALOHA. For the specific times of the experiments, the default settings of ALOHA were used.

All necessary atmospheric conditions were provided, except for the relative humidity values which required approximation because ALOHA only accepts integer inputs. The experimental study reported relative humidity values of 94.3% and 94.5% for tests 1 and 2, respectively. For the simulated experiment 3.1, the relative humidity in ALOHA was set to 94%, and for simulated experiment 3.2, it was set to 95%. The stability class suggested by ALOHA was D, which corresponds to the stability class used in Phast. For simulated experiment 3.2, a wind velocity of 1m/s was used, since the value of 0.83 m/s (Ekoto et al, 2012) is below the software limit. ALOHA can model a jet fire originating from gas pipelines and tank sources. For this study, the source term that best described the experimental setup was a leak from a tank. The tank volume was set to match the volume specified in Phast. To define the leak, a circular opening with the diameters specified in Table 13 was used. When a leak burns as a jet fire, ALOHA calculates the thermal radiation contours for the specified radiation levels.

The possibility of defining a direct source in ALOHA was also explored. This feature requires specifying the discharge rate, the release duration (for continuous releases), and the source height. The discharge rate and release duration were set according to the values calculated by Phast, while the source height was defined as specified in the experimental study. When the release is not a

ground release, meaning that the height is not equal to zero, ALOHA can perform the calculations only with the Gaussian model. The direct source does not allow for the calculation of a jet fire; it only calculates concentration contours, which correspond to the flammable area of the cloud.

#### **6.2.2.2 Results of the simulations**

The graphs generated as results from Phast include graphs of the radiation ellipse characterizing the jet fire and the radiation as a function of the downwind distance. Figures 36 and Figure 37 show the radiation ellipses obtained from the simulations where the radiation contours depicted are 3 kW/m<sup>2</sup>, 5 kW/m<sup>2</sup>, and 8 kW/m<sup>2</sup>. For each radiation level, the ellipse produced by the jet fire in the specified wind direction and the effect zone are represented. The ellipse shows that the radiation has a minor impact also on the area upstream of the release point. The effect zone encompasses all the radiation ellipses that the jet fire can produce for all possible wind directions. It is depicted as a circle with a radius equal to the maximum distance at which a specific radiation value is reached.

In the graph showing the radiation as a function of the downwind distance, the y coordinate is zero, indicating the direction of the release, and the z-axis represents the height of interest, set at 3.25 m, which corresponds to the elevation of the release point (Figure 38).

HyRAM provided a visualization of the flame through temperature plots, as illustrated in Figure 39. These plots show that as the release hole diameter increases, the flame length also increases. Notably, the largest flame exhibits a longer segment influenced by wind or buoyancy. In addition, near the release point, the temperature is low, indicating that the combustion reaction is not occurring in this region. This segment represents the lift-off.

From the Radiative Heat Flux window of HyRAM, radiation contours for fixed radiation levels can also be obtained. These radiation ellipses produced by the jet fire are represented in three different planes: the XZ plane (top view of the jet fire), the XY plane (side view) and the YZ plane (view at a fixed downwind distance). The results are shown in Figure 40.

In the XY and YZ representations, it is evident that the radiation contours account for the fact that the flame is partially lifted. Specifically, the XZ plane reveals that the flame tip is approximately 3 meters above the release point for simulated experiment 3.1, and about 15 meters above the release point for simulated experiment 3.2.

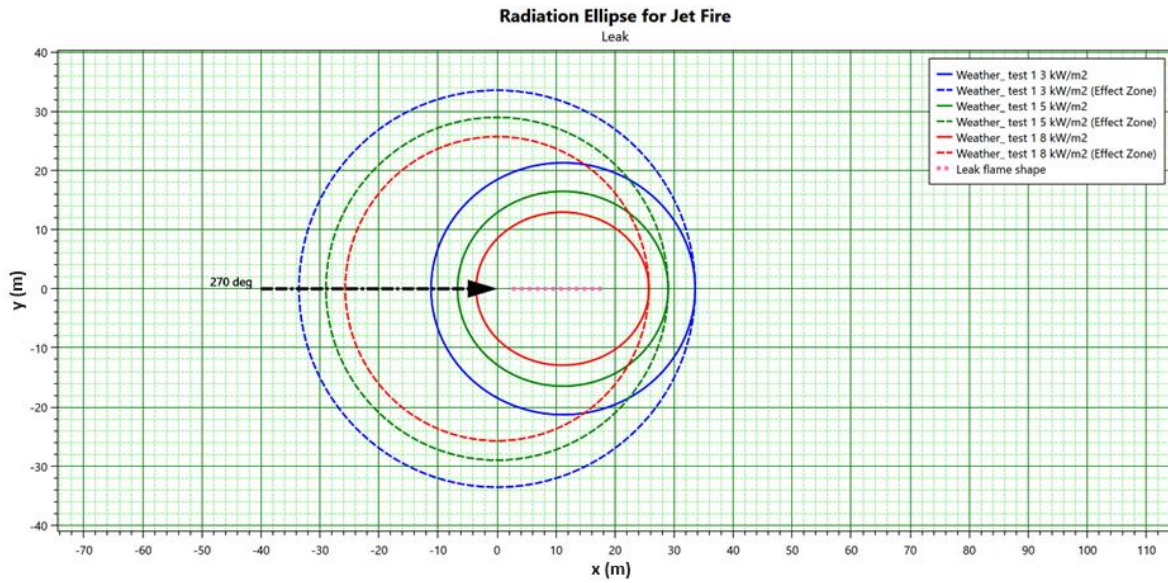


Figure 36: Graph generated by Phast representing the radiation ellipse and effect zone results for simulated experiment 3.1.

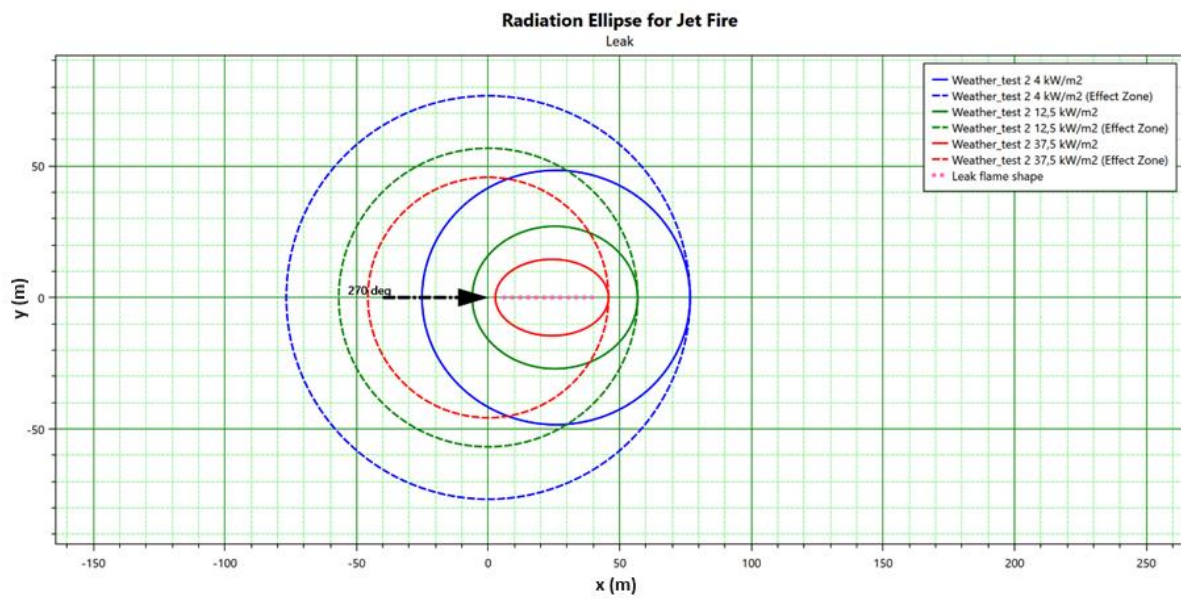
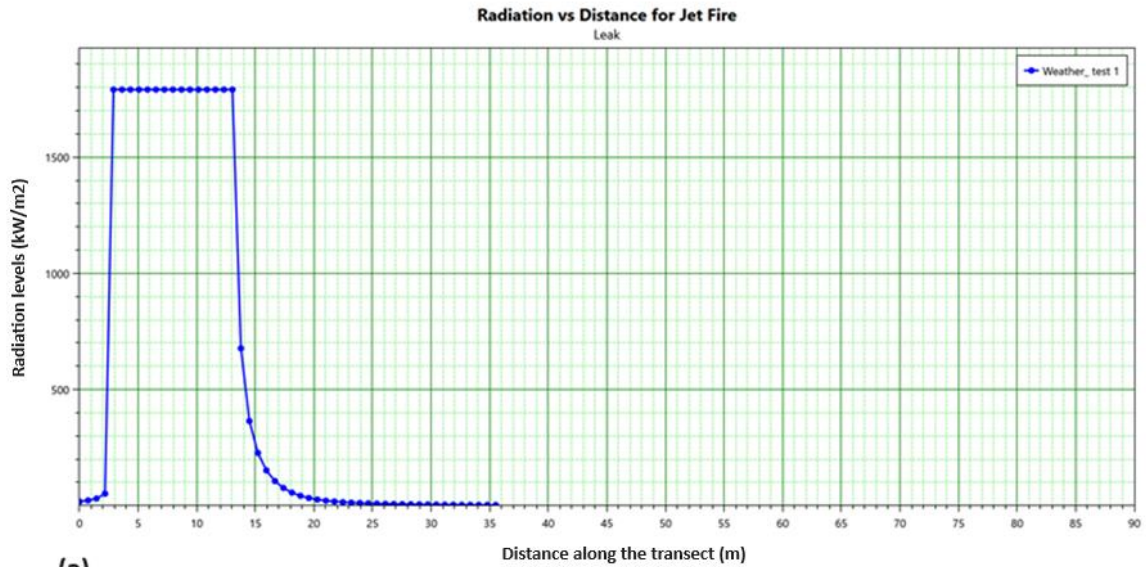
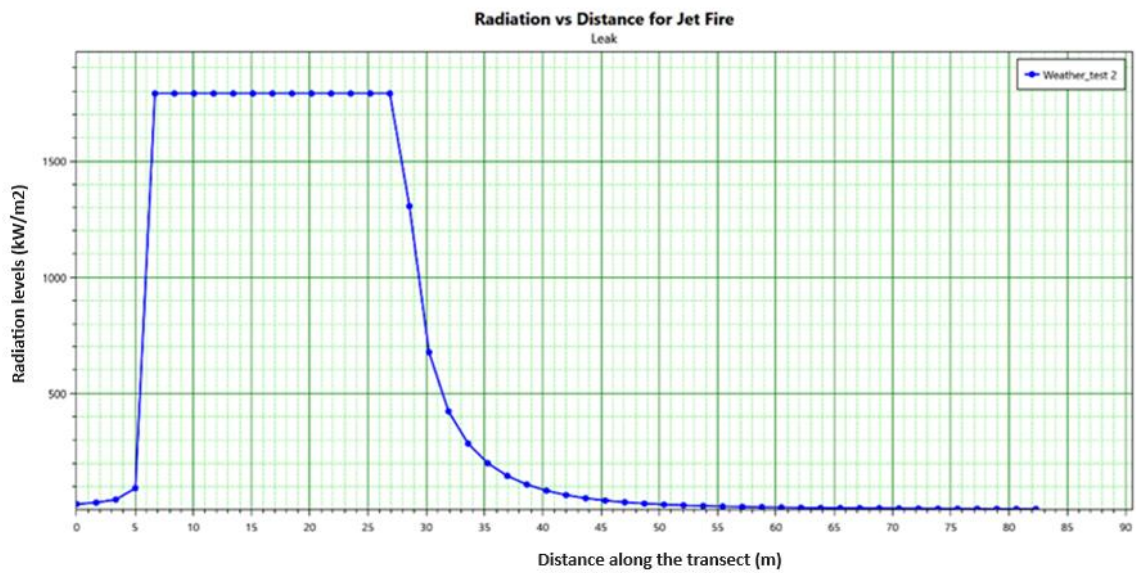


Figure 37: Graph generated by Phast representing the radiation ellipse and effect zone results for simulated experiment 3.2.



(a)



(b)

Figure 38: Graph generated by Phast representing the radiation (kW/m<sup>2</sup>) in function of the downwind distance (m) for (a) simulates experiment 3.1 and (b) simulated experiment 3.2.

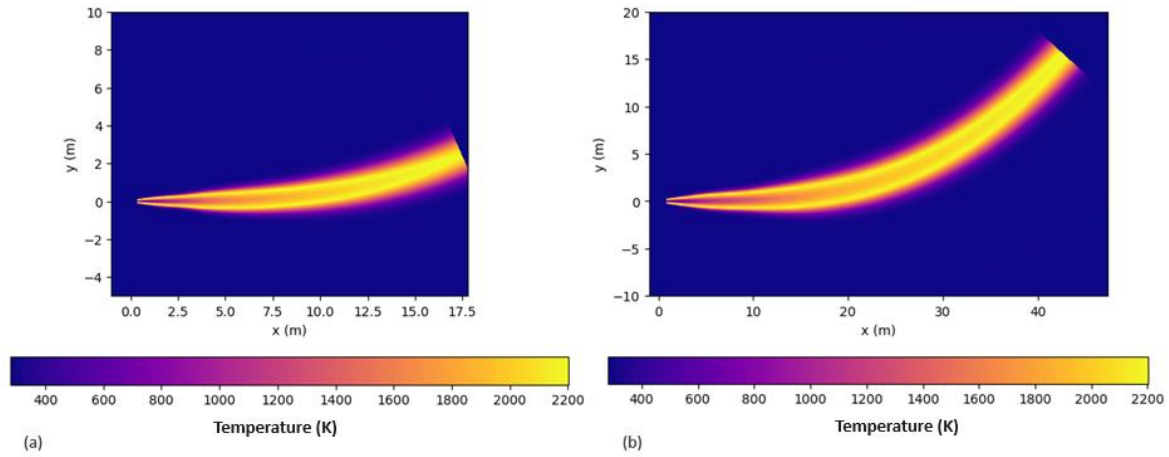


Figure 39: Temperature plots for (a) simulated experiment 3.1 and (b) simulated experiment 3.2 obtained with HyRAM.

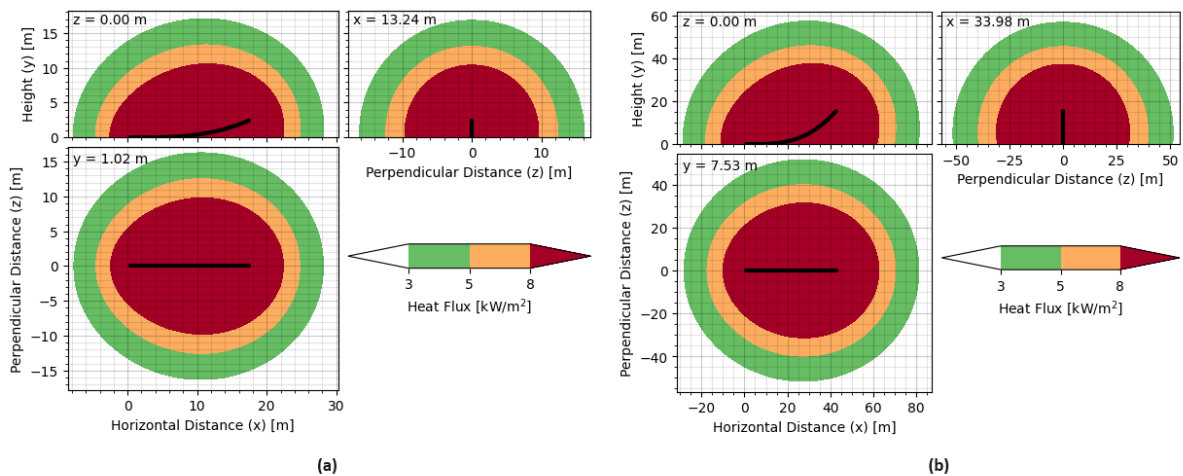


Figure 40: Radiation ellipses for (a) simulated experiment 3.1 and (b) simulated experiment 3.2 obtained with HyRAM.

The results from the ALOHA simulations for experiments 3.1 and 3.2 are shown as radiation contours for the defined radiation levels of 3.0 kW/m<sup>2</sup>, 5.0 kW/m<sup>2</sup>, and 8.0 kW/m<sup>2</sup> in Figure 40. The maximum flame length calculated by ALOHA is 5 meters for simulated experiment 3.2 and 2 meters for simulated experiment 3.1. These values are significantly smaller compared to the measured flame lengths in the study by Ekoto et al., which were an order of magnitude larger. This discrepancy arises because the Jet Fire model in ALOHA is designed for an upward vertical jet release, such as a vertically oriented pipe or a hole at the top of a tank (NOAA, 2013).

In Figure 42, the concentration contours for the UFL, LFL, and 0.5LFL are depicted. These results were obtained by setting a direct source in ALOHA using the discharge rates and duration calculated by Phast. The leak is represented with a jet shape. However, a comparison with the



results from Phast shows that the maximum downwind distances for the defined concentration levels are an order of magnitude higher in ALOHA than those calculated by Phast. Specifically, for simulated experiment 3.1, ALOHA calculates the LFL concentration distance as 136 m, while Phast calculates it as 27.76 m. For simulated experiment 3.2, ALOHA calculates the LFL concentration distance as 440 m, whereas Phast calculates it as 69.51 m.

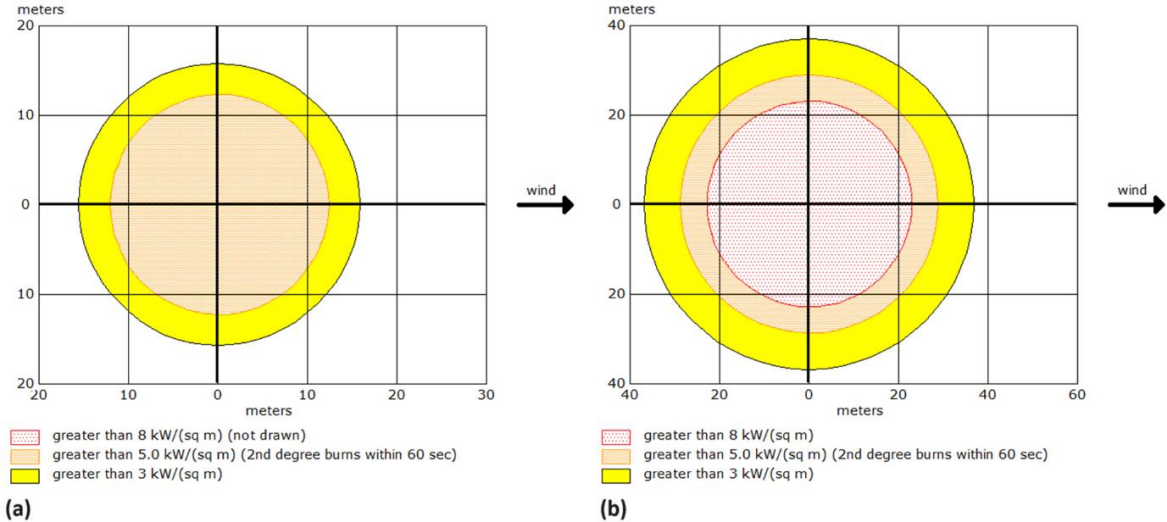


Figure 41: Radiation contours generated by ALOHA for simulated experiments (a) 3.1 and (b) 3.2.

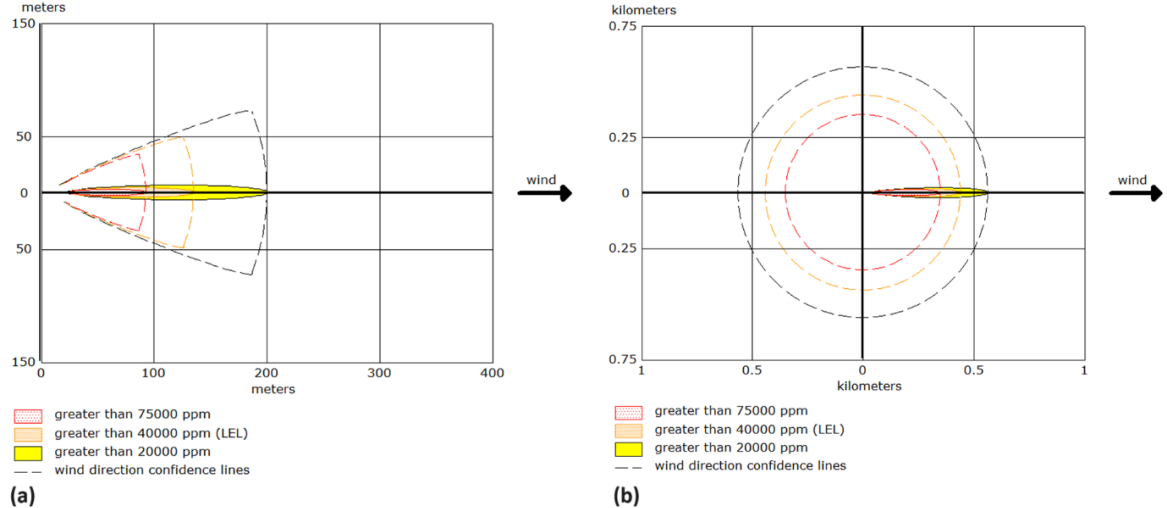


Figure 42: Concentration contours generated by ALOHA for simulated experiments (a) 3.1 and (b) 3.2.

Table 16 presents the dimensions of the radiation ellipses calculated by Phast, HyRAM, and ALOHA. The values computed by HyRAM are obtained from the graphs in Figure 40.

The smaller radiation contours generated by ALOHA can be attributed to its simulation of a vertical jet fire. Overall, Phast tends to predict larger downwind distances for the radiation contours, while HyRAM predicts larger extents of the contours in the direction perpendicular to the jet direction (y-axis for Phast and z-axis for HyRAM).

Table 16: Comparison of radiation ellipses dimensions for simulated experiments 3.1 and 3.2.

Software	Simulated experiment	Radiation level (kW/m <sup>2</sup> )	Maximum downwind distance (m)	Ellipse half length (m)	Ellipse half width (m)
Phast	3.1	3	33.55	22.37	11.19
		5	28.98	16.47	11.15
		8	25.71	12.93	11.08
	3.2	3	83.75	57.92	55.66
		5	71.85	46.12	43.27
		8	63.25	37.67	34.14
HyRAM	3.1	3	28	18	16.5
		5	24.3	14.3	12.7
		8	22	12.3	10
	3.2	3	82	54.8	52.5
		5	70	43.8	40.5
		8	62.5	36.25	32
ALOHA	3.1	3	16	-	-
		5	13	-	-
		8	<10 m	-	-
	3.2	3	37	-	-
		5	29	-	-
		8	23	-	-

### 6.2.2.3 Discussion

Figure 43 shows the comparison between the radiation values (kW/m<sup>2</sup>) calculated by the software tools and the experimental values measured by the radiometers. In the graph, the bisector represents the experimental results, with error bars indicating the  $\pm 5\%$  accuracy of the radiometers used in the experimental study by Ekoto et al.

For simulated experiment 3.1 (test 1), Phast consistently overpredicts the radiation levels or makes predictions within the error margin, while HyRAM tends to underpredict the radiation levels. For simulated experiment 3.2 (test 2), both software tools underpredict the radiation values at the radiometer positions.

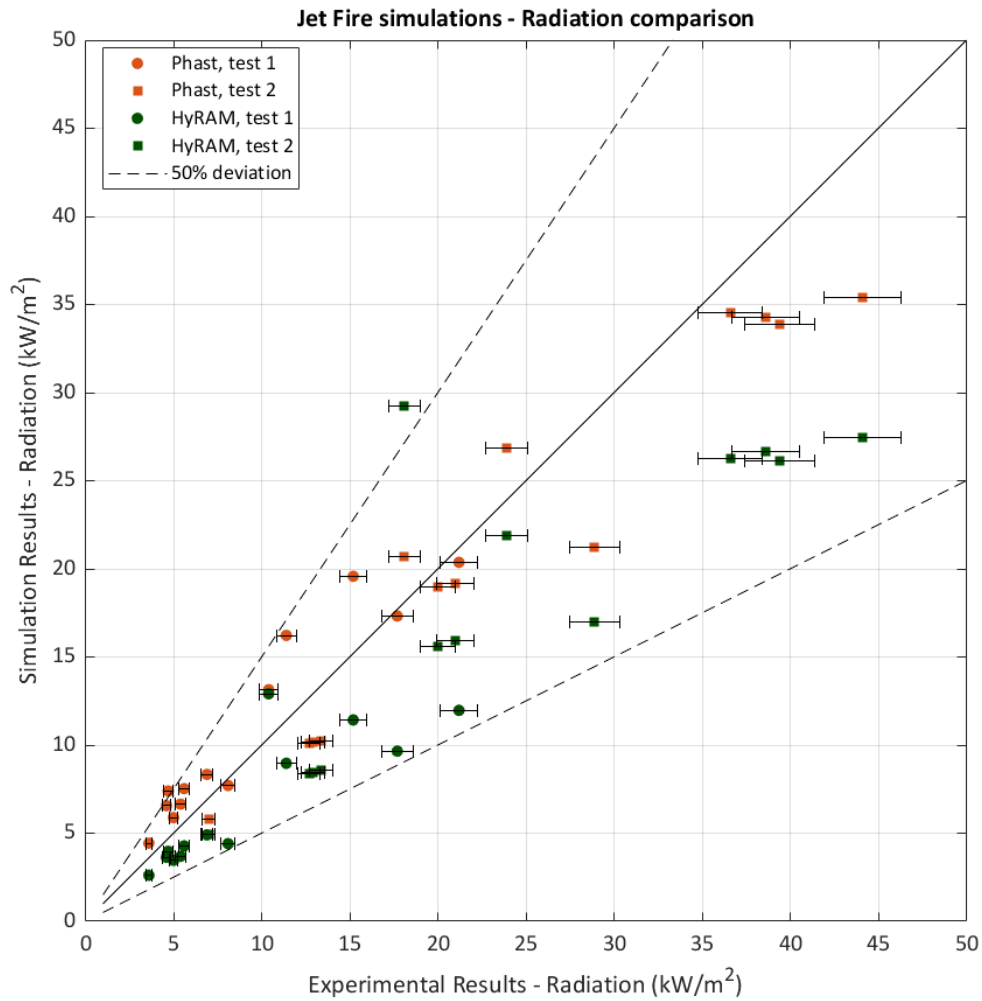


Figure 43: Jet fire radiation. Comparison between experimental results and simulation results.

The experimental study also provided the flame lengths for the two jet fires, determined from video recordings. These flames exhibited significant visible luminosity, which is typically not seen in smaller-scale hydrogen flames (Ekoto et al., 2012). The flame lengths predicted from Phast and HyRAM are larger than the experimental value for experiment 3.1 (Table 17). However, for simulated experiment 3.2, both software tools underpredict the flame length. Phast's prediction is approximately 10% shorter, while HyRAM's prediction is less than 1% shorter. Since the deviation in the calculated flame length in this case is not significant, it can be concluded that the flame length was accurately predicted in the case of the large-scale hydrogen jet fire.

Table 17: Flame length comparison with experimental results.

Test		Flame length (m)
3.1	Experimental	17.4
	Phast	18.43
	HyRAM	17.76
3.2	Experimental	48.5
	Phast	43.24
	HyRAM	47.33

One reason for the underprediction of radiation lies in the configuration of the experimental setup. Directly in front of the release point, a concrete pad was placed on the ground to prevent the entrainment of dirt particles and it was covered with steel sheeting (Ekoto et al.), as shown in Figure 35. Given the large scale of the second experiment, the jet was quite close to the ground. This is illustrated in Figure 44, where, one second after the release began, hydrogen in a flammable concentration almost reached the ground. Consequently, it is possible that part of the radiation emitted by the jet fire in this second experiment was reflected by the steel on the ground, thereby increasing the radiation detected by the radiometers. Since the two software tools are not capable to account for the reflectance of the material constituting the ground, this increase in the radiation level is not calculated.

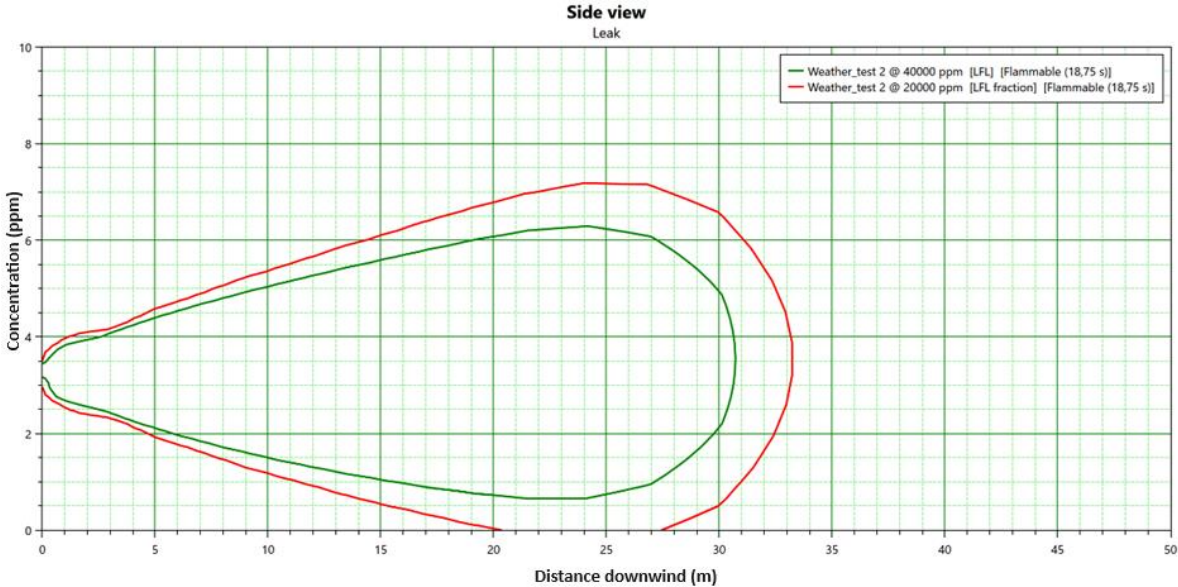


Figure 44: Side view of the simulated experiment 3.2 one second after the start of the release generated by Phast. LFL and 0.5LFL contours.

## 7 Conclusion

Accidents involving hydrogen have resulted in fatalities, injuries, and building damage, highlighting the urgent need for enhanced safety measures. Quantitative Risk Assessment is vital for identifying hazards and developing risk reduction strategies, combining failure probability with consequences to quantify overall risk. Consequence analysis evaluates impacts on human health and the environment by modelling dispersion, radiation and overpressure from accidental releases. Various software tools are employed for consequence analysis, each with distinct models and assumptions. Accuracy in consequence estimation directly influences risk assessments, underscoring the need to compare tools for understanding strengths and limitations.

In this thesis a benchmark analysis of Phast, HyRAM and ALOHA software tools for evaluating possible accidents related to hydrogen storage systems has been conducted. These studies were chosen in order to provide the ground truth with which the simulation results have been compared. Three different experimental studies were chosen to assess dispersion, flame length, and radiation from horizontal hydrogen jets. Simulated experiments covered pressure ranges of 60 to 400 bar, with release hole diameters spanning from 0.5 mm to 52.5 mm for large-scale hydrogen jets.

ALOHA demonstrated significant limitations in this study. It could not produce results for most of the experimental studies involving small and medium-scale hydrogen jets because it does not display distances shorter than 10 meters. Additionally, ALOHA is restricted to simulating vertical jet fires, providing outcomes only for flame length and radiation contours. For dispersion analysis, ALOHA employs a Gaussian model for buoyancy-neutral gases and a heavy gas model. These models are not well-suited for hydrogen, which is lighter than air and for which buoyancy significantly affects dispersion. Consequently, ALOHA's models are less effective for accurately analysing the consequences of hydrogen releases in the selected experimental studies.

Phast allows for the simulation of various scenarios and the generation of different types of results. When assessing hydrogen dispersion following a leak from a small hole in a pressurized tank, Phast could precisely simulate the position of sampling probes and the time evolution of hydrogen concentration. This enabled the determination of the moment at which a stationary regime is reached. In this case, the simulated results slightly underpredicted the experimental values, suggesting possible limitations in the software's functionality. It is important to consider that these results also depend on assumptions regarding weather conditions and the extraction of results from the experimental study.

For characterizing hydrogen jet fires, Phast uses the Miller model, which is specific to non-hydrocarbon/low-luminosity gases and accounts for buoyancy and wind effects. The flame length predicted by Phast was generally greater than the measured flame length. For assessing radiation emitted from a hydrogen jet fire, Phast could accurately simulate the positioning of radiometers.

The results showed that Phast overpredicted radiation levels in one test and underpredicted them in another. This highlights a limitation of Phast in accounting for the material of the ground and its reflectance, which could affect radiation levels reaching certain points.

HyRAM is a more simplified software as it does not account for wind effects or atmospheric stability. Additionally, the elevation of the release cannot be specified, meaning the interaction with the ground is not simulated. The results for dispersion generally showed an underprediction of concentrations. Moreover, it was not possible to set specific positions for calculating concentrations, so the values compared with experimental data were centreline concentrations. For jet fire characterization, the temperature plots indicated that the buoyancy effect was considered since the jet lifted in its final segment. Although HyRAM overestimated flame length, this overestimation was less pronounced than that of Phast. For radiation assessment, HyRAM allowed for the specification of coordinates to simulate the position of radiometers accurately. The calculated radiation values consistently underpredicted the experimental values.

The main limitations of this thesis work arise from several key factors. First, the assumptions made to gather all necessary inputs, particularly regarding atmospheric conditions and wind, introduce uncertainties. These assumptions may not accurately represent real-world ambient variables, such as temperature variations during experiments and wind velocity fluctuations. Secondly, the obtained results depend on experimental measurements where the potential errors are often unknown. This introduces an additional layer of uncertainty in validating the simulation outcomes. Lastly, the choice of experimental studies forming the ground truth is crucial, as the integral models implemented in the software tools are not capable of simulating interactions with complex geometries in the surroundings.

In future research, expanding the selection of experimental studies used for validation is recommended. This expansion should encompass a broader range of conditions and scenarios, including different scales of hydrogen releases and various environmental settings. Additionally, to gain a comprehensive understanding of the capabilities of the software tools in simulating hydrogen accidents, the analysis should extend to scenarios involving explosions and accidents stemming from liquid hydrogen storage.

Considering the highlighted characteristics of the software and its accuracy in obtaining results, Phast is recommended for analysing hydrogen jet dispersions and hydrogen jet fires. It should be noted, however, that further validation of the software is necessary for large-scale jets.

## **Glossary**

**ALOHA** Areal Location Of Hazardous Atmospheres

**CAMEO** Computer-Aided Management of Emergency Operations),

**COPV** Composite Pressure Vessel

**DNV** Det Norske Veritas

**EPA** Environmental Protection Agency

**GHS** Globally Harmonized System

**HIAD** Hydrogen Incidents and Accidents Database

**HyRAM+** Hydrogen Plus Other Alternative Fuels Risk Assessment Model

**ICSC** International Chemical and Safety Cards

**LOHC** Liquid Organic Hydrogen Carriers

**MOF** Metal Organic Frameworks

**NOAA** National Oceanic and Atmospheric Administration

**OSHA** Occupational Safety and Health Administration

**Phast** Process hazard analysis software tool

**QRA** Quantitative Risk Assessment

**UDM** Unified Dispersion Model

## References

- Abohamzeh, E., Salehi, F., Sheikholeslami, M., Abbassi, R., & Khan, F. (2021). Review of hydrogen safety during storage, transmission, and applications processes. *Journal of Loss Prevention in the Process Industries*, 72, 104569. <https://doi.org/10.1016/j.jlp.2021.104569>
- Barthelemy, H., Weber, M., & Barbier, F. (2017). Hydrogen storage: Recent improvements and industrial perspectives. *International Journal of Hydrogen Energy*, 42(11), 7254–7262. <https://doi.org/10.1016/j.ijhydene.2016.03.178>
- Bengaouer, A., Cariteau, B., Makarov, D., Molkov, V., Papanikolaou, E., Saffers, J.-B., Tkatschenko, I., & Venetsanos, A. (2009). Safety of Hydrogen as an Energy Carrier. ALLOWABLE HYDROGEN PERMEATION RATE FOR AUTOMOTIVE APPLICATIONS Deliverable D74 (InsHyde)-FINAL with Corr.1.
- Bhutta, K. S., & Huq, F. (1999). Benchmarking - best practices: an integrated approach. *Benchmarking: An International Journal*, 6(3), 254–268.
- Cadwallader, L. C., & Herring, J. S. (1999). Safety Issues with Hydrogen as a Vehicle Fuel.
- Campari, A., Nakhal Akel, A. J., Ustolin, F., Alvaro, A., Ledda, A., Agnello, P., Moretto, P., Patriarca, R., & Paltrinieri, N. (2023). Lessons learned from HIAD 2.0: Inspection and maintenance to avoid hydrogen-induced material failures. *Computers & Chemical Engineering*, 173, 108199. <https://doi.org/10.1016/j.compchemeng.2023.108199>
- Carboni, M., Pio, G., Mocellin, P., Pilo, F., Vianello, C., Russo, P., Maschio, G., & Salzano, E. (2022). Experimental and numerical characterization of hydrogen jet fires. *International Journal of Hydrogen Energy*, 47(51), 21883–21896. <https://doi.org/10.1016/j.ijhydene.2022.05.010>
- Department of energy. (2001). Hydrogen properties. In *Hydrogen Fuel Cell Engines and Related Technologies*. [https://www1.eere.energy.gov/hydrogenandfuelcells/tech\\_validation/pdfs/fcm01r0.pdf](https://www1.eere.energy.gov/hydrogenandfuelcells/tech_validation/pdfs/fcm01r0.pdf)
- DNV. Consequence analysis, Phast Software. Retrieved April 21, 2024, from <https://www.dnv.com/software/services/plant/consequence-analysis-phast/>
- DNV. (2023). Unified Dispersion Model (UDM) validation. [https://myworkspace.dnv.com/download/public/phast/technical\\_documentation/05\\_dispersion/udm/validation/UDM\\_Validation.pdf](https://myworkspace.dnv.com/download/public/phast/technical_documentation/05_dispersion/udm/validation/UDM_Validation.pdf)



- Dwivedi, S. K., & Vishwakarma, M. (2018). Hydrogen embrittlement in different materials: A review. *International Journal of Hydrogen Energy*, 43(46), 21603–21616. <https://doi.org/10.1016/j.ijhydene.2018.09.201>
- Ehrhart, B. D., Hecht, E. S., & Schroeder, B. B. (2023). *Hydrogen Plus Other Alternative Fuels Risk Assessment Models (HyRAM+) Version 5.1 Technical Reference Manual*.
- Ehrhart, B. D., Hecht, E. S., & Mohmand, J. A. (2021). *Validation and Comparison of HyRAM Physics Models*.
- Ekoto, I. W., Houf, W. G., Ruggles, A. J., Creitz, L. W., & Li, J. X. (2012). Large-Scale Hydrogen Jet Flame Radiant Fraction Measurements and Modeling. Volume 4: Pipelining in Northern and Offshore Environments; Strain-Based Design; Risk and Reliability; Standards and Regulations, 713–724. <https://doi.org/10.1115/IPC2012-90535>
- European Commission. (2020). A hydrogen strategy for a climate-neutral Europe. <https://www.eu2018.at/calendar-events/political-events/BMNT->
- European Commission. (2021). European Climate Law. <http://data.europa.eu/eli/reg/2021/1119/oj>
- E. Behrend, & Dr. U. Schmidtchen. (1995). Fortentwicklung technischer Regelwerke aus Anlaß von Schadensfällen.
- Fiorucci, A., Pontiggia, M., Derudi, M., Alba, M., Scaioni, M., Pendino, R., Uguccioni, G., & Rota, R. (n.d.). Risk assessment of dangerous products release and dispersion: a comparison between CFD and integral models.
- GeoHack. RAF Spadeadam. Retrieved May 27, 2024, from [https://geohack.toolforge.org/geohack.php?pagename=RAF\\_Spadeadam&params=55\\_01\\_30\\_N\\_002\\_36\\_08\\_W\\_region:GB\\_type:landmark](https://geohack.toolforge.org/geohack.php?pagename=RAF_Spadeadam&params=55_01_30_N_002_36_08_W_region:GB_type:landmark)
- Great Britain. HM Factory Inspectorate. (1976). *The explosion at Laporte Industries Ltd., Ilford, 5 April 1975 : a report*. H.M. Stationery Off.
- Groth, K. M., & Hecht, E. S. (2017). HyRAM: A methodology and toolkit for quantitative risk assessment of hydrogen systems. *International Journal of Hydrogen Energy*, 42(11), 7485–7493. <https://doi.org/10.1016/j.ijhydene.2016.07.002>
- Han, S. H., Chang, D., & Kim, J. S. (2014). Experimental investigation of highly pressurized hydrogen release through a small hole. *International Journal of Hydrogen Energy*, 39(17), 9552–9561. <https://doi.org/10.1016/j.ijhydene.2014.03.044>

- Hansen, O. R. (2019). Workshop Hydrogen Safety: Kjørbo-incident, overview and perspectives. [https://mozees.no/wp-content/uploads/2019/10/Hansen\\_Hydrogen-safety\\_Kjoerbo-incident-overview-and-perspectives.pdf](https://mozees.no/wp-content/uploads/2019/10/Hansen_Hydrogen-safety_Kjoerbo-incident-overview-and-perspectives.pdf)
- HyResponders. (2021). Hazard distances from hydrogen flames and fire fighting. In European Train the Trainer Programme for Responders. [https://hyresponder.eu/wp-content/uploads/2021/06/L9\\_HyResponder\\_Level4\\_210618.pdf](https://hyresponder.eu/wp-content/uploads/2021/06/L9_HyResponder_Level4_210618.pdf)
- INSTRUCCIÓ 11/2010 SIE, criteris per l'elaboració i l'avaluació de l'informe de seguretat a presentar pels establiments afectats en nivell alt per la legislació vigent en matèria d'accidents greus. (2010). <http://www.ictonline.es/pdfsno/20172542.pdf>
- Kahl, J. D. W., & Chapman, H. L. (2018). Atmospheric stability characterization using the Pasquill method: A critical evaluation. *Atmospheric Environment*, 187, 196–209. <https://doi.org/10.1016/j.atmosenv.2018.05.058>
- Løkke Jon André. (2019). THE KJØRBO INCIDENT. <https://www.sintef.no/globalassets/sintef-industri/arrangement/sh2ift/learnings-from-the-kjoerbo-incident-nel.pdf>
- Markus Sommerfeld. (2021, October 5). „Blick zurück“: Wasserstoff-Explosion bei Heraeus Quarzglas am 5. Oktober 1991 – „Tausende Schutzengel über Hanau“. <https://www.erlensee-aktuell.com/2021/10/05/blick-zurueck-wasserstoff-explosion-bei-heraeus-quarzglas-am-5-oktober-1991-tausende-schutzengel-ueber-hanau/>
- Marx, J., Cornwell, J., Marx, J. D., & Cornwell, J. B. (2001). What is a QRA and What Can It Tell You?
- Miller, D. (2017). New model for predicting thermal radiation from flares and high pressure jet fires for hydrogen and syngas. *Process Safety Progress*, 36(3), 237–251. <https://doi.org/10.1002/prs.11867>
- Molkov, V., & Saffers, J.-B. (2013). Hydrogen jet flames. *International Journal of Hydrogen Energy*, 38(19), 8141–8158. <https://doi.org/10.1016/j.ijhydene.2012.08.106>
- Moradi, R., & Groth, K. M. (2019). Hydrogen storage and delivery: Review of the state of the art technologies and risk and reliability analysis. *International Journal of Hydrogen Energy*, 44(23), 12254–12269. <https://doi.org/10.1016/j.ijhydene.2019.03.041>
- Muntasir Shovon, S., Ahamed Akash, F., Abdur Rahman, M., Rahman, W., Chakraborty, P., Monir, M. U., Sarkar, S. M., Abd Aziz, A., & Chowdhury, S. (2024). Advancements in hydrogen generation, storage, and utilizations: A comprehensive review of current

trends in Bangladesh. Energy, 292, 130477.  
<https://doi.org/10.1016/j.energy.2024.130477>

National Oceanic and Atmospheric Administration (NOAA). (2013). ALOHA® (Areal Locations Of Hazardous Atmospheres) 5.4.4: Technical Documentation.

National Oceanic and Atmospheric Administration (NOAA). (2020). ALOHA Fact Sheet.  
<https://response.restoration.noaa.gov>

NOAA, & Office of Response and Restoration. (2012, October 31). ALOHA's Limitations.  
<https://response.restoration.noaa.gov/oil-and-chemical-spills/chemical-spills/response-tools/alohas-limitations.html>

Okuyama, T., Hiroshi Koseki, J., Kobayashi, M., & Tamura, M. (1973). Explosion of Acetylene Hydrogenation Section in Ethylene Plant.

Rum, A., Landucci, G., & Galletti, C. (2018). Coupling of integral methods and CFD for modeling complex industrial accidents. *Journal of Loss Prevention in the Process Industries*, 53, 115–128. <https://doi.org/10.1016/j.jlp.2017.09.006>

Schefer, R. W., Houf, W. G., Williams, T. C., Bourne, B., & Colton, J. (2007). Characterization of high-pressure, underexpanded hydrogen-jet flames. *International Journal of Hydrogen Energy*, 32(12), 2081–2093. <https://doi.org/10.1016/j.ijhydene.2006.08.037>

Shen, R., Jiao, Z., Parker, T., Sun, Y., & Wang, Q. (2020). Recent application of Computational Fluid Dynamics (CFD) in process safety and loss prevention: A review. *Journal of Loss Prevention in the Process Industries*, 67, 104252.  
<https://doi.org/10.1016/j.jlp.2020.104252>

Spain. (2020). INTEGRATED NATIONAL ENERGY AND CLIMATE PLAN 2021-2030.

Vianello, C., Guerrini, L., Maschio, G., & Mura, A. (2014). Consequence Analysis: Comparison of Methodologies under API Standard and Commercial Software. *Chemical Engineering Transactions*, 36, 511–516. <https://doi.org/10.3303/CET1436086>

West, M., Al-Douri, A., Hartmann, K., Buttner, W., & Groth, K. M. (2022). Critical review and analysis of hydrogen safety data collection tools. *International Journal of Hydrogen Energy*, 47(40), 17845–17858. <https://doi.org/10.1016/j.ijhydene.2022.03.244>

Yadav, A., Verma, S. S., & Dafedar, A. A. (2021). Design and Development of High Pressure Hydrogen Storage Tank Using Glass Fiber as the Stress Bearing Component (pp. 41–48). [https://doi.org/10.1007/978-981-16-0976-3\\_5](https://doi.org/10.1007/978-981-16-0976-3_5)

- Yang, F., Wang, T., Deng, X., Dang, J., Huang, Z., Hu, S., Li, Y., & Ouyang, M. (2021). Review on hydrogen safety issues: Incident statistics, hydrogen diffusion, and detonation process. *International Journal of Hydrogen Energy*, 46(61), 31467–31488. <https://doi.org/10.1016/j.ijhydene.2021.07.005>
- Yin, L., & Ju, Y. (2020). Review on the design and optimization of hydrogen liquefaction processes. *Frontiers in Energy*, 14(3), 530–544. <https://doi.org/10.1007/s11708-019-0657-4>
- Yin, L., Yang, H., & Ju, Y. (2024). Review on the key technologies and future development of insulation structure for liquid hydrogen storage tanks. *International Journal of Hydrogen Energy*, 57, 1302–1315. <https://doi.org/10.1016/j.ijhydene.2024.01.093>
- Züttel, A. (2004). Hydrogen storage methods. In *Naturwissenschaften* (Vol. 91, Issue 4, pp. 157–172). <https://doi.org/10.1007/s00114-004-0516-x>

# Annex A: Sustainability report

## A.1 Sustainability matrix

In the two following paragraphs, a brief evaluation of the sustainability of the work is undertaken. In particular, it will be focused on the environmental and economic sustainability of the development of the thesis work.

### A.1.1 Environmental sustainability

The environmental impact of this work can be assessed by quantifying the main source of emissions, which is the electricity consumed during the research activities. Specifically, these emissions can be calculated based on the energy mix of Spain. Figure A1 illustrates the daily distribution of electricity production sources, with wind, photovoltaic, and nuclear energy being the three primary sources, as indicated by the Electricity Map. This tool also provides data on the average mass of equivalent CO<sub>2</sub> emissions per kWh consumed for each hour of the day (Table A1). Carbon dioxide equivalent, as defined from the European Environment Agency, is measure used to compare the emissions from various greenhouse gases based upon their global warming potential (GWP).

To estimate the amount of equivalent CO<sub>2</sub> emitted during the development of this master thesis, a standard electricity consumption value for a computer was used. On average, most of the computers use between 0.8 and 2.5 kWh per hour. The activities primarily took place in the morning, from 9 am to 1 pm. Considering four hours per day and 80 days as extent of the thesis work, the total amount of equivalent CO<sub>2</sub> emitted resulted to be between 30.4 and 95 kgCO<sub>2</sub> eq.

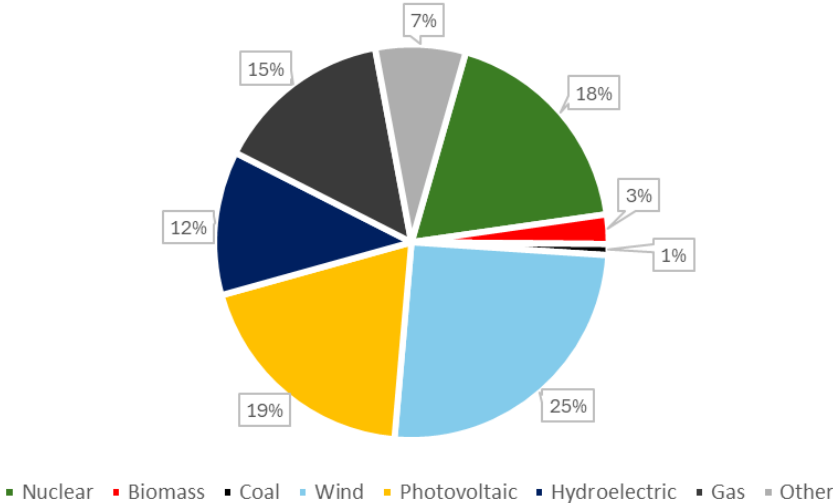


Figure A1: Energy mix of Spain.

Table A1: Equivalent CO<sub>2</sub> emission per kWh during the morning hours.

Hour	Emissions (gCO <sub>2</sub> eq/kWh)
From 9 a.m. to 10 a.m.	140
From 10 a.m. to 11 a.m.	129
From 11 a.m. to 12 a.m.	109
From 12 a.m. to 1 p.m.	97

Additional sources of emissions that should be considered include the energy required to power and cool the data center systems that host the servers supporting the software. The use of the internet itself, involving the transmission and reception of data, also relies on communication networks, which have their own environmental impact. These elements, however, are difficult to estimate numerically without precise data from the software providers.

### **A.1.2 Economic sustainability**

Quantifying the costs associated with the thesis work involves considering both human and material resources. Regarding material resources, the software tools utilized play a significant role. While two of these tools were open source and incurred no direct financial cost, the third tool, Phast, required a license, resulting in a financial expense.

In terms of human resources, the costs encompass the personnel involved in the project, including the student's own time spent on research, writing, and analysis, as well as any expenses related to supervision or tutoring provided by academic supervisors. Estimating the number of hours contributed by each person involved is crucial for accurate cost assessment. For example, the student's personal involvement in the project averaged four hours per day, resulting in a total of 420 hours.

Additional material resources include the use of computer hardware, office supplies and other equipment necessary for simulations and data analysis. Indirect costs, such as electricity consumption for running the software and hardware, internet usage and other utilities, should be also considered.

## **A.2 Ethical implications**

This thesis work responds to the growing need for safe and efficient hydrogen storage and usage, particularly in the context of the global shift towards sustainable energy solutions. Specifically, it addresses the needs of enhancing safety by identifying and mitigating risks associated with hydrogen storage and usage, improving efficiency through reliable risk assessment models to better industrial processes and contributing to sustainability by advancing clean energy technologies.

Beyond the immediate scope of the project, focused on hydrogen, there are several potential consequences. The benchmark methodology developed could be adapted for other types of energy storage, substances and scenarios requiring safety assessments.

This work adheres to the ethical standards and deontological codes relevant to engineering and scientific research. This involves accurately reporting and honestly interpreting all data and findings. Additionally, the work is committed to practices that support long-term environmental sustainability. Transparency is ensured in the methodologies employed, ensuring that all procedures utilized throughout the thesis work are explicitly described and documented, allowing others to comprehend and evaluate the work undertaken.

### A.3 Relationship with the Sustainable Development Goals

The Sustainable Development Goals (SDGs), also known as the Global Goals, were adopted by the United Nations in 2015. United Nations aim to achieve 17 goals by 2030, addressing the global challenges we face, including those related to poverty, inequality, climate change, environmental degradation, peace and justice.

This thesis work contributes in part to the Sustainable Development Goals (SDGs) illustrated in Figure A2. Hydrogen, as previously mentioned, is a clean fuel because its combustion does not emit carbon dioxide. When produced through sustainable methods, it serves as a source of clean energy. By analysing potential accidents in hydrogen storage scenarios and identifying reliable ways to predict their consequences, this research can help develop and innovate industrial processes while enhancing urban safety. Specifically, one of the targets of Goal 11 is to provide access to safe and sustainable transport systems. Consequently, as hydrogen-powered vehicles are being developed, addressing their safety is crucial to achieving this target.



Figure A2: SDGs related to the thesis work.





## Annex B: Inputs of dispersion simulations

Phast:

Ambient conditions	Simulation ID	Ambient temperature (°C)	Wind velocity (m/s)	Atmospheric stability class
	1.1	10	Varying depending on the simulation	F
	1.2	10	Varying depending on the simulation	F
	1.3	10	Varying depending on the simulation	F
	1.4	10	Varying depending on the simulation	F
	1.5	10	Varying depending on the simulation	F
	1.6	10	Varying depending on the simulation	F
	1.7	10	Varying depending on the simulation	F
	1.8	10	Varying depending on the simulation	F
	1.9	10	Varying depending on the simulation	F
	1.10	10	Varying depending on the simulation	F
	1.11	10	Varying depending on the simulation	F

<b>Equipment</b>	<b>PRESSURE VESSEL</b>	<b>Simulation ID</b>	<b>Material</b>	<b>Volume (L)</b>	<b>Fluid pressure (abs)</b>	<b>Fluid temperature (°C)</b>
		<b>1.1</b>	Hydrogen	50	100	10
		<b>1.2</b>	Hydrogen	50	100	10
		<b>1.3</b>	Hydrogen	50	100	10
		<b>1.4</b>	Hydrogen	50	200	10
		<b>1.5</b>	Hydrogen	50	200	10
		<b>1.6</b>	Hydrogen	50	200	10
		<b>1.7</b>	Hydrogen	50	300	10
		<b>1.8</b>	Hydrogen	50	300	10
		<b>1.9</b>	Hydrogen	50	300	10
		<b>1.10</b>	Hydrogen	50	400	10
		<b>1.11</b>	Hydrogen	50	400	10

<b>Scenario (Initiating event)</b>	<b>LEAK</b>	<b>Simulation ID</b>	<b>Orifice diameter (mm)</b>	<b>Elevation (m)</b>	<b>Release direction</b>
		<b>1.1</b>	0,5	Varying depending on the simulation	Horizontal
		<b>1.2</b>	0,7	Varying depending on the simulation	Horizontal
		<b>1.3</b>	1	Varying depending on the simulation	Horizontal
		<b>1.4</b>	0,5	Varying depending on the simulation	Horizontal
		<b>1.5</b>	0,7	Varying depending on the simulation	Horizontal
		<b>1.6</b>	1	Varying depending on the simulation	Horizontal
		<b>1.7</b>	0,5	Varying depending on the simulation	Horizontal
		<b>1.8</b>	0,7	Varying depending on the simulation	Horizontal
		<b>1.9</b>	1	Varying depending on the simulation	Horizontal
		<b>1.10</b>	0,5	Varying depending on the simulation	Horizontal
		<b>1.11</b>	0,7	Varying depending on the simulation	Horizontal

**HyRAM:**

<b>Fuel</b>	Hydrogen
<b>Percent (vol %)</b>	100 %
<b>Fluid phase</b>	Fluid
<b>Notional nozzle model</b>	Yuceil/Otugen

<b>Simulation ID</b>	<b>Tank fluid pressure (abs)</b>	<b>Tank fluid temperature (°C)</b>	<b>Ambient temperature (°C)</b>	<b>Ambient pressure (Mpa)</b>	<b>Discharge coefficient</b>
<b>1.1</b>	100	10	10	0,101325	0,862887
<b>1.2</b>	100	10	10	0,101325	0,862887
<b>1.3</b>	100	10	10	0,101325	0,862887
<b>1.4</b>	200	10	10	0,101325	0,859323
<b>1.5</b>	200	10	10	0,101325	0,859323
<b>1.6</b>	200	10	10	0,101325	0,859323
<b>1.7</b>	300	10	10	0,101325	0,855561
<b>1.8</b>	300	10	10	0,101325	0,855561
<b>1.9</b>	300	10	10	0,101325	0,855561
<b>1.10</b>	400	10	10	0,101325	0,851911
<b>1.11</b>	400	10	10	0,101325	0,851911

<b>Simulation ID</b>	<b>Leak diameter (mm)</b>	<b>Angle of jet (rad)</b>
<b>1.1</b>	0,5	0
<b>1.2</b>	0,7	0
<b>1.3</b>	1	0
<b>1.4</b>	0,5	0
<b>1.5</b>	0,7	0
<b>1.6</b>	1	0
<b>1.7</b>	0,5	0
<b>1.8</b>	0,7	0
<b>1.9</b>	1	0
<b>1.10</b>	0,5	0
<b>1.11</b>	0,7	0

## Annex C: Inputs of jet fire flame length simulations

Phast:

Ambient conditions	Simulation ID	Ambient temperature (°C)	Wind velocity (m/s)	Atmospheric stability class
	2.1	20	1	Varying depending on the simulation
	2.2	20	0,5	Varying depending on the simulation
	2.3	20	0,5	Varying depending on the simulation
	2.4	20	2	Varying depending on the simulation
	2.5	20	2	Varying depending on the simulation
	2.6	20	2	Varying depending on the simulation
	2.7	20	1	Varying depending on the simulation
	2.8	20	2	Varying depending on the simulation
	2.9	20	0,1	Varying depending on the simulation
	2.10	20	1	Varying depending on the simulation
	2.11	20	0,5	Varying depending on the simulation
	2.12	20	0,1	Varying depending on the simulation
	2.13	20	2	Varying depending on the simulation
	2.14	20	0,5	Varying depending on the simulation
	2.15	20	2	Varying depending on the simulation
	2.16	20	2	Varying depending on the simulation
	2.17	20	1,5	Varying depending on the simulation

Equipment	PRESSURE VESSEL	Simulation ID	Material	Volume (m <sup>3</sup> )	Fluid pressure (abs)	Fluid temperature (°C)
		2.1	Hydrogen	0,8	365	20
2.2	Hydrogen	0,8	360	20		
2.3	Hydrogen	0,8	350	20		
2.4	Hydrogen	0,8	450	20		
2.5	Hydrogen	0,8	420	20		
2.6	Hydrogen	0,8	380	20		
2.7	Hydrogen	0,8	340	20		
2.8	Hydrogen	0,8	300	20		
2.9	Hydrogen	0,8	270	20		
2.10	Hydrogen	0,8	240	20		
2.11	Hydrogen	0,8	220	20		
2.12	Hydrogen	0,8	340	20		
2.13	Hydrogen	0,8	270	20		
2.14	Hydrogen	0,8	240	20		
2.15	Hydrogen	0,8	125	20		
2.16	Hydrogen	0,8	120	20		
2.17	Hydrogen	0,8	90	20		

Scenario (Initiating event)	LEAK	Simulation ID	Orifice diameter (mm)	Elevation (m)	Release direction	Jet fire model
		2.1	1	1	Horizontal	Miller
2.2	1	1	Horizontal	Miller		
2.3	1	1	Horizontal	Miller		
2.4	3	1	Horizontal	Miller		
2.5	3	1	Horizontal	Miller		
2.6	3	1	Horizontal	Miller		
2.7	3	1	Horizontal	Miller		
2.8	3	1	Horizontal	Miller		
2.9	3	1	Horizontal	Miller		
2.10	3	1	Horizontal	Miller		
2.11	3	1	Horizontal	Miller		
2.12	5	1	Horizontal	Miller		
2.13	5	1	Horizontal	Miller		
2.14	5	1	Horizontal	Miller		
2.15	5	1	Horizontal	Miller		
2.16	5	1	Horizontal	Miller		
2.17	5	1	Horizontal	Miller		

**HyRAM:**

<b>Fuel</b>	Hydrogen
<b>Percent (vol %)</b>	100 %
<b>Fluid phase</b>	Fluid
<b>Notional nozzle model</b>	Yuceil/Otugen

<b>Simulation ID</b>	<b>Tank fluid pressure (abs)</b>	<b>Tank fluid temperature (°C)</b>	<b>Ambient temperature (°C)</b>	<b>Ambient pressure (Mpa)</b>	<b>Discharge coefficient</b>
2.1	365	20	20	0,101325	0,853781
2.2	360	20	20	0,101325	0,853956
2.3	350	20	20	0,101325	0,854309
2.4	450	20	20	0,101325	0,850851
2.5	420	20	20	0,101325	0,851873
2.6	380	20	20	0,101325	0,853256
2.7	340	20	20	0,101325	0,854662
2.8	300	20	20	0,101325	0,85609
2.9	270	20	20	0,101325	0,857173
2.10	240	20	20	0,101325	0,858262
2.11	220	20	20	0,101325	0,85899
2.12	340	20	20	0,101325	0,854662
2.13	270	20	20	0,101325	0,857173
2.14	240	20	20	0,101325	0,858262
2.15	125	20	20	0,101325	0,862354
2.16	120	20	20	0,101325	0,862517
2.17	90	20	20	0,101325	0,863406

<b>Simulation ID</b>	<b>Leak diameter (mm)</b>	<b>Angle of jet (rad)</b>
2.1	1	0
2.2	1	0
2.3	1	0
2.4	3	0
2.5	3	0
2.6	3	0
2.7	3	0
2.8	3	0
2.9	3	0
2.10	3	0
2.11	3	0
2.12	5	0
2.13	5	0
2.14	5	0
2.15	5	0
2.16	5	0
2.17	5	0

## Annex D: Inputs of jet fire radiation simulations

### Phast:

Ambient conditions	Simulation ID	Ambient temperature (°C)	Wind velocity (m/s)	Atmospheric stability class	Relative humidity (%)
	3.1	6,85	2,84	D	94,3
	3.2	6,85	0,83	D	94,5

Equipment	PRESSURE VESSEL	Simulation ID	Material	Volume (m3)	Fluid pressure (abs)	Fluid temperature (°C)
		3.1	Hydrogen	1	60,8	35,55
		3.2	Hydrogen	1	63,1	14,65

Scenario (Initiating event)	LEAK	Simulation ID	Orifice diameter (mm)	Elevation (m)	Release direction	Jet fire model
		3.1	20,9	3,25	Horizontal	Miller
		3.2	52,5	3,25	Horizontal	Miller

### HyRAM:

Fuel	Hydrogen
Percent (vol %)	100 %
Fluid phase	Fluid
Notional nozzle model	Yuceil/Otugen

Simulation ID	Tank fluid pressure (abs)	Tank fluid temperature (°C)	Ambient temperature (°C)	Ambient pressure (Mpa)	Discharge coefficient
3.1	60,8	35,55	6,85	0,01022	0,864212
3.2	63,1	14,65	6,85	0,01011	0,863832

Simulation ID	Leak diameter (mm)	Relative humidity	Release angle (°)
3.1	20,9	0,943	0
3.2	52,5	0,945	0



**ALOHA:**

<b>Simulation ID</b>			<b>Simulation ID</b>		
<b>3.1</b>	<b>SITE DATA</b>		<b>3.2</b>	<b>SITE DATA</b>	
	Location	Cumbria, UK		Location	Cumbria, UK
	Latitude	55°3' N		Latitude	55°3' N
	Longitude	2°35' W		Longitude	2°35' W
	<b>CHEMICAL DATA</b>	Hydrogen		<b>CHEMICAL DATA</b>	Hydrogen
	<b>ATMOSPHERIC DATA</b>			<b>ATMOSPHERIC DATA</b>	
	Wind	2,84 m/s		Wind	0,83 m/s
	from	1,5°		from	1,5°
	at	10 m		at	10 m
	Cloud cover	10 tenths		Cloud cover	10 tenths
	Air Temperature	6,85 °C		Air Temperature	6,85 °C
	Stability class	D		Stability class	D
	Relative humidity	94%		Relative humidity	95%
	<b>SOURCE STRENGHT</b>			<b>SOURCE STRENGHT</b>	
	<b>TANK</b>	Vertical cylindrical		<b>TANK</b>	Vertical cylindrical
	Diameter	4,81 m		Diameter	4,81 m
	Length	5,5 m		Length	5,5 m
	Temperature	35,55 °C		Temperature	14,65 °C
	Pressure	60,005 atm		Pressure	62,275 atm
	Opening shape	Circular		Opening shape	Circular
Opening diameter	2,09 cm	Opening diameter	5,25 cm		
<b>DIRECT</b>		<b>DIRECT</b>			
Source	Continuous	Source	Continuous		
Amount released	1,12763 kg/s	Amount released	7,29627 kg/s		
Duration of the release	7 min	Duration of the release	3 min		
Source height	3,25m	Source height	3,25m		



## Ringraziamenti

Mi piacerebbe esprimere la mia gratitudine alla Professoressa Elsa Pastor Ferrer e alla Professoressa Eulalia Planas Cuchi per il loro prezioso consiglio e assistenza durante il mio lavoro di tesi. Vorrei inoltre ringraziare la professoressa Micaela Demichela per il suo supporto sebbene da remoto. Grazie per il tempo dedicato a rispondere alle mie domande, discutere le mie idee e offrirmi incoraggiamento in ogni fase del processo.

Inoltre, desidero esprimere il mio profondo apprezzamento a tutti i membri del CERTEC. Sin dal primo giorno sono stata accolta con gentilezza e calore, facendo sì che la mia esperienza si svolgesse all'interno di un ambiente di lavoro collaborativo e gratificante.

Sono profondamente grata ai miei genitori e a mio fratello Gabriele per il loro sostegno incrollabile. La vostra costante fiducia in me e il vostro amore incondizionato sono stati i miei pilastri di forza lungo questo percorso. Grazie per aver celebrato ogni mio successo con me e avermi dato conforto e motivazione durante i momenti difficili.

Desidero ringraziare i miei nonni, zii e cugini per tutto l'amore e il sostegno che mi avete sempre dimostrato.

Un ringraziamento speciale ad Adriana e Rachele, con cui ho avuto il privilegio di condividere questo percorso. Il legame che abbiamo formato e i ricordi che abbiamo creato insieme sono inestimabili. Non vedo l'ora di continuare a festeggiare i nostri successi e i nostri traguardi insieme per molti anni a venire.

Ringrazio Giulia perché mi è sempre stata vicina seppur nell'ultimo anno geograficamente lontana. La tua presenza è stata preziosa e significativa per me. Sei una persona speciale e voglio farti sapere che sarò sempre qui per te, pronta a sostenerti in ogni tua scelta.

Grazie a Francesco, Angela e Lorenzo per il sostegno, l'amicizia e le esperienze condivise durante questo percorso accademico.

Un grazie anche a Mattia, per il supporto durante questi anni di studio. Mi mancheranno molto le nostre serate in casa a Torino con cena e film durante la sessione. Un ringraziamento alle mie amiche storiche Gloria, Marie, Alice, Agnese, Sara e Francesca, siamo cresciute insieme e adesso siamo delle donne sparse per il mondo, ma ci sarà sempre un legame che ci unisce.

Infine, grazie ad Aníbal, perché il tuo premuroso incoraggiamento e la tua sincera fiducia nelle mie capacità sono stati una fonte di immensa motivazione.